Transparent Hemicellulose-DWCNT Electrode

Hannu Pasanen

Master's Thesis
University of Jyväskylä, Department of Physics
30.10.2015
Supervisors: Markus Ahlskog
Jouko Korppi-Tommola

JYVÄSKYLÄN YLIOPISTO
UNIVERSITY OF JYVÄSKYLÄ

Abstract

Carbon nanotubes (CNTs) and graphene have shown promising potential as next-generation transparent conducting materials due to their high electrical and thermal conductance, flexibility and transparency in both visible and infrared spectral regions. In this study transparent and conductive thin films with a novel hemicellulose and double-walled carbon nanotube (HC-DWCNT) hybrid material were produced with spray-coating, droplet casting and vacuum filtration deposition methods. HC-DWCNT material is easily dispersed in water and usable for mass-production. These films showed good conductivity, stability at ambient air, very good transparency in the visible and excellent transparency in the infrared spectral regions while having few percent haze. The best sample had sheet resistance of $115 \pm 9\ \Omega/sq$ and direct transmittance of 81.6 % at 550 nm wavelength. The properties of the prepared films were compared to CNT, graphene and their hybrid films reported by research groups by reviewing their fabrication methods and film performances. While many of these other films have shown higher short-term quality, it was found that the performances of HC-DWCNT films were quite promising for future development considering the stability of the films and the fact that dopants or post-treatments were not used for enhancing the performance of the best samples.

Acknowledgements

I would like to thank these following people for helping me with this work:

-Markus Ahlskog and Jouko-Korppi Tommola for supervising this work although transparent conductors are neither of theirs field of specialty.

-Peerapong Yotprayoonsak, Pasi Myllyperkiö, Matti Hokkanen, Kimmo Kinnunen, Tarmo Suppula, Mikko Laitinen and Jussi Toppari for helping me with the practical issues. Additional thanks to Toppari for letting me borrow his equipment.

-The personnel at Department of Chemistry and Department of Biological and Environmental Sciences for helping me find the equipment I needed.

-nEMCel for providing me with the HC-DWCNT material.

Abbreviations

AF	aerosol filtration
AgNP	silver nanoparticle
AgNW	Silver nanowire
AuNP	gold nanoparticle
CNT	carbon nanotube
CuNW	copper nanowire
CVD	chemical vapor deposition
DD	dispersion deposited
DOS	density of states
DSSC	dye-sensitized solar cell
DWCNT	double-walled carbon nanotube
GO	graphene oxide
HC-DWCNT	hemicellulose - double walled carbon nanotube
HPLC	high-performance liquid chromatography
IR	infrared
ITO	indium-tin oxide
LB	Langmuir-Blodgett
MCE	mixed cellulose-ester
MNP	metal nanoparticle
MWCNT	multi-walled carbon nanotube
OA	triethyloxonium hexachloroantimonate
OLED	organic light emitting diode
PEDOT:PSS	poly-(3,4-ethylenedioxythiophene):poly(styrenesulfonic acid)
PMMA	polymethylmethacrylate
polyHMAM	poly-N-hydroxymethyl acrylamide
PU	polyurethane
RGO	reduced graphene oxide
SEC	size-exclusion chromatography
SEM	scanning electron microscope
TCF	transparent conducting film
TCNQ	tetracyanoquinodimethane
TCO	transparent conductive oxide

Symbols

μ	absorption coefficient
A	absorbance
A_{cs}	cross-sectional area
A_{sc}	surface area of a spherical cap
A_d	spherical cap covered by detector
a_I	current to voltage amplification factor
a_V	voltage amplification factor
h	height
I	electrical current
I	intensity
I_{bg}	background electrical current
I_d	detected intensity
l	length
n_{dt}	portion of directly transmitted light of total transmittance
n_s	portion of scattered light of total transmittance
P_{dt}	power of directly transmitted light
P_{gdt}	power of directly transmitted light through glass
P_{gs}	power of scattered light through glass
P_d	detected power
P_s	total power of scattered light
R	electrical resistance
r	radius
r_d	radius of detector
R_s	sheet resistance
T	transmittance
V	voltage difference
V_{bg}	background voltage difference
z	position in z-axis

Contents

1 Introduction

Transparent conducting films (TCFs) have multiple applications including organic light emitting diodes (OLEDs), touch screens and most importantly next generation solar cells. It has been estimated that the markets for these products will grow to $5.1 billion by 2020 [1]. Indium-tin oxide (ITO) and other transparent conductive oxides (TCOs) have dominated markets with their very low sheet resistance and high transmittance in visible light, for example commercial ITO has sheet resistance of less than 10 Ω/sq and over 80 % transmittance [2]. They do however have several drawbacks such as many of them, especially ITO, contain rare and expensive metals and their deposition method, sputtering in vacuum, is expensive. They are also inflexible and their transparency in infrared (IR) region is poor. Hence many alternative matrials have been looked for, such as carbon nanotube (CNT) based electrodes, graphene, metal nanowires, conductive polymers and hybrid materials that are mixtures of these or other substances. None of these alternatives are however yet in commercial use because they have not yet reached the quality of TCOs.

While many common applications only require transparency in visible light some applications also demand transparency in the infrared. These include IR sensing and emission devices such as long wavelength vertical cavity surface emitting lasers (VCSELs), IR solar cells that could turn regular windows into solar cells, transportation of energy generated by satellites with solar cells and fiber-optic communication. Few TCOs are transparent in the infrared while CNTs have very high IR transparency, in fact they are more transparent in IR region than in visible light. Other common candidates for transparent conductive films such as silver nanowires and conductive polymers are also opaque in IR [3], which makes CNTs the best candidate for many IR applications.

Another field of growing interest is flexible electronics. Flexible electrodes could for example be used in new kind of sensors or artificial muscles. By combining flexibility with transparency we could create foldable solar cells, displays and so on. Because TCOs cannot be used in these applications as they easily break when bent, IR applications or flexible electronics will be the first commercial use for the new conductive materials.

Transparency and conductivity are features that are theoretically in contradiction with each other [4, p. 1]: excellent transparency requires that the band gap between the conduction band and valence band is large enough so that photons cannot excite electrons from valence band to conduction band, which would cause the photon to lose energy and decrease transparency. Good electrical conductivity on the other hand requires electrons in conduction bands. Transparent conductive materials always have to trade off some of transparency in exchange for better conductivity or vise versa.

Deposition methods must also be cost-efficient. ITO for instance has to be deposited

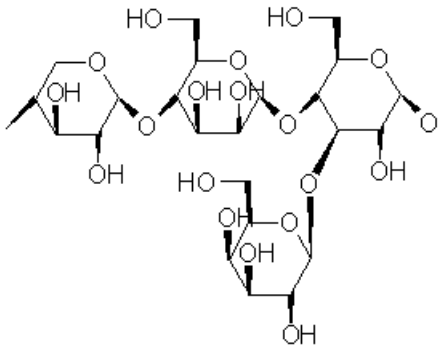

Figure 1: An example of molecular motif of hemicellulose. Adapted from Wikimedia Commons.

by sputtering and then annealed at high temperatures [5] which limits the substrates it can be used with. High quality aligned CNT thin films that have all the CNTs pointing to same direction can also be prepared by directly transferring the synthesized films from growth substrate to another substrate [6] but such methods have problems in scaling them to mass production, which is why CNTs are usually first dispersed in solvents and then deposited with different methods. Dispersing CNTs in solvents also has its issues: it often requires addition of surfactants that may need to be removed afterwords and it results in loss of alignment as the CNTs land randomly on the substrate.

In this study transparent and conductive thin films have been prepared with a novel hybrid material that is a 1:1 mixture of hemicellulose and double-walled carbon nanotubes (HC-DWCNT), produced by a local company nEMCel. Hemicellulose is a common matrix polysaccharide found in plants, consisting of many different monomers with many C-O-C and OH groups as shown in figure 1, which makes it soluble in water. Since it does not have delocalized electron structure it is not electrically conductive material but it can be utilized as a surfactant for dispersing CNTs in water.

HC-DWCNT material is potentially transparent in both the IR and visible spectral regions, flexible and easily dispersed in water, unlocking efficient and cheap deposition methods for mass-production. The films were characterized by measuring their sheet resistance, transmittance from visible light to mid infrared and scattering. In addition different deposition methods were compared and the resilience of the films was tested by annealing them and immersing them in solvents. In order to compare the results obtained in the Thesis with the results reported previously for TCFs a review of different carbon-based transparent electrodes, CNTs, graphene and hybrid materials is given.

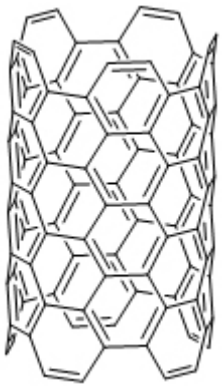

Figure 2: Single-walled carbon nanotube. Adapted from Wikimedia Commons.

2 Carbon nanotubes and graphene

2.1 Properties

Carbon nanotubes are hollow tubes consisting only of carbon atoms as shown in figure 2. Both graphene and CNTs are bound by sp^2 bonds: each carbon atom is bound to three other carbon atoms in such way that one electron from each atom is delocalized, which is the reason for their many useful properties. Single walled CNTs (SWCNT) have a diameter of about 1 nm, but CNTs with multiple walls (MWCNT) can have diameters of dozens of nanometers, and the length of a CNT can be up to 550 mm [7], granting them the largest length-to-diameter ratio among known materials. The smallest multi-walled nanotubes are double-walled nanotubes (DWCNTS). A very similar material to CNTs is graphene which is only one atom thick layer of carbon, and a CNT can be considered as a sheet of graphene rolled to a tube.

Since CNTs can be conceptualized by rolling up a sheet of graphene, they are presented by a pair of chiral indices (n,m) that are the coefficients of the unit vectors of a honeycomb crystal lattice of graphene. These vectors are visualized in figure 3. The sum of these vectors multiplied by their coefficients is called the chiral vector and it tells which way the sheet of graphene has to be wrapped in order to get a certain type of CNT. There are three types of SWCNTs: zigzag (m=0), armchair (m=n) and the rest are called chiral CNTs. Armchair CNTs are metallic while the other CNTs, zigzags and chirals, are semiconductive. Chirality is a very important factor in determining the properties of a CNT, and MWCNTs can consist of many nanotubes with different chiralities, which makes their properties and identification much more complicated.

Materials can be classified into metals, semimetals, semiconductors and insulators. Metals are materials that have no energy difference or so called band gap between the lowest unfilled energy level (conduction band) and the highest filled energy level (valence

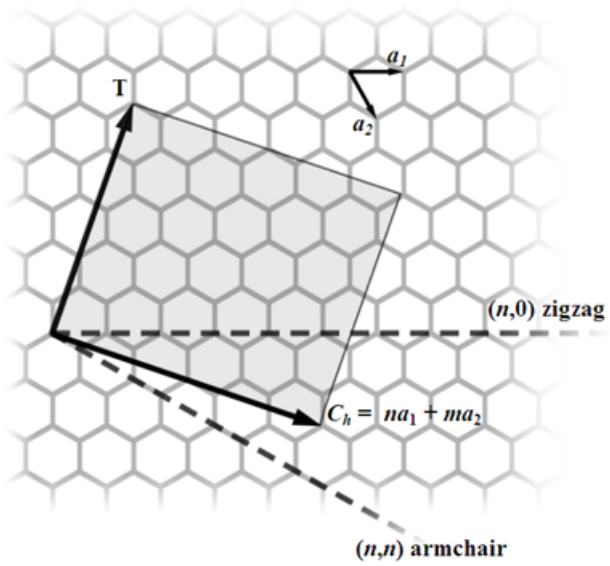

Figure 3: Unit vectors of the crystal lattice of graphene and an example of a chiral vector. The chiral indices of the chiral vector are (4,2) and the CNT would be wrapped of the darkened area so that T denotes the tube axis. Adapted from Wikimedia Commons.

band), in other words an electron needs next to no energy in order to move from one energy level to another, which makes it possible for the electrons to move between atoms and the material to conduct electrical current. Semimetals have a very small overlap between conduction band and valence band. Semiconductors have a small band gap, in other words electrons need some energy in order to move from valence band to conduction band, and insulators have a large band gap. CNTs can be either semiconductive, metallic (if m=n) or semimetals, which depends on their chiral indices, but graphene is a special zero-overlap semimetal that has no electrons in the conduction band but no band gap between it and valence band.

CNTs and graphene have several interesting properties and potential applications. Due to their sp^2 bonds and delocalized electrons individual SWCNTs can have very high conductivity in scale of 10^4 S/m and they are called one-dimensional conductors while graphene is a unique two-dimensional material. Thanks to the strength of carbon - carbon bonds they are very strong materials: graphene is in fact the strongest material ever discovered, having a tensile strength of 130 GPa and a Young's modulus of 1 TPa [8]. Graphene also has good thermal conductivity [9] and while graphene is not originally magnetic researches have recently been successful in making graphene magnetic [10]. CNTs share most of these properties of graphene but compared to graphene CNTs are a very heterogeneous group of materials due to chirality.

Graphene has a very high opacity as it absorbs 2.3 % of white light [11], considering

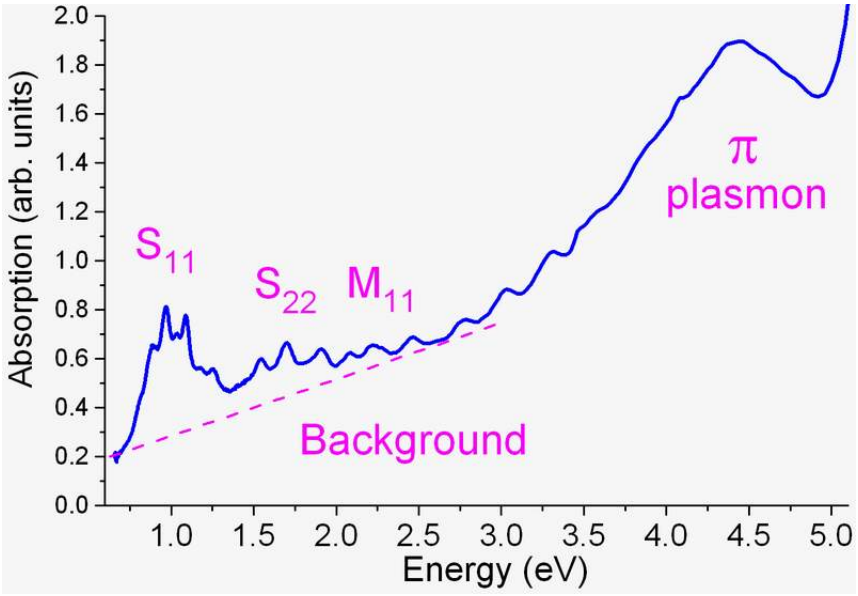

Figure 4: Optical absorption of dispersed SWCNT. The spikes such as S_{11} are caused by Van Hove singularities. Adapted from Wikimedia Commons.

that it is only one atom thick. Because of its high opacity compared to its thickness the amount of photons graphene can absorb is limited, in other words the absorption becomes saturated and graphene begins to absorb less than 2.3 % if it is exposed to light of high intensity [12]. CNTs have also been used in applications requiring saturable absorption [13].

The optical absorption in CNTs differs from graphene and three-dimensional solids because of Van Hove singularities that cause the fine structure in the absorption spectrum shown in figure 4. As SWCNTs are one-dimensional particles they do not have continuous density of states (DOS), they also have sharp peaks in DOS called Van Hove singularities [14]. The spikes in figure 4 correspond to the energy differences of these singularities in figure 5 and can be used for identifying different SWCNTs.

Another common optical method for identifying CNTs is Raman spectroscopy which can be used for detecting for example vibrational and rotational energy levels. In Raman spectroscopy the sample is first excited with a laser from a ground state to a very short lived virtual energy state. When excited form the ground vibrational state the molecules can return to first excited vibrations state by emitting a photon with energy of the excitation energy minus vibrational energy. Such transition is called a Stokes scattering process. Excitation could start also from the first vibrationally excited state. In this case the emitted photon has an energy of excitation energy plus the vibration energy. This process is called anti-Stokes scattering. For CNTs the vibrational mode of interest is the carbon-carbon stretching mode around 1600 cm^{-1}. The location of this band in

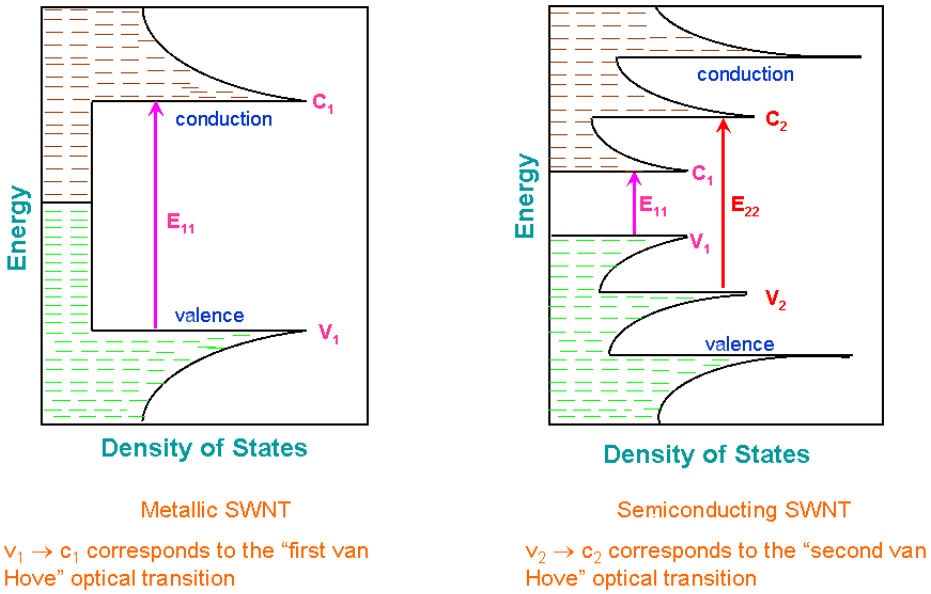

Figure 5: Density of states in SWCNTs. The spikes represent Van Hove singularities. Adapted from Wikimedia Commons.

the Raman spectrum is sensitive to for example chirality of the tube and hence can be used to identify CNTs.

There are many new forms of carbon that are based on carbon nanotubes, graphene and fullerenes which are hollow carbon molecules in form of spheres, ellipsoids and so on. These new forms include for instance peapods [15] and nanobuds [16] that are fullerene functionalized SWNTs with the fullerene groups inside or outside the tube. Carbon nanotubes may even have graphitic foliages grown along their sidewalls [17]. These materials add to the potential of use of basic carbon materials even further by allowing development of additional useful properties. Of these materials, nanobuds have been used for producing transparent conductive electrodes [18], but carbon based materials in general have multitude of applications, for instance they are used in electrical circuits [19], supercapacitors [20] and solar cells [21].

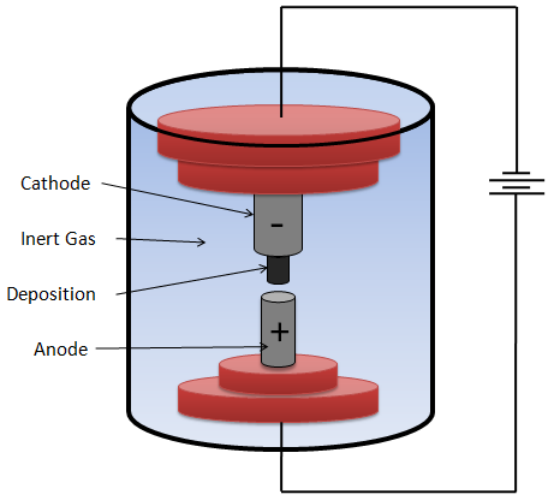

Figure 6: Arc discharge setup for CNT synthesis. Adapted from Wikimedia Commons.

2.2 Synthesis

2.2.1 Synthesis of CNTs

This section shortly describes the most common methods for producing CNTs. While there are multiple methods available, many of them are not suitable for large-scale production of quality CNTs.

Arc Discharge

In arc discharge method a strong electrical current is used for evaporating carbon in an inert atmosphere, most commonly helium or argon, by passing it through two graphite electrodes [22]. As carbon evaporates it condenses on the walls of the system and on the cathode where the nanotube growth happens. Growth of SWCNTs requires metal catalyst particles such as cobalt or nickel that are added to the anode and are vaporized alongside with carbon. Without catalyst particles MWCNTs and fullerenes are produced instead.

Laser Ablation

To make CNTs by laser ablation a composite of about 98.8 % graphite and 1.2 % of cobalt or nickel is first heated to 1200 $°C$ in an inert atmosphere. Either laser pulses or continuous laser is then used for vaporizing carbon atoms together with metal nanoparticles that act as catalysts for nanotube growth. By using pure graphite without catalysts MWCNTs are produced just like in arc discharge.

Laser ablation and arc discharge methods are very similar in their basic principle that

the catalyst particles are vaporized alongside carbon from graphite. Both methods can be used for large-scale production of CNTs and they also produce fullerenes and other carbon materials as by-products. So far arc discharge has been more successful of the two in production of high-quality SWCNTs.

Chemical Vapour Deposition

While arc discharge and laser ablation methods are good for mass-production of CNTs they are less suited for selective synthesis of nanotubes with desired chiralities or other characteristics. In chemical vapour deposition (CVD) the catalyst particles are first deposited or formed on the growth substrate, which allows control over their size and shape that are crucial in acquiring only certain kinds of CNTs [23]. The substrate is then placed into a furnace where a flow of gaseous carbon compounds such as methane, carbon monoxide or other hydrocarbon comes into contact with the substrate. The catalyst particles and carbon compounds undergo chemical reactions that cause CNTs to grow from the particles. In CVD there are multiple factors that affect the properties of the CNTs, such as furnace temperature, the pressure and concentration of carbon compounds, the properties of the catalyst particles and so on. CVD can also be used for growing aligned "towers" of CNTs [24]. Despite the possibility of selective properties of CNTs, CVD commonly also produces amorphous carbon, graphite and other impurities.

There are also other versions of CVD such as alcohol catalytic CVD that uses alcohols instead of metal catalyst particles, which is cheaper and requires lower temperature of 550 $°C$ while regular CVD requires at least 650 $°C$. A very well-known version of CVD is high pressure carbon monoxide reaction (HiPco) in which the catalyst particles are also introduced in gas phase, which has many advantages such as continuous operation [25]. HiPco uses iron carbon monoxide to form the iron catalyst particles. Other aerosol CVD methods have also been developed that utilize carbon monoxide as the carbon source with iron catalyst obtained by decomposition of ferrocene [26]. The advantage of carbon monoxide is that it produces very clean CNTs without amorphous carbon or other detrimental impurities.

2.2.2 Purification of CNTs

Oxidation methods

Since synthesized CNT material contains metal catalyst particles and various forms of carbon, it has to be purified before it can be used. This requires selective oxidation of the synthesized material, and one way is to reflux CNTs in mineral acid such as nitric acid or to use some other oxidant [27]. The effectiveness of the procedure depends on

temperature, reflux time and the type of acid. If oxidation is too strong the CNTs will be damaged, cut into short fragments or have their surfaces chemically modified. One interesting phenomena relating to oxidation is the opening of the end of the nanotube: The end carbon atoms are less stable than the rest of the tube, which makes them chemically more reactive and vulnerable to oxidation.

Air oxidation means oxidizing the impurities simple by heating the material in air. It can be used for removing the catalyst particles and amorphous carbon in so-called dynamic oxidation which means that the temperature is gradually increased during the process. It is the most common gas phase oxidation method, while other gasses that have been used are CO_2, H_2 and NH_3.

Liquid Br can also be used for purification of CNTs by mixing CNTs in liquid Br under nitrogen atmosphere. Bromide bath alters the reactivity of carbon materials with oxygen, allowing the selective oxidation of impurities without damaging CNTs.

Physical purification methods

Physical and chemical purification methods are often both used in multi-step procedures in order to gain high-purity CNTs. Filtration is one of the most basic separation techniques, and with filtration membranes that have small pore size distribution it is possible to separate nanotubes by their length in addition to separating them from impurities.

Chromatography, especially high-performance liquid chromatography (HPLC) and size-exclusion chromatography (SEC), is another method that can separate CNTs by their size. For example in HPLC dispersed CNTs are pushed through a column filled with a solid adsorbent material. Different CNTs have different flow rates through the column, which allows length-based separation with narrow distribution.

Third technique that can be used for mass or length-based separation of CNTs is centrifugation [28, 29]. Centrifugation means rotating a dispersion with high enough angular velocity that the centrifugal force forces the particles to the bottom of the container. Using it on CNT dispersion causes sedimentation in such way that the heaviest CNTs end up to the bottom of the sediment, and by removing the upper part of sediment one can separate CNTs according to their length.

One downside to physical purification methods is that they require CNTs to be dispersed in a solvent, which usually requires sonication and surfactants. Sonication utilizes high intensity ultrasonic waves which separate CNTs from each other while surfactants modify the chemical properties of CNTs.

2.2.3 Synthesis of graphene and graphene oxide

Graphene was first discovered by K.S. Novoselov et al. in 2004 [30] by manually peeling off layers of graphite with Scotch tape. Mechanical peeling of graphite is however not suitable for industrial production, so graphene sheets are either produced by synthesizing it with CVD, epitaxial growth method or solution exfoliation or by reducing graphene oxide [31]. In CVD method graphene is grown on transition metals, usually nickel or copper which act as a catalyst [32]. The method is very similar to CNT synthesis with CVD, including the use of hydrocarbons as carbon source. Graphene growth in CVD stops at monolayer or few layers, so additional layers must be stacked with transfer methods. Epitaxial growth method also produces a graphene monolayer but it uses silicon carbide as both the substrate and carbon source. By heating silicon carbide at about 1300 $^{\circ}C$ in vacuum silicon sublimes while carbon undergoes graphitization.

Solution exfoliation, in which graphite is exfoliated into layers of graphene in a solvent such as methanesulfonic acid with the aid of sonication, is a method that can effectively produce multi-layered graphene but the exact amount and quality of layers can be difficult to control [33]. Since graphite is easy to acquire solution exfoliation is a very promising method for mass production. Purification of the product however usually requires oxidation or some other chemical modification which increases the amount of defects in the graphene sheets.

Graphene oxide (GO) is commonly produced by oxidizing graphite with sodium nitrate, potassium permanganate and concentrated sulfuric acid [34]. The layers are then exfoliated with sonication and dispersed in water or some organic solvent without surfactants. If the size distribution of the GO flakes is too great, smaller flakes can be removed with for example by centrifugation or pH-assisted selective sedimentation [35].

3 Transparent carbon-based electrodes

3.1 Preparation methods

Usually synthesized CNTs and graphene need to be transferred to another substrate for the application. CNTs can be either transferred directly from the growth substrate to the desired substrate or they can be first dissolved or dispersed in a solution by adding surfactants. CNTs can be dispersed without surfactants to some degree with sonication which separates individual CNTs from each other, but it is only temporary as they will eventually re-aggregate and sonication has to be used with many surfactants as well for proper dissolution. Surfactants and their removal and sonication can damage the CNTs and solution deposition methods usually cause the CNTs to align randomly on the substrate, which is why the solution processed CNT films are most likely of lesser quality than the directly deposited or dry-transferred films, in which the alignment and the quality of CNTs can be preserved better. Removal of the surfactants is required because they can decrease conductivity in tube-tube junctions. The dry-transfer methods however are much more difficult to scale up for industrial purposes, and so solution based transfer methods are often used instead because they can be easily scaled for mass-production.

Graphene, just like pristine CNTs, is insoluble in water. Instead of surfactants, graphene can be oxidized to graphene oxide (GO) which is soluble in water. This is done by using strong oxidizing agents. Graphene oxide is however an insulator, and so it has to be reduced back to graphene after depositing graphene oxide flakes on substrate. Graphene deposited in this way is called reduced graphene oxide (RGO).

What usually limit the conductivity of CNT and graphene thin films are defects in their structure and connections between individual CNTs or graphene flakes. Mainly because of the bad connections in tube-to-tube intersection, CNT thin films have much lower conductivity than individual CNTs, and synthesis of ultra-long CNTs that could reach from one edge to another of for example a solar cell is very challenging. Because of the importance of good connections between CNTs the formation of CNT bundles is also a negative thing: bundles have multiple CNTs attached to each other and have same alignment but the connection between two bundles is not much better than it is for individual tubes. Instead the bundles have multiple layers of CNTs which decreases transmittance. The same principle applies to multi-walled CNTs: MWCNTs have multiple carbon walls that increase absorbance but do not have direct contact with other MWCNTs in junctions.

Thus there are many ways to improve properties of CNT and graphene thin films. First of all the synthesis methods could be improved to produce longer tubes or graphene sheets with lower density of defects. Secondly the film transfer or deposition techniques

should cause as few defects as possible and avoid bundling while preferably either aligning or maintaining the alignment of the tubes. In addition film transfer should be cost efficient and scalable. Thirdly the conductivity of the connections between tubes or sheets can be enhanced for example by chemical doping or by adding some other conductive material to the contact points. Such hybrid films usually contain conductive polymers or metal nanoparticles.

3.1.1 Deposition methods for CNT and graphene dispersions

Vacuum filtration

Vacuum filtration is a common filtration technique in which pressure difference is used for pushing a solvent through a filter membrane. Wu et al. [36] were the first ones to use the method to make transparent CNT thin films in 2004 and since then it has become one of the most common methods for producing CNT thin films in laboratories [37, p. 69]. While the solution containing CNT or graphene oxide is being pushed through the filter the particles form a layer on the filter membrane. The resulting film is uniform if the dispersion is uniform, but the accumulation of the particles also slows down the solvent flow speed so that the possibility of a particle landing to some other thinner spot on the film increases. Because the film is attached to the filter membrane it is usually removed by dissolving the membrane for instance into acetone while the film is either pressed to the desired substrate or it floats to the surface of the liquid from where it can be collected. Although the method is widely used in laboratories, including this study, vacuum filtration technique has problems such as small sample size [38, p. 397] and cost of the filters and their dissolution, which makes it difficult to utilize it in commercial applications and mass-production.

Solvent evaporation

The most simple solvent evaporation deposition method is droplet casting, placing a droplet of solution with dispersed nanoparticles and letting it dry. Since a droplet always dries in such a way that the formed CNT film is not uniform, multiple techniques have been developed for producing more uniform films. All of the solvent evaporation methods are fairly simple such as spray-coating which was used also in this study. Some of these methods require that the CNT or GO ink has high viscosity such as spin-coating in which the solution is spread by spinning the substrate. Doctor-blading, or wire bar, is another method that requires viscosity and it means spreading the CNT ink by pressing and spreading it with a blade or other object with a fixed distance from the substrate. Dip-coating can either mean dipping the substrate into CNT or GO solution and either

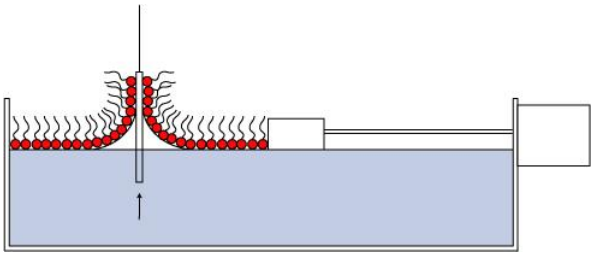

Figure 7: Vertical deposition of floating nanoparticles with LB trough. Adapted from Wikimedia Commons.

letting the solution evaporate or slowly pulling the substrate out with a constant speed.

Langmuir-Blodgett trough

Langmuir-Blodgett (LB) trough can be used for depositing nanoparticles which form a monolayer on liquid surface such as water. The nanoparticle film is compressed from one or both sides while the substrate is lifted from the liquid and the floating particles attach to the substrate as in figure 7. The LB method can be used for precise control of how many particle layers are deposited on the substrate by repeating the process. The compression pressure can have an effect on the deposition: the greater the pressure the higher the particle surface density. CNTs can actually also be aligned with the LB method by adjusting the pressure [39], although in order to avoid aggregation into bundles CNTs require surface functionalization.

Electrodeposition

Electrodeposition utilizes electric field for gathering charged particles from a colloidal dispersion and attaching them to an electrode [40]. This can be simply achieved by using a power source to apply a voltage difference over two electrodes that are placed into CNT dispersion which contains CNTs with electrically charged surfactants. This method can however be only used for coating conductive surfaces and so it is very impractical for producing transparent electrodes expect maybe for some hybrid materials, such as using CNTs or GO as a coating for silver nanowires.

Layer-by-layer self-assembly

Layer-by-layer self-assembly also requires use of surfactants that are electrically charged in a colloidal dispersion. By having a substrate that also has electrically charged surface a monolayer of CNTs can be easily deposited on the substrate by placing it into the dispersion. Another layer can be formed by placing the same substrate to another dispersion in which the CNTs have opposite electrical charge and this can be continued

until desired thickness is achieved. Hybrid materials can also be easily crafted by adding a layer of the other material instead of CNTs.

Sol-gel method

Sol-gel method is usually used for fabrication of metal oxide thin films but it can also be used for fabrication of CNT and metal or silicon oxide hybrid films such as CNT-ITO [41]. Sol-gel method functions by having a colloidal solution of nanoparticles that turns into a wet gel as it dries where the particles have formed continuous networks. A thermal treatment is usually required after the gelation for removing the rest of the solvent and improving film quality. The precursor solution can be deposited on the substrate with for example dip-coating or spin-coating.

3.1.2 Dry-transfer

Dry-transfer, commonly stamping or press transfer, is a simple transfer method in which the CNTs grown or deposited on a substrate are transferred to another substrate by pressing the substrates against each other so that the CNT thin film forms stronger bonds with the new substrate than the original one. The method can preserve orientation and quality of the tubes and be used for patterning [39]. Dry-transfer is usually used with CVD produced CNTs or graphene. Nasibulin et al. [42] have developed an aerosol CVD method that is similar to vacuum filtration: the CNTs are grown in gas phase and filtered with a microporous filter and then press transferred onto the substrate. This filtration method is relatively cheap and can be scaled up but many of the CVD growth and dry-transfer techiques are too impractical for industrial use.

Graphene CVD faces similar issues, and Sukang Bae et al. [43] have developed a scalable method for transferring graphene produced with CVD. Graphene is grown on a thin sheet of copper and then attached to a polymer by pressing them together and etching the copper, leaving the graphene sheet on the polymer to be press transferred to another substrate. The downside of the method is that it requires etching of copper which makes the process expensive. Many alternative methods for dry-transferring graphene have also been developed [44–48] but polymethylmethacrylate (PMMA) and Cu etching based transfer has been the most popular for producing TCFs. Among graphene transfer methods the one developed by Deng et al. has been successful at fabricating graphene and copper nanowire hybrid films with roll-to-roll technique that transfers graphene layers without destroying the copper growth substrate and even allows reuse of the same substrate. This electrochemical delamination transfer method has been investigated earlier by other groups [49–51] but it has not seen much use in production of TCFs.

3.1.3 Doping

Doping means introducing impurities to a pure material in order to change its properties. Doping can refer to substituting carbon atoms with some other element, adding atoms or ions outside or inside the tubes, covalent functionalization or attaching functionalization groups via π-stacking [52]. In case of transparent CNT films it is used for improving the conductivity of the individual tubes by increasing the carrier concentration in semiconducting CNTs and decreasing contact resistance in CNT junctions, of which tube-tube junction resistance decrease has been determined as the most important factor for transparent conductive CNT films [53]. Doping rarely affects the transparency of CNT films [54]. Doping has been an important factor for improving CNT films and various dopants have been tested, such as vapor treatment with bromine and potassium, acid baths and treatments with other common dopants NO_2, $SOCl_2$, I_2 and tetracyanoquinodimethane [2]. Graphene has also been successfully doped with HNO_3 [43, 55]. In addition to doping, HNO_3 has been used for removing surfactants and other impurities.

Doping typically however suffers from instability and degradation of conductivity over time, for example NO_2 and NO_3^- are compounds that tend to detach from the CNTs. Instability is the major drawback in many of the new transparent conductor materials, including silver nanowires [56], conductive polymers as well as modified CNT films. Doping with strong oxidants also limits the substrates. Hongjun Gao et al. [57] have shown that it is possible to improve stability of HNO_3 doped CNT films by using vapor doping instead of acid bath, but after the initial decrease of sheet resistance to about 23 % of the original resistance it still increased back to about one half of the original value. New dopants have also been suggested, for example Chandra et al. [53] have used triethyloxonium hexachloroantimonate as dopant and shown that the doped CNT film is stable in room air.

3.2 Performance of transparent carbon-based conductive films

This section lists the top performances of transparent electrodes which utilize CNTs and graphene. Performance of TCFs is commonly given as sheet resistance R_s and transmittance T of the film. Important stability test results for the films are much less frequently reported, probably due to time consuming follow up measurements. Stability can be measured in different ways: in regular room conditions, in high humidity or temperature (85 % relative humidity and 85 $°C$) or under constant electric current.

Sheet resistance refers to the resistance of a film with a square shape, for instance the electrical resistance of a film with dimensions of $1cm$ x $1cm$ is the same as the sheet resistance of the same film. Hence sheet resistance is only dependent on thickness and conductivity.

There are two types of transmittance: direct transmission, also known as specular or regular transmission, and scattered transmission, also called diffusion transmission. In direct transmission measurement intensity of the incoming light beam is measured only in the direction of the incoming beam. Measurement of scattered transmission requires use of integrated sphere measurement instrumentation, which allows measurement of the intensity of the off-axis transmitted light as well. Scattering can be advantageous in some cases, such as in the study of solar cells, but detrimental in other cases such as displays where it causes blurring.

In the literature transmittancies of transparent films are is usually given as the total transmittances at 550 nm wavelength, which includes both diffusion and direct transmission especially when the diffused portion is significant. Hence most of the transmittance values in this chapter are given in total transmittance values. This is however not the case in the experimental section of this study where transmittance was mostly measured only as direct transmittance without including scattering. Scattering was measured separately for some of the samples.

3.2.1 SWCNT films

Most of the top-performing SWCNT TCFs found in literature are listed in figure 8. The state-of-the-art dry-transferred transparent SWCNT electrodes have been developed by Mustonen et al. [58] with aerosol vacuum filtration, dry-transfer and doping with strong nitric acid, having sheet resistance of 63 Ω/sq and 90 % transparency. They used a new synthesis method that produces mainly CNTs with near armchair chiralities: an aerosol CVD system where the iron catalyst particles are formed by applying voltage between two iron electrodes separated by nitrogen gas so that the electrical discharges vaporize iron particles. Carbon monoxide was used as the carbon source. Other aerosol synthesis

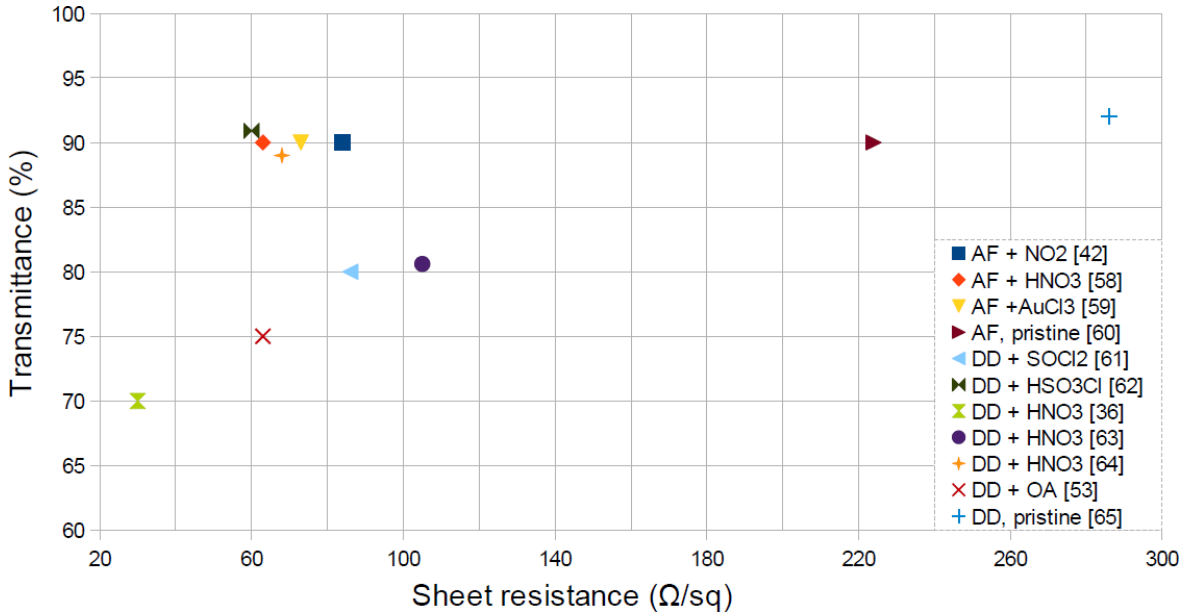

Figure 8: Performances of different transparent SWCNT electrodes with their dopants and deposition methods. AF means aerosol filtration method and DD refers to dispersion deposited films.

methods by the same group with ferrocene as the catalyst source have achieved sheet resistance of 86 Ω/sq, Reynaud et al. [60], and 73 Ω/sq, Anoshkin et al. [59], at 90 % transparency with hydrocarbon as the carbon source in first case and combination of carbon monoxide and ethylene in the second. Gold chloride, $AuCl_3$, was used as the dopant and it showed much better stability than nitric acid doping.

Jing Gao et al. [61] used highly purified arc discharge SWCNT dispersion with spray-deposition and thionyl chloride as dopant to create films with 86 Ω/sq sheet resistance and 80 % transmittance. Sae Jin Sung et al. [63] used strong acids for oxidizing SWCNTs and then neutralized the SWCNTs with filtration until the acids were removed. The oxidized SWCNTs were then further purified with centrifugation, vacuum filtered of a dispersion and doped with nitric acid. The best of their films had sheet resistance of 105 Ω/sq and 80.6 % transparency. A thicker film by Wu et al. [36] with the same dopant had performance of 30 Ω/sq R_s and 70 % T. More stable doping with triethyloxonium hexachloroantimonate (OA) as the dopant developed by Chandra et al. [53] achieved 63 Ω/sq and 75 % respectively.

Kim et al. [64] produced CNT films with 68 Ω/sq R_s and 89 % T by creating CNT ink with hydroxypropylcellulose, spreading the ink with doctor-blading and removing the cellulose with isopropanol. They also used nitric acid as dopant but in addition to doping they irradiated the SWCNT film beforehand with a xenon flash lamp to remove rest of the cellulose, which also improved conductivity.

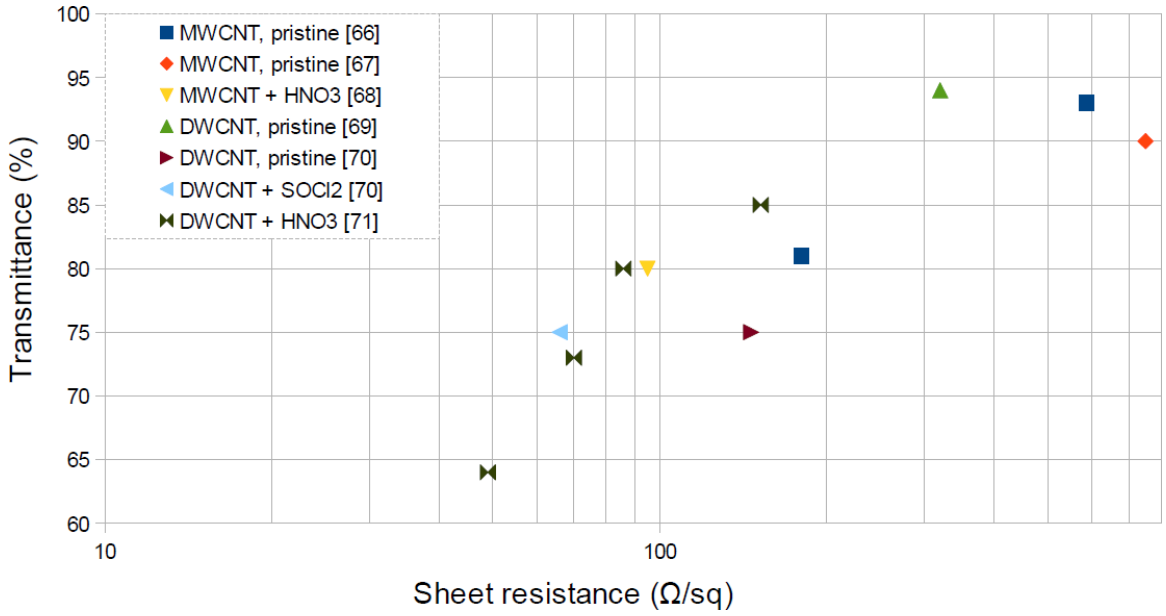

Figure 9: Performances of different transparent MWCNT electrodes.

Hecht et al. [62] on the other hand have produced the best dispersion-deposited CNT films with vacuum filtration by doping the film with chlorosulfonic acid, resulting in a sample with values of 60 Ω/sq R_s and 90.9 % T. This result was achieved by using very high-grade CNTs produced with CVD and unstable superacid doping that significantly degraded in few days.

Record numbers of 60 Ω/sq R_s and 90 % transmittance of SWCNT films have not improved over the last two years. Degradation of the doping of these films is also still an unresolved problem. The sheet resistance of pristine SWCNTs is usually too high for practical purposes, which is why stable doping is essential for production of SWCNT films. For instance the pristine sheet resistance of the film produced by Reynaud et al. before doping was 224 Ω/sq with 90 % transparency. Regarding dispersion-deposited films, Yanqing Wang and Bunshi Fugetsu [65] produced SWCNT films by only using very long tubes. They achieved sheet resistance of 286 Ω/sq with 92 % transmittance without oxidant-based doping.

3.2.2 MWCNT films

Transparent and conductive multi-walled carbon nanotube films have been investigated less than SWCNTs. Resistance in CNT junctions is a major contributor to the overall resistance of the film but MWCNTs do not necessarily have any better contact to each other than SWCNTs have while having more carbon walls which increase absorbance. Peng et al. [68] have created high-quality MWCNT films with traditional vacuum filtration of MWCNT dispersion and doping with nitric acid. One of their samples for instance had

a sheet resistance of 95 Ω/sq with 80 % transmittance, which are the best values found for MWCNT transparent electrodes expect the ones using DWCNTs as seen in figure 9.

Double-walled CNTs, the smallest possible type of MWCNTs, are an exception to the quality of MWCNT films. Hou et al. [71] fabricated a DWCNT film with values of 83 Ω/sq R_s and 79 % T. They used an aerosol CVD method for synthesis and air oxidation and dilute HCl for purification to obtain DWCNTs of good purity, structure and uniformity and vacuum filtration for the deposition after dispersing them in water with sodium dodecyl sulfate. HNO_3 was used as dopant. Green and Hersam [70] also produced transparent DWCNT films with a very different method but their films ended up being of similar quality of 146 Ω/sq without doping and 65 Ω/sq with $SOCl_2$ doping and 75 % transmittance. DWCNT films showed better stability after doping than SWCNT films. While DWCNTs have higher absorbance than SWCNTs, the reasons why dispersion deposited DWCNT films can compete with similar SWCNT films are the longer average tube length of DWCNTs and lesser vulnerability to defects, but they are still evidently behind SWCNT films in short-term quality. Their better stability and lesser vulnerability however give them an important advantage over SWCNTs in developing films that need to last long.

In addition to thicker films Hou et al. produced a DWCNT sample with respective values of 326 Ω/sq 90 % and Izamu et al. [69] also used DWCNTs to fabricate a dispersion-deposited film with values of 320 Ω/sq and 94 %. Comparing these films to pristine SWCNT films of Wang et al., 286 Ω/sq at 92 %, and Reynaud et al., 224 Ω/sq at 90 %, is difficult because a small change in transmittance can make a large difference in the amount of CNT junctions when the films are very thin. These films are still however much better than pristine MWCNT films with about 90 % transmittance which can have sheet resistance of over 500 Ω/sq, which clearly shows that while MWCNTs absorb a lot more per tube than SWCNTs the amount of contact points between the tubes remains the same, so in order to have the same absorbance a MWCNT film has to have much fever tubes and junctions than a SWCNTs film.

3.2.3 Graphene

The different performances of graphene electrodes reported in the literature are shown in figure 10. The large-scale synthesis and transfer process for graphene developed by Bae et al. [43] which was described in the synthesis section also produced the graphene sheets with very high performance of 30 Ω/sq R_s with 90 % transmittance. Without nitric acid doping the sheet resistance was about 40 Ω/sq. This result has however not been reported by any other research group after many years since its publication, so it has remained an anomaly that has been difficult to reproduce. Only very recently another research

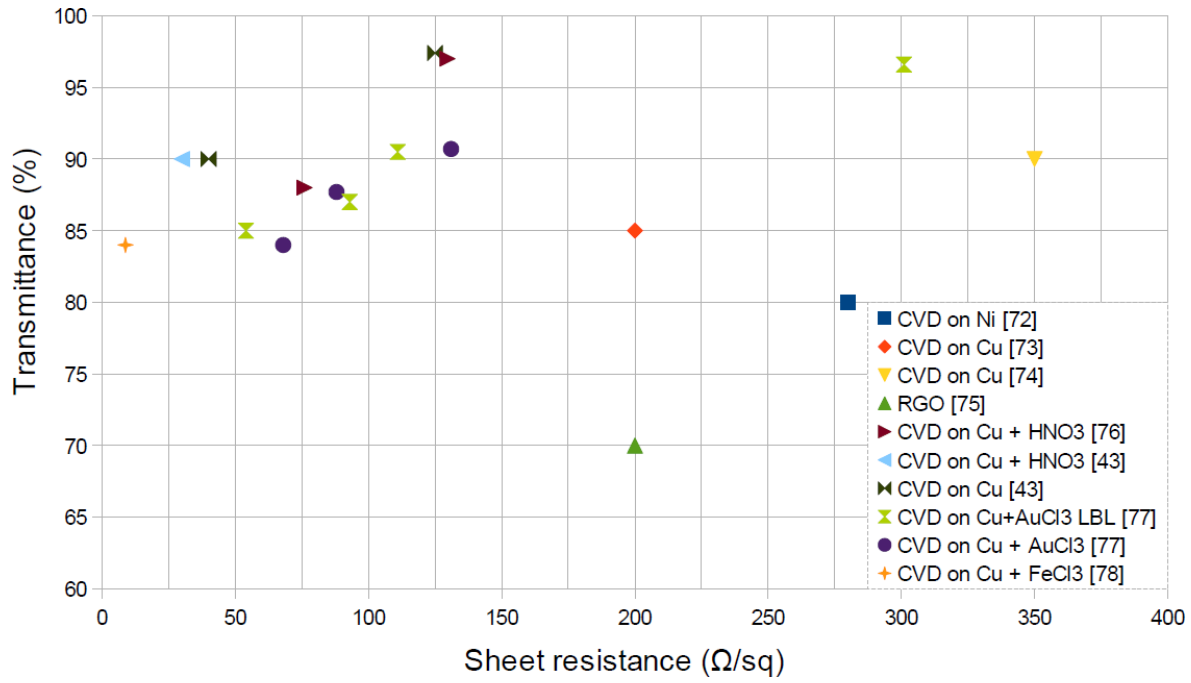

Figure 10: Performances of different transparent graphene electrodes. For CVD grown graphene the growth substrate and possible dopant are mentioned.

group has claimed to have produced graphene electrodes with 20 Ω/sq sheet resistance and 88 % transmittance with HNO_3 doping but this measurement was performed with a non-contact measurement setup while the actual 4-probe measurement gave a sheet resistance value of 76 Ω/sq [76]. This 4-probe value was used in figure 10 but it is still a remarkable improvement compared to common CVD grown graphene electrodes: for instance pristine graphene films have been produced with performance of 350 Ω/sq and 90 % by Li et al. [74], with 200 Ω/sq and 85 % by Cai et al. [73] and with 280 Ω/sq and 80 % by Kim et al. [72]. Doping with $AuCl_3$ has also been successful and produced films with R_s of 88 Ω/sq and 87.7 % T [77].

Graphene electrodes with higher quality have also been achieved but these methods have been very expensive or impractical for large-scale production. These methods include doping each CVD grown layer separately with $AuCl_3$ [77] and graphene electrodes produced with micromechanical cleaving of graphite and $FeCl_3$ doping [78]. The former had performance of 54 Ω/sq with 83.5 % while the latter had record quality of 8.8 Ω/sq with 84 %. $FeCl_3$ doping was carried out in vacuum with a two-zone vapor transport method and showed fairly good stability, but the method overall with micromechanical cleaving and vacuum processes is very difficult to utilize in mass-production.

Reduced graphene oxide films have been less succesful than CVD grown. The best performing RGO film fabricated by Nekahi et al. [75] had sheet resistance of 200 Ω/sq with 70 % transmittance while most RGOs have sheet resistances in range of kiloohms.

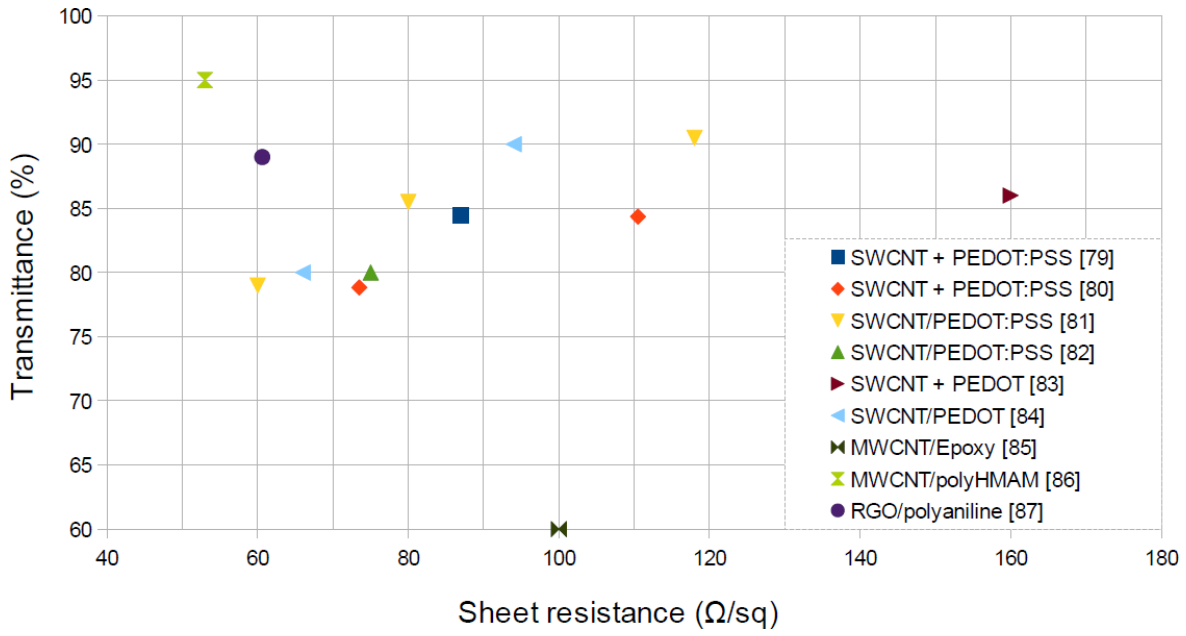

Figure 11: Transmittance as function of sheet resistance for conducting polymer and CNT or graphene hybrid films. The materials are in their order of deposition or denoted with / in case of mixtures.

In comparison to CNT films graphene is in a surprisingly similar state: Reaching over 90 % transparency while having less than 75 Ω/sq R_s is very difficult and even this level requires doping which usually makes the film to become unstable. The difference is that unlike CNTs graphene has actually proved that it can achieve much higher quality but the issue remains how to do it in a chemically stable and economically viable way.

3.2.4 Conducting polymers and CNT or graphene hybrid films

In principle the conductivity of polymers is based on the same delocalization of electrons in conjugated sp^2 carbon bonds as in CNTs and graphene. Poly-(3,4-ethylenedioxythiophene) (PEDOT) is the most common conducting polymer and it is usually doped with poly(styrenesulfonic acid) (PEDOT:PSS). PEDOT:PSS films have achieved higher quality than CNT films, for example 25 Ω/sq with 85 % transmittance [88]. However, just like CNTs, PEDOT:PSS requires additional doping and has problems with stability [89]. Hybrid films of CNT materials and PEDOT:PSS have not reached the quality of the best PEDOT:PSS films but they could possess higher stability instead if they do not require additional doping: CNT and PEDOT hybrid films have been able to achieve performance of 66 Ω/sq R_s with 80 % [84] T.

The performance of these kind of films is illustrated in figure 11 and it shows that films prepared of mixtures of PEDOT or PEDOT:PSS and SWCNTs are generally better than films that have them added as separate layers. In mixtures PEDOT can coat the

CNTs from all sides in such a way that it improves the contacts of CNTs while in separate layer deposition PEDOT may not have access to the tube junctions, which restrains its ability to act as an intermediate.

Regarding other conductive polymers, Nayak et al. [86] produced highly transparent MWCNT N-hydroxymethyl acrylamide (polyHMAM) composite films with 53 Ω/sq R_s and 95 % transmittance. Reduced graphene oxide and polyaniline hybrid by Domingues et al. [87] achieved 60.6 Ω/sq R_s with 89 % T. Although the initial results are promising, the long-term stability of these films was not reported. Generally PEDOT:PSS is considered the best conductive polymer due to its properties that outclass other conducting polymers, such as better stability than the others have. Since even PEDOT:PSS has problems with stability, the stability of the films based on other polymers is even more questionable.

Graphene oxide, without reduction, has been successfully used with PEDOT:PSS for improving OLEDs but since GO is insulating it increased sheet resistance of PEDOT:PSS, making the films less optimal for other purposes [90]. GO and RGO in general have met much more success and use in hybrid materials than on their own as the presence of other conductive material improves contacts between graphene flakes, radically improving the film conductivity. Nonetheless in case of TCFs graphene and conducting polymer hybrids have been rare compared to CNT and polymer hybrids. Graphene based hybrid TCF research has been more focused on graphene and metal nanowire hybrids described in the next section.

3.2.5 Carbon and metal hybrid films

Metal nanowires

Silver nanowires (AgNWs) have very high potential to replace ITO as the main transparent conductive material: AgNWs have already reached quality of less than 10 Ω/sq sheet resistance with over 80 % transmittance which is comparable to ITO [107]. The downside was that the films are easily oxidized and especially unstable when subjected to electric current. Copper nanowires (CuNWs) have also been investigated but they were very prone to oxidation and so even less stable than (AgNWs). The degradation of of these films is caused by the different behavior of nanoscale materials and macroscale materials: for instance metal nanowires have much lower melting points than their macroscopic versions, so when an electric current heats the wires they can undergo structural changes even in relatively low temperatures and their chemical reactivity can be very high. Pristine AgNWs films also suffer from hollow spaces between the nanowires which can be detrimental in many applications. Another issue of these films is high optical haze, in other words they scatter a large portion of incoming light [108, 109] making them not an ideal electrode for displays.

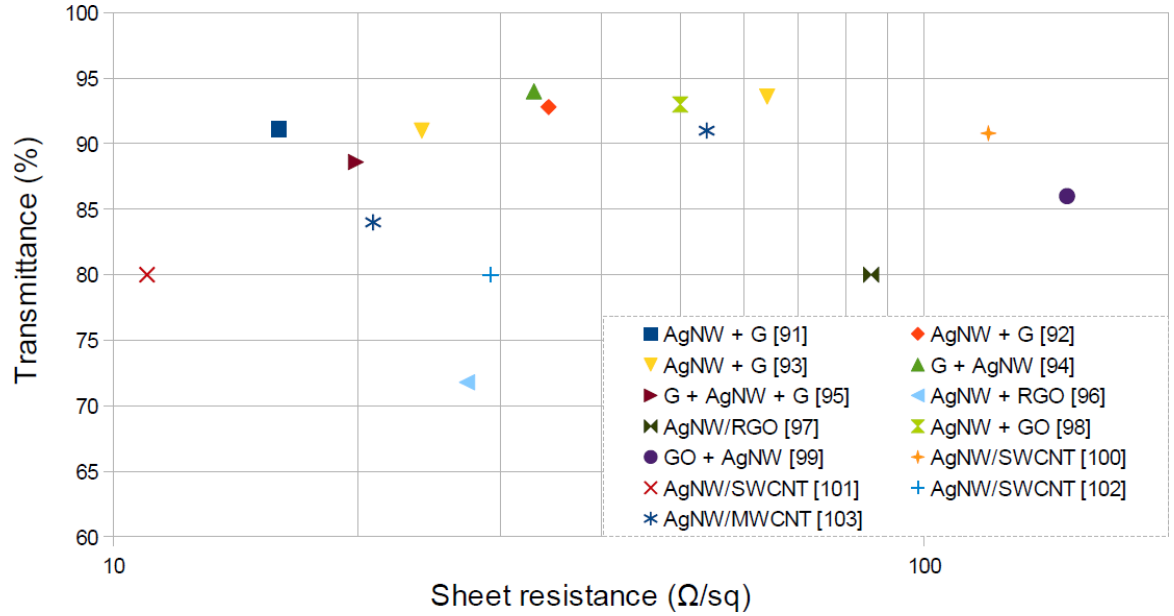

Figure 12: Transmittances and sheet resistances of silver nanowire and carbon hybrid films with the different layers given in their order of deposition starting from bottom or with / in case of mixtures. G refers to CVD grown and directly transferred graphene.

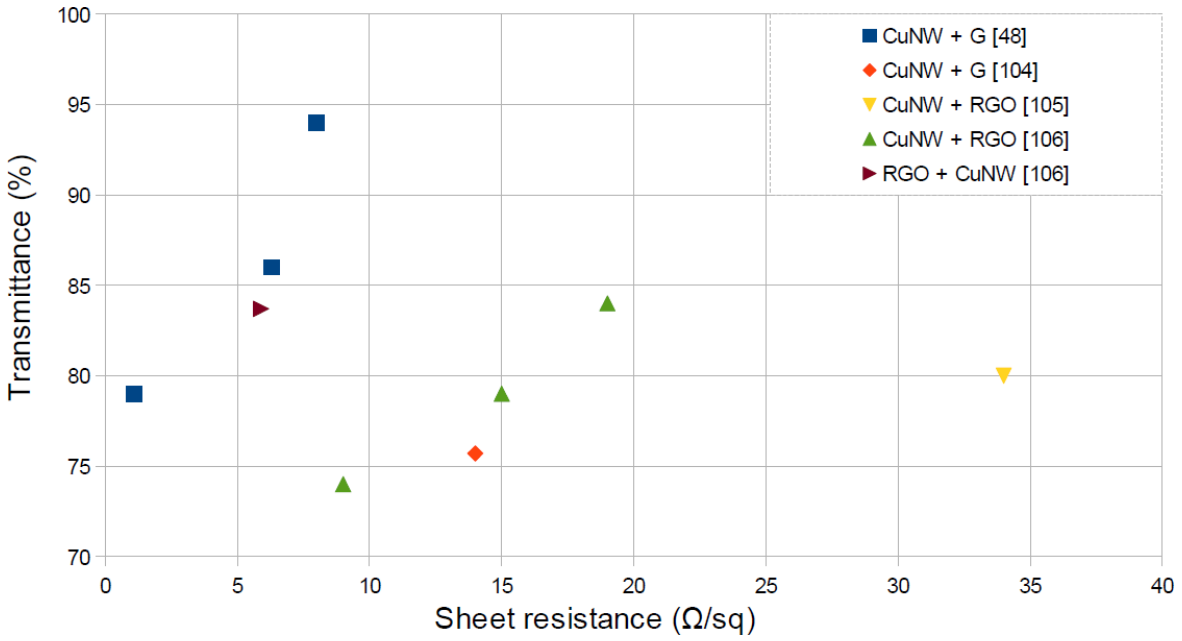

Figure 13: Performances of copper nanowire and graphene hybrid films with the different layers given in their order of deposition starting from bottom.

Oxidation of these films in ambient conditions can be reduced with coatings, for which graphene has been utilized in numerous cases displayed in figure 12 for AgNWs and 13 for CuNWs. Since the nanowires are vulnerable to Joule heating graphene is also required to act as heat conductor to keep the wires from melting and reorganizing into some less conductive form but this aspect of improved stability still remains to be seen. In other words the purpose of graphene coating on metal nanowires is not to improve their conductivity but to help them maintain it.

The most successful AgNW and graphene hybrid film has R_s of 16 Ω/sq with 91.1 % T [91], which was prepared by adding an extra layer of PMMA on the PMMA layer used for transferring the graphene. The re-coating with PMMA relaxed the underlying graphene and improved its contact to AgNWs. Among the best of these films are also those by Lee et al. [95] with 19.9 Ω/sq R_s and 88.6 % T which were produced by placing AgNWs between two layers of CVD grown graphene which were transferred directly from growth substrate without dispersing them in solvent. This sandwich-structure also protected AgNWs and increased their stability. CuNW and CVD grown graphene hybrid films with 8 Ω/sq R_s and 94 % T also showed improved corrosion resistance [48]; CuNW based films have in general shown on one hand higher short-term quality and on the other lower stability than AgNWs. CNTs have also been used with AgNWs [102, 103] but the stability of those films is questionable whether they have improved stability or not in comparison to pristine AgNWs.

AgNW and RGO hybrid films have been less successful with performances such as 86 Ω/sq R_s with 80 % T [97]. Similar CuNW and RGO hybrids have however achieved performance of 5.9 Ω/sq R_s with 83.7 % T [106]. Interestingly AgNW and GO hybrid films have been of higher quality of 50 Ω/sq R_s with 93 % T [98] than AgNW and RGO hybrids and despite GO being an insulator and RGO a conductor, which was attributed to a change in AgNW energy states due to presence of GO. However, having an insulating layer on the conductor severely limits the applications. Similarly Cytop and PMMA polymers can be used for flattening and improving the film quality [110] but they are insulators between the conducting film and application. The films using them are listed in figure 16 along with other less common hybrids.

Metal nanoparticles

Unlike metal nanowires which have excellent conductivity on their own but require protective and stabilizing layers, smaller metal nanoparticles (MNPs) are used for similar purposes as doping: for improving conductivity in CNT junctions or between graphene sheets. This way of doping with nanoparticles has good chances to prove to be more stable than HNO_3 and other chemical doping as nanoparticles are less likely to sublime

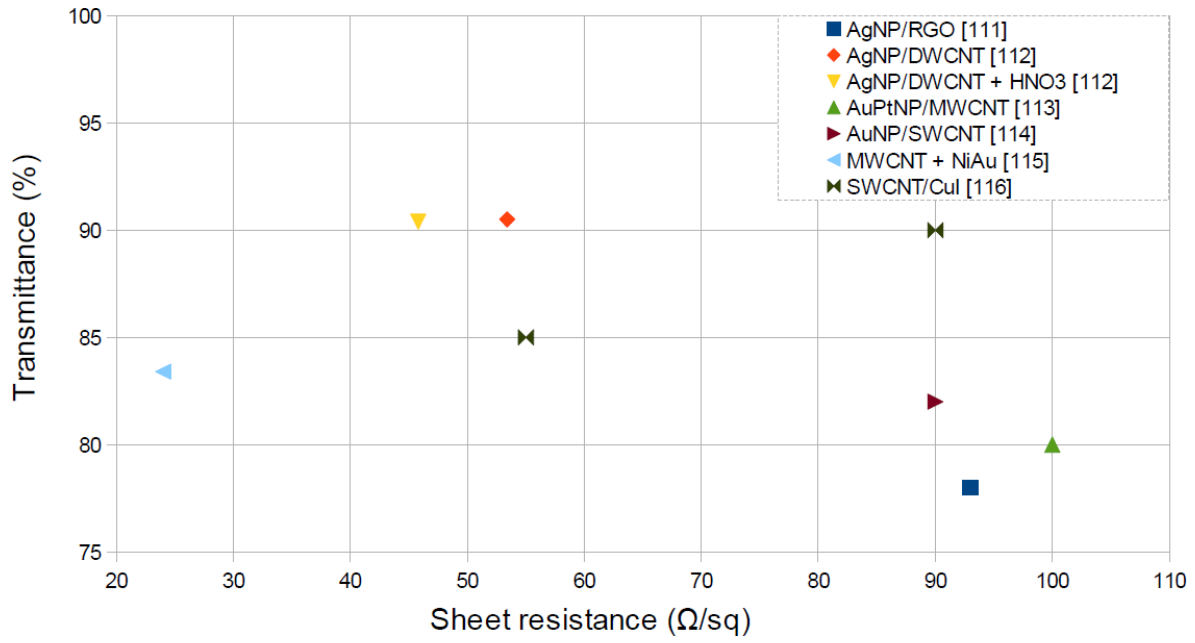

Figure 14: Performances of metal nanoparticles and CNT or graphene hybrid films.

or otherwise detach from the film. Some of the MNPs such as gold nanoparticles (AuNPs) are also chemically fairly inert.

The performance of nanoparticle films can be seen in figure 14. DWCNT and silver nanoparticles (AgNPs) hybrid film has achieved 53.4 Ω/sq R_s with 90.5 % T and after nitric acid doping and annealing the sheet resistance decreased further to 45.8 Ω/sq [112]. Annealing contributed to melting and rearrangement of the silver nanoparticles, which improved the tube junction contacts. These result outclassed the plain SWCNT and DWCNT films. SWCNT gold nanoparticle hybrid films [114] and graphene AgNP hybrids [111] have been less successful.

Recently copper halide nanoparticles have also been utilized for connecting SWCNTs, which resulted in about 55 Ω/sq sheet resistance with 85 % transmittance [116]. Despite the films having good stability the fabrication method in the study was troublesome for industrial use: copper halide layer was deposited on the SWCNT film with vacuum evaporation which is an expensive method. Feng et al. [115] also used vacuum evaporation and magnetron sputtering for depositing nickel and gold on aligned MWCNTs and achieved TCFs with R_s of 24 Ω/sq and 83.4 % T.

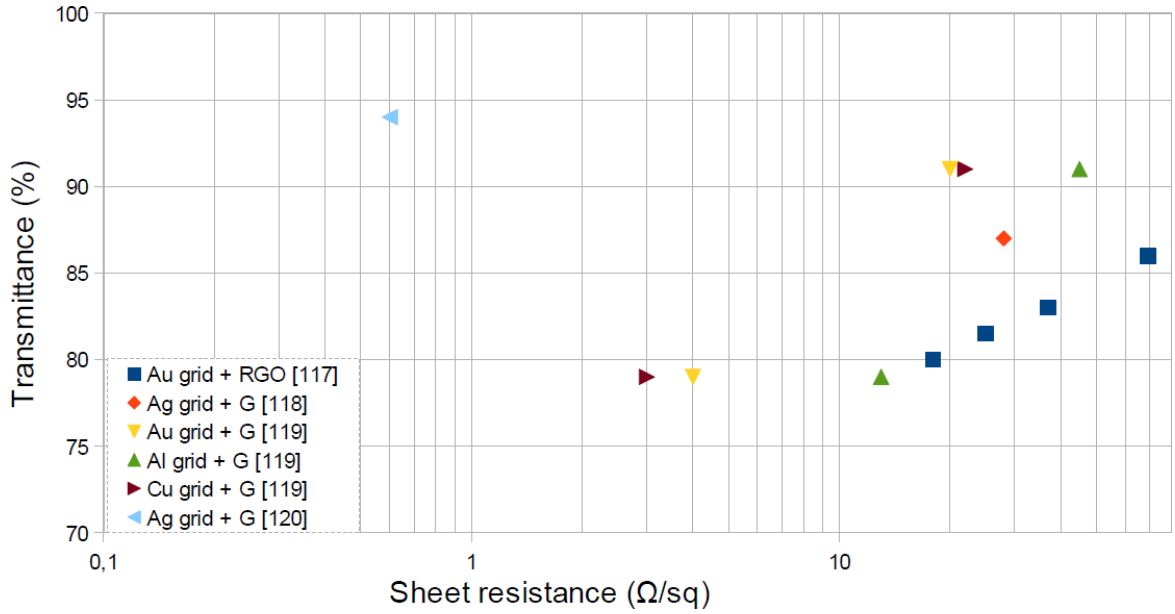

Figure 15: Performances of metal grid and graphene hybrid films.

Metal grids

Patterned metal grids or meshes with nanometer-scale metal wires commonly have quite good conductivity and transparency that rivals ITO, and in a sense metal nanowires are also a metal mesh so the properties and possible problems of the two are very similar; metal grids especially require graphene to fill the large portion of empty space which has practically no contact with the metal electrodes. Their main difference is in their production method: whereas nanowires are synthesized and deposited from dispersion, patterned grids are produced for example by creating a pattern with photolithography and filling it with evaporated metal. Hence the distances between patterned electrodes are in micrometer scale while in case of deposited nanowires they are in nanometers. Combinations with graphene have created films with sheet resistance as low as 0.6 Ω/sq with 94 % [120] in case of CVD grown graphene and 18 Ω/sq [117] R_s with 80 % T in case of RGO as seen in figure 15. However, it is questionable whether sheet resistance and transmittance alone are enough for describing these films: since the sheet resistance of unmodified graphene, especially only a single layer, is commonly very high it might not have good enough conductivity to actually cover and conduct electricity over the large holes in metal grids although the grid itself in macroscopic scale has very good conductivity. Most of the surface area only has contact with the graphene and it has to have good enough conductivity to transport the charge carriers to the nearest metal wire without major losses, and this can be especially important in solar cells and other applications where the conductivity and contact to the electrode has to be good in every part of the film.

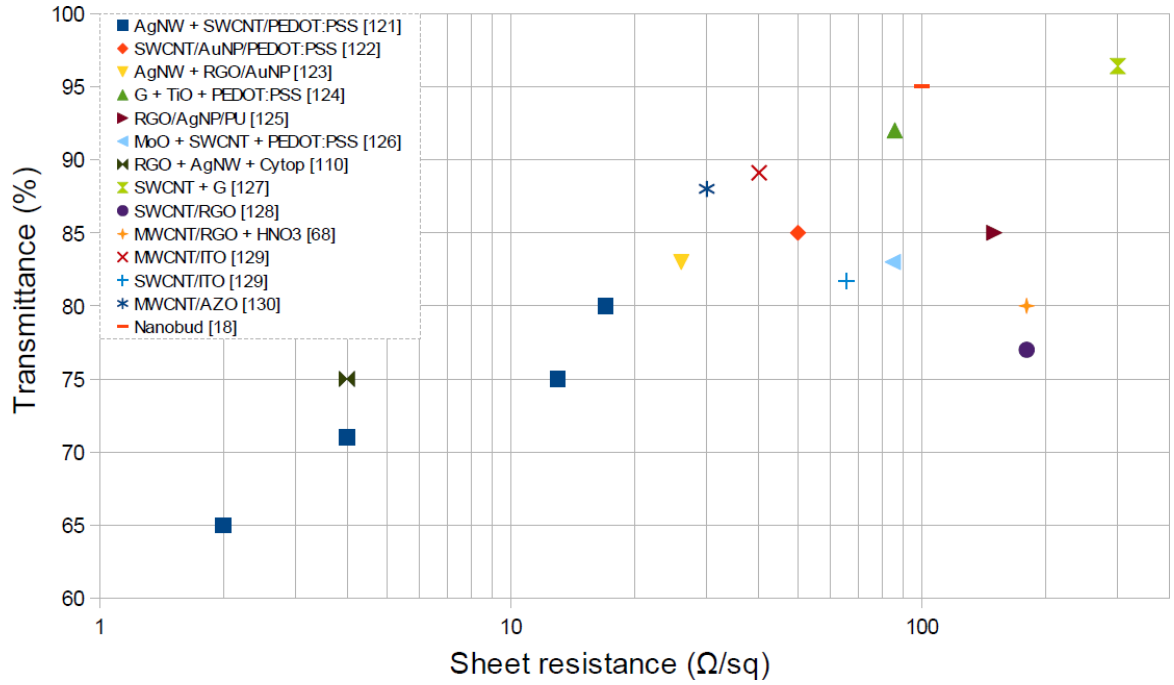

Figure 16: Performances of other notable carbon-based TCFs. PU refers to polyurethane [125].

3.2.6 Other carbon-based materials and hybrids

This section includes all kinds of other carbon-based conducting films and hybrids that are unique or rarely studied. Their performances are illustrated in figure 16.

Combinations of three different conductive materials

Combinations of all three major candidates for next-generation transparent conductive films have also been prepared. Hwang et al. [121] used AgNWs coated with a thin layer of SWCNT/PEDOT:PSS and the resulting film had sheet resistance of 17 Ω/sq and transmittance of 80 % without additional doping. However, the films were not stable and the resistance kept increasing over several months. A transparent film of SWCNTs, gold nanoparticles and PEDOT:PSS was fabricated by Shin et al. [122] and had respective values of 50 Ω/sq and 85 %. The hybrid version had better quality than pristine CNT and PEDOT:PSS films, and adding AuNPs increased the quality even further. Another group that used AuNPs with RGO and AgNWs achieved 26 Ω/sq R_s with 83 % T [123]. Zhu et al. [124] on the other hand used CVD grown graphene, titanium suboxide TiO_x and PEDOT:PSS in a tri-layer film which had performance of 86 Ω/sq R_s with 92 % T.

Combinations of CNTs and graphene

Combining CNTs and graphene is fairly rare because their combination alone does not solve their most basic issue: bad connections between individual CNTs and graphene sheets. Hence these materials are more used in other applications than transparent films [131–133]. Nonetheless transparent CNT and graphene hybrid films with 96.4 % transmittance have shown sheet resistance of 300 Ω/sq [127] and SWCNT/RGO have had 77 % and 180 Ω/sq respectively [128], which are relatively good results for non-doped carbon films.

Transparent conductive oxides with CNTs

The purpose of incorporating CNTs into TCOs is to open new cheaper production methods instead of the current expensive deposition method used by industries: the cheaper methods cause microscopic cracks in pure TCO films, which greatly weaken their performance. By mixing CNTs into the TCO film during sol-gel deposition the CNTs act as conducting bridges across the cracks [129]. MWCNT doped ITO films fabricated by Golobostanfard et al. with inexpensive sol-gel method had performance of 40.2 Ω/sq R_s with 89.1 % T. Another example is aluminum-doped zinc oxide and MWCNT hybrid by Ian Y.Y. Bu and Matthew T. Cole [130] also produced with sol-gel method and with respective values of 30 Ω/sq and 88 %.

Carbon nanobuds

Carbon nanobuds are in principle not hybrid films but another form of carbon allotropes, fullerene functionalized SWNTs, discovered by Nasibulin et al in 2006. [16]. They posses properties from both materials, such as reactivity of fullerenes and electrical and mechanical properties of CNTs. Commercial transparent films made of nanobuds have sheet resistance of 100 Ω/sq with very high transmittance of 95 % [18].

While nanobud films are of quite good quality, their synthesis and many applications have been patented by a Finnish company and the material itself is very new. Hence the amount of scientific publications relating to this new material is still scarce compared to CNTs and graphene.

4 HC-DWCNT sample fabrication

This section describes the methods used in this study for producing HC-DWCNT thin films and samples.

4.1 Substrate preparation

Most of the samples were prepared on Thermo Scientific Menzel-Gläser microscope slides. Each slide was cut in half so that the dimensions of the substrates were about 3.6x2.5 cm^2. Then the slide was cleaned with ethanol before evaporation of the electrodes with BAL-TEC BAE 250 Coating System. The thin film is produced by heating a piece of metal in a crucible so that the evaporated metal atoms and particles are ejected to the substrate. Vacuum is required because otherwise the metal to be evaporated might be oxidized instead and air can block the route of the evaporated particles.

For the evaporation the glass was covered with aluminum foil which acted as a mask, the foil had been cut to reveal the desired electrode pattern shown in figure 17. Only the revealed parts of the substrate will be covered with metal. Vaporization chamber was pumped until pressure inside the chamber was about $2 \cdot 10^{-5}$ mbar. The evaporated titanium and gold films were 5 nm and 120 nm thick, respectively. Titanium film was required to act as an adhesive between the gold electrode and glass surface. The electrodes had to be as thin as possible because they were to be covered with nanotube films that are only few dozen nanometers thick.

Samples used for IR absorbance measurements were prepared on CaF_2 windows but did not have metal electrodes evaporated on them. CaF_2 windows were cleaned with acetone and isopropanol before sample deposition.

4.2 Thin film deposition

4.2.1 Spray-coating

Spray-coating with an airbrush is a common method for depositing CNTs as it is an easy and cheap method for producing large-scale films with controlled film thickness. Because HC-DWCNT is easily dispersed in water there is no need for any other surfactants that are usually required for dispersing CNTs in solutions nor there is any required chemical post-processing for removing them. The solution was only mildly shaken in order to disperse any minor aggregates: sonication was not used as it had no positive effect on the film quality.

The substrate has to be heated in order to quickly vaporize the solvent once it hits the substrate surface. In this work the substrate was placed in a 500 ml beaker which

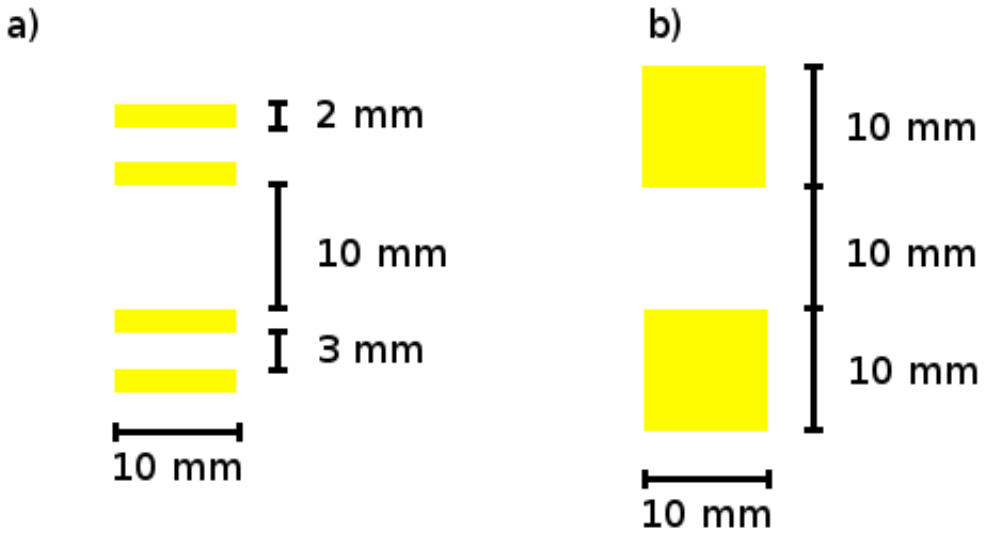

Figure 17: Electrode schematics. Schematics a) was used for most samples while b) was used for some of the vacuum-filtered samples. Some of the microscope slides had two series of a) type electrodes side by side so that two samples could be prepared simultaneously.

was heated with a heat plate set to 200 $°C$. The beaker was used to prevent HC-DWCNT spray from contaminating the surroundings. Excess HC-DWCNT was cleaned with wet cotton stick to make the film width match the width of the electrodes of 1 cm.

4.2.2 Droplet casting

Droplet casting simply means placing a droplet of the HC-DWCNT solution on the substrate and letting the solvent evaporate. While the method is simple and cheap it is in fact a very complex process and acquiring uniform large-scale films is very difficult. For example a drying droplet of a CNT solution typically forms a concentrated ring of CNTs along the edge of the droplet because the rate of evaporation is much higher there and there is a constant flow of solution from the middle of the droplet to its edge. Hence the middle of the resulting film is different from its edge, and if the droplet is large the uniformity of the film can be very random. Excess film on the edges was removed in a similar way as for spray-coated films.

Spin-coating is also a very common method for producing thin films, and it is done by placing a droplet of the CNT dispersion on the substrate and then spinning it so that the solution spreads uniformly on the substrate. This method was also attempted in this work but it wasted way too much HC-DWCNT solution and it did not produce any successful samples because spinning always hurled most the solution off the substrate because the HC-DWCNT dispersion was not viscous enough.

4.2.3 Vacuum filtration with dissolution of the filter membrane

The vacuum filtration setup in this work is shown in figures 18 and 19. Diluted HC-DWCNT solution is first placed in the funnel: the filter membrane is too thick for water to pass through without external force. The filters used in this work were 25 mm mixed cellulose ester (MCE) filters with pore size of 25 nm by Merck Millipore. Then a water aspirator is used for producing vacuum inside the Büchner flask, creating pressure difference that pushes water through the filter. A more sturdy filter is also required for upholding the actual filter membrane. As the solution is pushed through the filter HC-DWCNT sticks to its surface because the pore size of the filter membrane is too small for the HC-DWCNT to pass through. As HC-DWCNT accumulates on the surface of the filter it slows down water flow speed, making it more likely for the next HC-DWCNT particle to land in a spot that has low amount of HC-DWCNT. Hence the procedure is self-regulating and automatically creates homogeneous films, especially when the HC-DWCNT solution is also originally homogeneous. Figure 20 shows that there are two white spots on the filter that have no HC-DWCNT, which means that water did not flow through those spots. In order to produce quality thin films with vacuum filtration the filter must be very uniform, but it also means that the filtration technique can be used for patterning. Rinsing is often used for removing the surfactants and impurities but in this work it was not deemed necessary because there was no great enough need for removing the hemicellulose and risk causing defects to DWCNTs.

The filtration and formation of the thin film itself is quite simple and it is easy to control the thickness of the film by the concentration and volume of HC-DWCNT solution. What makes vacuum filtration complicated is transfer of the film off the MCE filter membrane to the desired substrate. If the film is very thick and strong, such as buckypaper that is a non-transparent macroscopic layer of CNTs, then it can be simply peeled off the filter but transparent CNT films are too thin to withstand such procedure. Hence more complicated methods are required, the most common of them being dissolution of the filter in an organic solvent, usually acetone. In the dissolution method the filter is pressed against the substrate so that the CNT film is between the filter and the substrate and then dipped in acetone to dissolve the filter membrane so that the film gets attached to the substrate instead. Alternatively the filter can be first dissolved in acetone, leaving the CNT film to float on the liquid surface from where it can be collected to the substrate.

In this work both of these methods were attempted but only the pressing produced intact HC-DWCNT films and only with equipment shown in figures 21 and 22. Dissolution of the MCE filter without press caused too many wrinkles and bubbles which resulted in major defects in the HC-DWCNT film. Pressing the filter with a metal weight that was

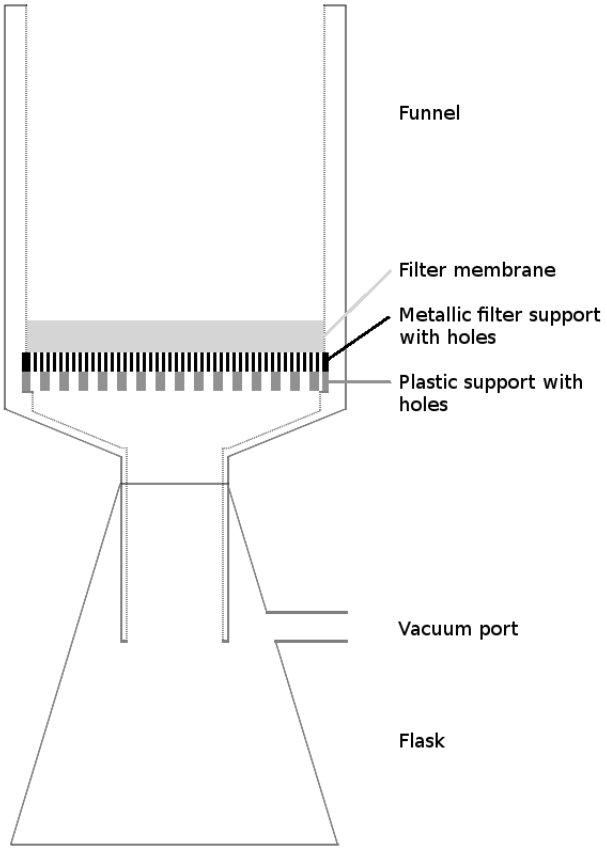

Figure 18: Schematics for vacuum filtration setup.

Figure 19: Photograph of the actual vacuum filtration setup.

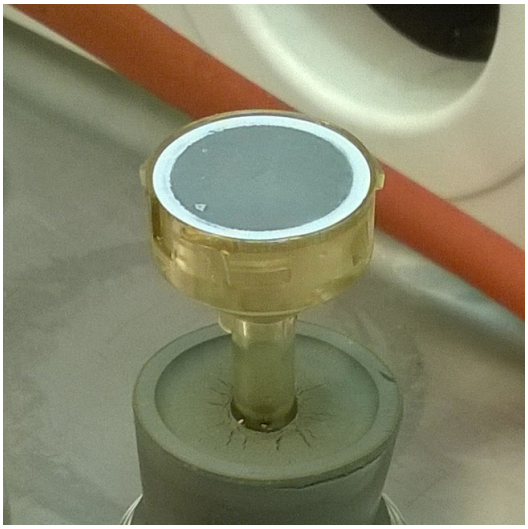

Figure 20: Photograph of the HC-DWCNT film after filtration. The HC-DWCNT film is the circular gray area on the filter membrane.

kept in place with a controllable xyz-stage was required to keep the MCE filter in place but the problem was that the filter attached to the metal while dissolving, which also caused bubbling and tearing of the film once the weight was lifted. Another problem was that because the metal weight covered the filter it could only dissolve from the small gap in the side, which slowed down the dissolution process to last for several days so dissolving the filter entirely to prevent attachment to the metal was not a practical option nor possibly possible because the MCE filter always left some impurities on the substrate and HC-DWCNT film that could not be removed. Heating of the solvent hastened the dissolution but also caused bubbling and defects to the film. Hence a cover paper was placed in between the weight and the filter. The paper had originally been a cover for the filter in the package but it turned out that the filter did not attach strongly to the paper even once it had been partially dissolved.

After some of the filter membrane had dissolved, the metal weight could be lifted and the paper peeled off without damaging the HC-DWCNT film. Figure 23 shows how there is still a major amount of MCE on the substrate but the amount was low enough to be dissolved without wrinkling or bubbling of the film as shown in figure 24. Not all of the filter could be removed so it always left behind some impurities on the substrate and the HC-DWCNT film.

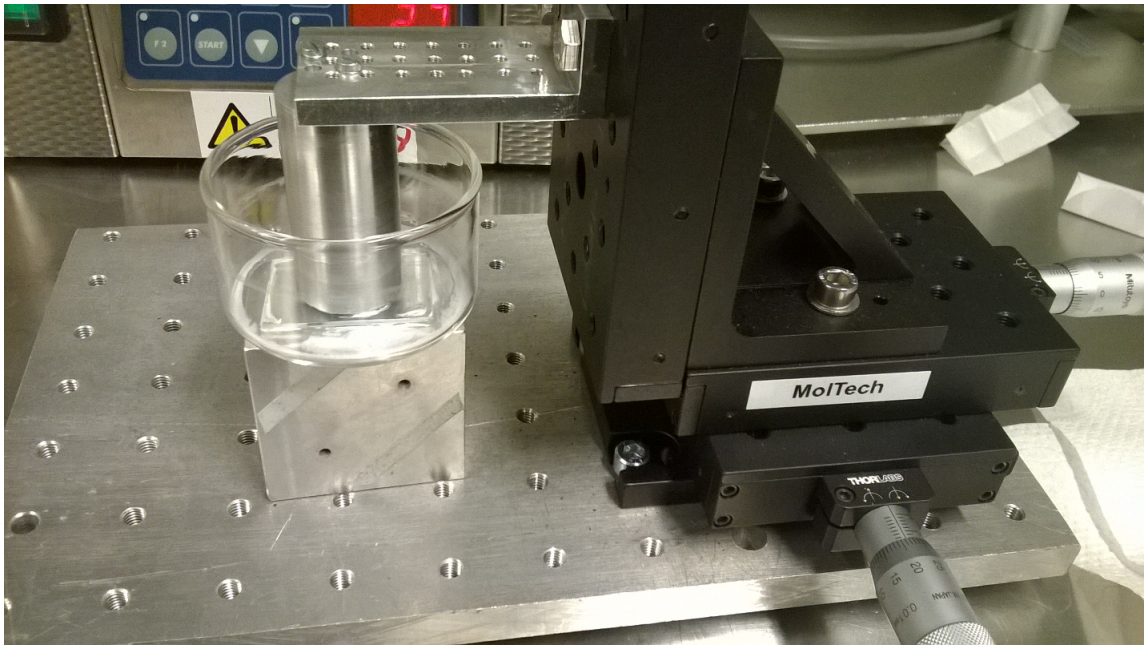

Figure 21: Photograph of the setup for initial dissolution of the filter. Acetone used for dissolution has already evaporated leaving behind a white layer of MCE that had dissolved off the filter.

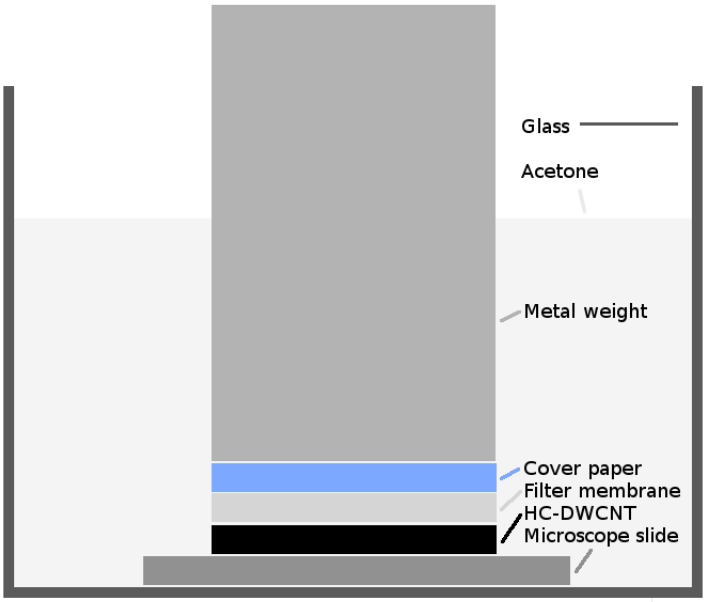

Figure 22: Schematics of the initial dissolution setup shown in figure 9. The space between the metal weight and the microscope slide is smaller in reality than in the image as can be seen in figure 9.

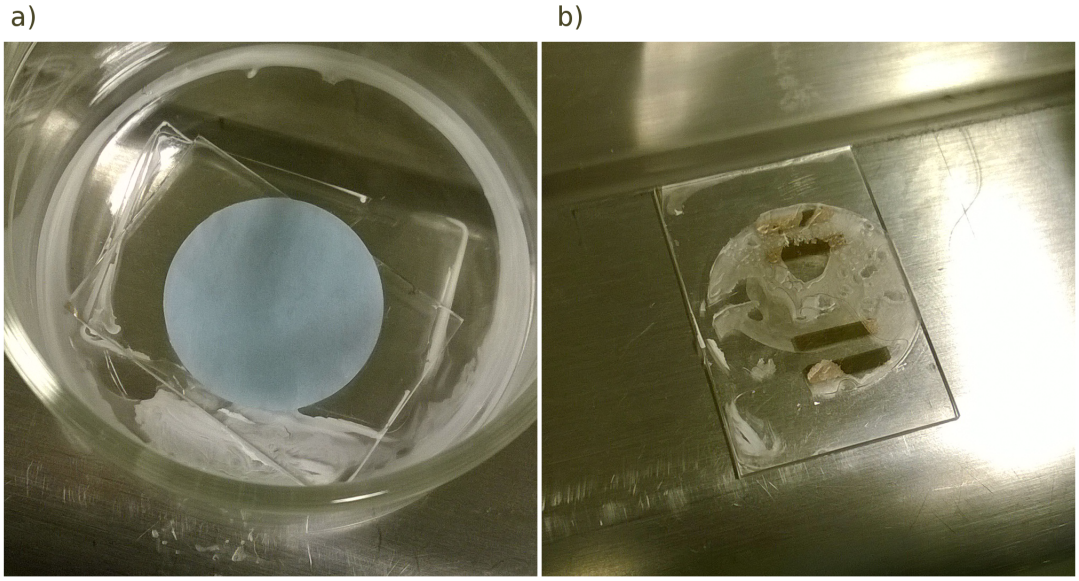

Figure 23: a) Sample after initial dissolution with the blue cover paper on the HC-DWCNT film. The white substance in the beaker is re-deposited MCE that had been dissolved by acetone. b) Sample after initial dissolution without cover. Some of the remaining MCE had turned transparent and it covers the electrodes even though they look exposed.

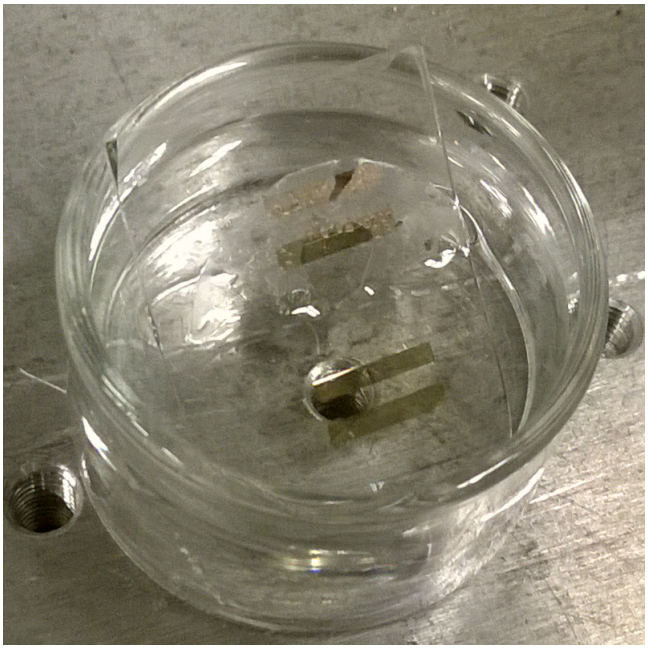

Figure 24: Removal of the rest of the filter by dissolving it in acetone.

Step-by-step procedure for sample preparation with the vacuum filtering and dissolution method:

1) Dilute HC-DWCNT solution and shake mildly to disperse the HC-DWCNT evenly.

2) Filter the HC-DWCNT solution with vacuum suction.

3) Let the filter and HC-DWCNT film on it dry in room conditions.

4) Place the substrate in glass container and put filter upside-down on the substrate so that HC-DWCNT film is in contact with the substrate. Place cover paper on the filter.

5) Lower the metal weight on the cover paper and filter with the xyz-stage and tighten until the paper and filter are firmly in place.

6) Pour about 40 ml acetone to the container and let it evaporate.

7) Clean the re-deposited MCE off the container with a cotton stick or paper dipped in acetone.

8) Repeat points 6 and 7.

9) Lift the metal weight and carefully peel off the cover paper.

10) Place the substrate at an angle in acetone. If not all of the MCE dissolved, replace the acetone and repeat until MCE no longer dissolves.

11) Dip the sample in isopropanol to clean the remains of acetone.

4.2.4 Peeling the HC-DWCNT film with water interface after filtration

Because the dissolution method was very time-consuming and left the sample with impurities only few samples were prepared with it. Most of the vacuum-filtered samples were instead produced with a method that uses water surface for peeling the HC-DWCNT film off the filter [134]. Instead of letting the filter completely dry after filtration, air was drawn through the film for 3 minutes and then it was let to dry for about 10 minutes in room air and temperature. This way the film is only partially dry and can be detached from the filter by immersing it into water as shown in figure 25. HC-DWCNT film will float on the water surface. The same metal support used in filtration was also used for keeping the filter from bending during the immersing. Once the HC-DWCNT film floats on the water surface it can be collected to the substrate by lifting the substrate from beneath.

With this technique it is important to control how dry the film and filter are: if they are too dry then the film sticks too strongly to the filter and cannot be peeled off, if they are too wet then the film agglomerates. In figure 25 the defects in the film are most likely caused by letting the film dry for too long causing some parts of to attach more strongly to the filter. Especially the edge of the film has to be wet enough because if the edge does not peel off then the rest of the film will not be peeled off either. It will take a lot

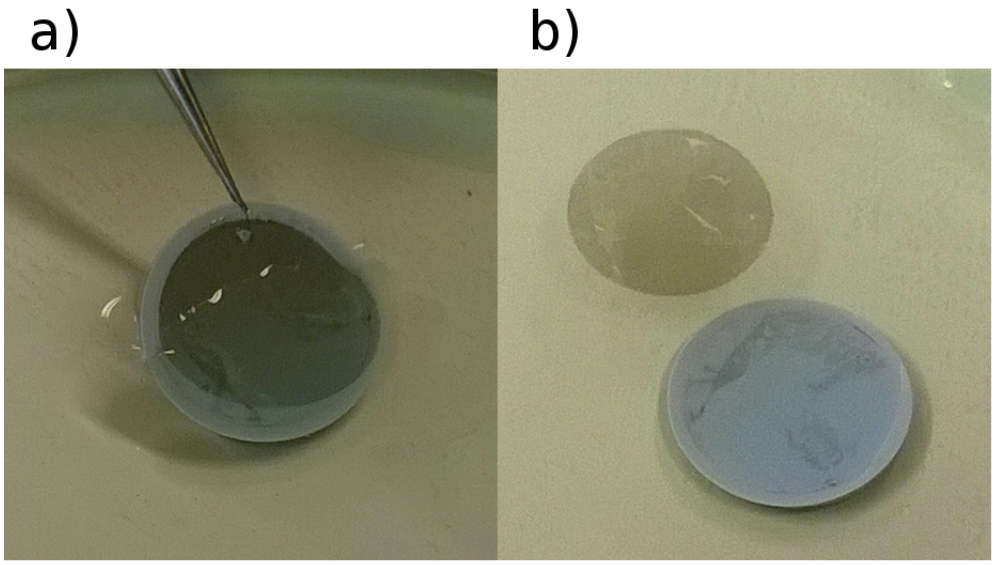

Figure 25: a) Removal of the HC-DWCNT film off the filter membrane with water. b) HC-DWCNT film is floating on the water surface. In this particular case not all of the HC-DWCNT was detached of the filter.

of time for HC-DWCNT to re-dissolve, if it re-dissolves at all, so there is no particular hurry in transferring the film to the substrate.

4.2.5 Method comparison

Figure 26 shows that vacuum filtration and spray-coating produce homogenous and uniform films with controllable thickness while droplet casting is very unreliable: where the agglomerates of HC-DWCNT happened to land on the substrate was uncontrollable, resulting in varying film thickness. The advantage of spray-coating and droplet casting is that they can cover a large area while vacuum filtration sample size is limited. Vacuum filtration is also not perfectly reliable because peeling could cause defects such as in figure 25 and dissolution could also go wrong if the remains of the filter were attached too strongly to the cover paper and teared the film when it was removed.

Resource-wise a problem with spray-coating was that it wasted a lot of HC-DWCNT solution because a large portion of the sprayed solution ended up elsewhere than on the substrate. A similar issue was with droplet casting as there was an agglomerate of HC-DWCNT around the edge of the substrate where it was of no use but it still wasted less HC-DWCNT than spray-coating. Vacuum filtration did not waste HC-DWCNT almost at all, only peeling with water surface caused a minor loss of material. Of the two film transfer techniques peeling with water interface is much more efficient, both time and

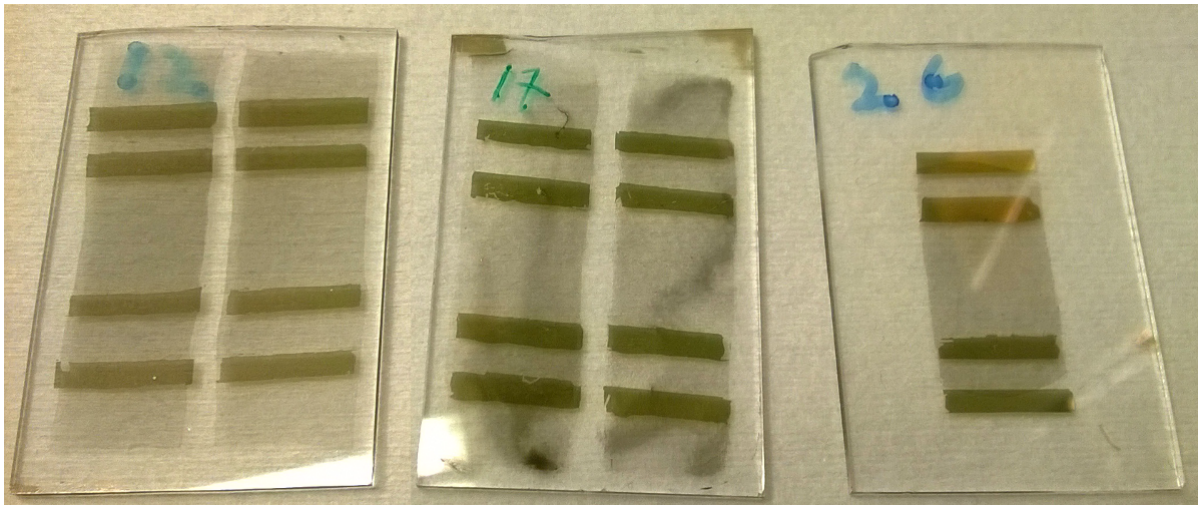

Figure 26: Photograph of three samples prepared with different methods: spray-coated sample is on the left, droplet-dried is in the middle and vacuum filtered sample (film transferred from water surface) is on the right.

cost-wise, than dissolution of the filter because with the peeling method the filter could be reused and it does not require use of additional chemicals. With peeling method possible defects in the film can be detected while it floats on the water surface before attaching it to the substrate so the damaged HC-DWCNT film can be easily re-dispersed and reused if necessary. With dissolution method if something goes wrong the substrate will most likely be already contaminated by MCE and neither the filter nor HC-DWCNT can be recycled. Time-wise vacuum filtration with peeling method proved to be also the fastest method as it could produce a sample in less than 30 minutes.

5 Resistance and transmittance measurements and effects of post-treatments

5.1 Sheet resistance measurements

The middle area between the electrodes in the figure 17 is 1 cm x 1 cm so the sheet resistance R_s of the HC-DWCNT film can be measured by measuring the voltage difference V between the electrodes and the current I through the film. From Ohm's law

$$R_s = \frac{V}{I}. \tag{1}$$

Some of the square resistance measurements were quickly done with Finest 203 multimeter which had indium contacts for connecting it to the gold electrodes on the samples. The resistance of the gold electrodes and indium contacts themselves was 1 Ω which was negligible in comparison to the resistance of the samples.

More accurate measurements were done with 4-probe station (Janis Research Company, model: ccr10-2cx-2tx-2mw67) for which the schematics are presented in figure 27. The current was measured as voltage after amplification with a current to voltage amplifier (Stanford Research Systems, model: SR570). The current source was Keithley 6221 AC and DC current source. The current through the sample was 10 μA and the current to voltage amplification a_I was 1 V for 10 μA for earlier measurements and 1 V for 100 μA for the rest. The amplification a_V of voltage difference V across sample was 100 and the amplifier used was Stanford Research Systems model SR560. The measurement program measured the voltages several times each second so the given values are averages of those measurement points. The background voltage V_{bg} and current amplified to voltage $V_{I(bg)}$ without any current through the sample was also measured for each sample and it was taken into account by subtracting it off the measured value. Hence the formula for calculating the square resistance is

$$R_s = \frac{(V - V_{bg})/a_V}{(V_I - V_{I(bg)})/a_I}. \tag{2}$$

For example for sample 5 A the current measured as voltage was 1001.36 mV with amplification of 1 V for 10 μA and the voltage drop was 518.25 mV, with the respective background values being -92.00 mV and -31.39 mV, then the sheet resistance would be

$$R_s = \frac{(518.25\ mV - [-31.39\ mV])/100}{(1001.36\ mV - [-92.00\ mV])(\frac{V}{10\mu A})^{-1}},$$

$$R_s \approx 502.7\ \Omega/sq,$$

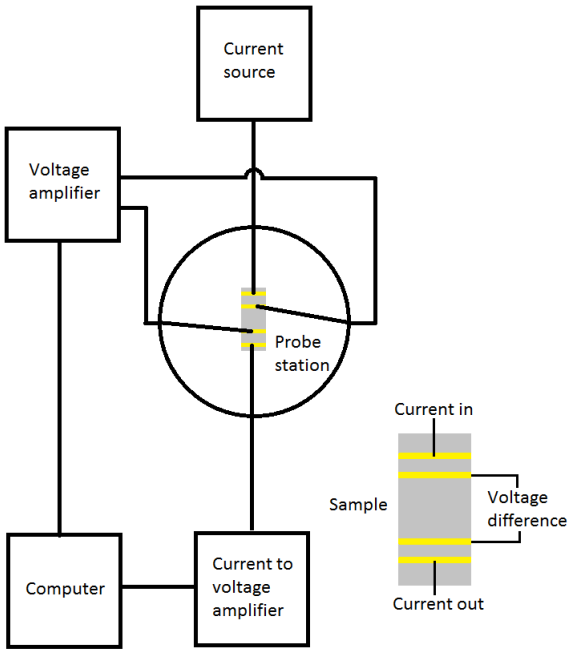

Figure 27: Schematics for 4-probe measurements

5.1.1 Sheet resistance measurement errors

Sheet resistance error was calculated with the equation

$$\delta R_s = \sqrt{\sum_i \left(\frac{\partial R_s}{\partial x_i}\delta x_i\right)^2} \tag{3}$$

in which x_i is one source of error. Since the error sources are the film width (0.5 mm or 5 % of total length), length (0.5 mm or 5 % of total width) and the measurement device (0.005 times reading + 3 digits with 0.1 resolution for Finest 203) the error for multimeter measurements is

$$\delta R_s = \sqrt{2(0.05R_s)^2 + (0.005R_s)^2 + (0.3[\Omega/sq])^2}$$

as the resistance is directly proportional to length and inversely proportional to width.

In the case of 4-point measurements the sheet resistance was measured hundreds of times and the result was an average of those measurements with the background taken into account, so the random errors are minimized and the only major sources of error are the dimensions of the sample. Hence by using equation (3) the error for 4-point measured sheet resistance values is

$$\delta R_s = \sqrt{2}(0.05R_s) \tag{4}$$

.

5.2 Transmittance measurements

Transmittance T describes how large portion of the light passes through the sample. Absorbance A is a logarithmic scale of how large portion of light is absorbed instead:

$$A = log_{10}\frac{1}{T} \tag{5}$$

assuming that none of the light is reflected of the surface or scattered. Scattered light also passes through the sample but it deviates of the original trajectory. According to Beer-Lambert law, absorbance is directly proportional to the thickness l of the sample:

$$A = \mu l \tag{6}$$

in which μ is the absorption coefficient.

Transmittance in the visible spectrum, from 300 to 895 nm, was measured with PerkinElmer Lambda 850 UV/VIS Spectrometer. Lambda 850 has two light sources, a deuterium lamp and a tungsten halogen lamp, but only the tungsten halogen lamp was used for these measurements. The spectrometer uses a monochromator for separating the different wavelengths of the light source and then it measures the amount of light that goes directly through the sample and compares it with the measured background. Lambda 850 only measures the light that passes directly through sample, it does not measure reflectance or scattering so it presumes that all light that is scattered or reflected is instead absorbed by the sample.

Microscope slide of the same stock as the substrate was used for background measurements after cleaning it with ethanol. This way the spectrometer will only measure the transmittance of the HC-DWCNT film itself, without adding the reflectance and absorption of the substrate to the absorption of the HC-DWCNT film.

The transmittance measurements were performed immediately after film deposition to ensure that dust would not affect the results. The light beam of Lambda 850 was also spread over about 1 *cm* in vertical direction so in order to ensure that all parts of the beam hit the sample its transmittance was measured before cleaning the excess film: the sample dimensions were 1 *cm* x 1 *cm* so without the excess film a small part of the beam could have bypassed the sample.

Because the droplet-dried films were so uneven their transmittance had to be measured from three different spots and calculate the average value. For other samples only a single measurement was required.

5.2.1 Transmittance in infrared

Transmittance in infrared, from 800 nm to 7000 nm, was measured with Nicolet Magna-IR 760 Spectrometer. Air inside the system was replaced with nitrogen gas in order to remove water vapor off the system because water absorbs IR radiation and can disrupt the measurement. Three samples were prepared on CaF_2 glass that has good infrared transmittance and a clean CaF_2 glass was used for measuring the background. Two of the samples were prepared with vacuum filtration, one with peeling method and the other with dissolution, and one sample was prepared with droplet casting method in order to detect if vacuum filtration methods added or removed any impurities compared the original HC-DWCNT solution. The transmittance of the vacuum filtered samples in visible part of the spectrum was also measured with Lambda 850, but it was not measured for the droplet-dried film because it was not enough uniform: aligning both of the measurement devices to measure exactly the same spot was too unreliable.

5.3 Annealing

Annealing is heat treatment that is meant to improve the quality of the film by oxidizing or vaporizing impurities or by altering its microstructure. Basically it means heating the sample in a suitable atmosphere. It is an advantage if the film requires no annealing because it can then be deposited on many different substrates that may not withstand heating, but for some applications annealing can be required because of other components: for example dye-sensitized solar cells (DSSC) require a layer of TiO_2 nanoparticles that has to be annealed. Hence the film is also required to withstand annealing, and annealing with a coating of TiO_2 nanoparticles was used for testing if these films can be used in DSSCs.

In this study annealing was done with two different setups: with a heat blower or in an oven without air blow. The heat blower had three blow speeds, of which the two fastest could be used in temperature range of 200 $^{\circ}C$ to 400 $^{\circ}C$ and the slowest mode was for lower temperatures. Annealing was always performed in room air. The square resistance of each sample was always measured before annealing and after annealing they were allowed to cool down for at least 20 minutes before measuring the resistance again.

5.3.1 Annealing with TiO_2

The TiO_2 nanoparticles used in this study were produced by Solaronix (11421 Ti-Nanoxide T BN395c/092113 Fm). Ti-Nanoxide T was dispersed in terpineol and mixed to produce homogeneous paste. The paste was spread over the HC-DWCNT film by covering the edges with tape, placing a droplet of the paste on the film and spreading it with a glass

rod. The rod was gently pressed against the tape so that the thickness of the paste on the film was roughly equal to the thickness of the tape. Each layer of tape is about 20 μm thick so two layers of tape is about 40 μm thick and three layers results in 60 μm thick layer of TiO_2.

For annealing the heat blower with the second fastest mode was used. Three samples were prepared with 40 μm of TiO_2 and annealed at temperatures of 300, 350 and 400 $°C$ for 30 minutes. One additional sample was prepared with 60 μm of TiO_2 and annealed at 400 $°C$. Sheet resistance was measured with 4-point method right before and after adding TiO_2 and annealing and the samples. Then they were kept in room air for 11 days and R_s was measured again.

5.4 Immersing the HC-DWCNT film in solvents

Since vacuum filtration with dissolution method requires washing the film with different solvents that other methods do not require some spray-coated samples were used for checking if solvents such as acetone and isopropanol could effect the sheet resistance of HC-DWCNT films. Samples were kept in three solvents, water, acetone, and isopropanol for 30 minutes and their square resistance was measured before and after the procedure.

5.5 Results and discussion

5.5.1 Initial sheet resistance and transmittance

Figure 28 shows a typical absorbance spectrum of a HC-DWCNT film. There were no differences in the visible region spectra among films prepared with different methods. Similar to other CNT based thin films, HC-DWCNT films showed smooth continuous spectra, the absorbance increasing towards UV wavelengths.

Figure 29 shows the initial resistance of some of the samples after letting the resistance settle for at least a few hours. Especially the conductivities of sprayed samples greatly improved within few hours after the preparation of the HC-DWCNT film. Not all of the samples were included in the figure because some of them had defects: for instance the peeling after filtering did not always peel the entire film or it did not land properly on the electrodes and some of the droplet-dried films did not spread properly over the electrodes and had very bad connection. For better comparison only good quality samples are presented in the figure.

The initial resistance was usually measured with the multimeter which always showed slightly higher readings than 4-point measurements. The difference was not large though, on average 8 Ω while the resistance of the samples was usually over 100 Ω/sq and the dif-

ference in resistance between samples with similar transmittance but different deposition methods was several tens of ohms.

With the earliest version of HC-DWCNT used in this study, batch 1, the difference between the methods is very clear: the initial resistance of spray-coated samples can be over twice as much as the resistance of droplet-dried or filtered samples. The best batch 1 sample prepared with droplet casting method had initial sheet resistance of 188 Ω/sq and transmittance of 74.4 % at 550 nm while corresponding spray-coated sample had resistance of 338 Ω/sq and transmittance of 74.3 %. Only one successful sample was prepared of batch 1 with vacuum filtration method but it was at least as good as the similar droplet-dried samples.

The latest version of HC-DWCNT, batch 3, proved to be much better than batch 1. Samples of batch 3 show the same result as batch 1 samples: the sheet resistance of filtered samples is about half of corresponding spray-coated samples. The best sample had resistance of 115 Ω/sq and transmittance of 81.6 % while the best spray-coated sample had 199 Ω/sq and 77 %.

Two successful samples were prepared with filtration and dissolution method but only one of them had transmittance of 76.0 %, in the same range as the samples prepared with peeling method. But since its resistance was 110 Ω/sq it was overall slightly worse than the films prepared with peeling method.

Some of the thinnest spray-coated batch 2 samples were quite good with transmittance of over 90% and sheet resistance of 415 - 440 Ω/sq. A corresponding batch 3 sample prepared with filtration and dissolution was in fact worse than them as it had the same sheet resistance but lower transmittance. This was the only case where spray-coated samples were better than filtered samples but the batch 2 samples with transmittance of bit over 80 % were on average similar to spray-coated batch 3 samples that were much worse than the filtered batch 3 samples.

5.5.2 Effects of annealing

Table 1 shows the results of annealing films in temperature range of 200 to 300 $°C$. Generally the sheet resistances of spray coated films were reduced on annealing while for all the other samples the resistances increased on annealing. The resistances of spray-coated samples were reduced by annealing the films in an oven at 250 $°C$. The resistance already increased when temperature was rised to 270 $°C$ but still remained much lower than the initial resistance. With the heat blower at the second fastest flow speed the optimal annealing temperature was between 270 and 280 $°C$ and with the fastest flow speed it was only 230 $°C$.

For spray-coated samples the decrease in resistance was rather large, in many cases

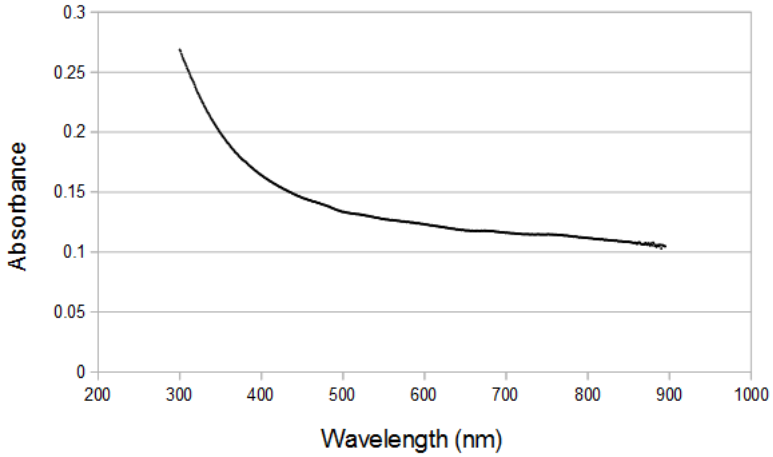

Figure 28: Absorbance spectrum of HC-DWCNT in the visible spectral region. This particular sample was prepared with droplet casting method and had a transmittance of 74 % at 550 nm.

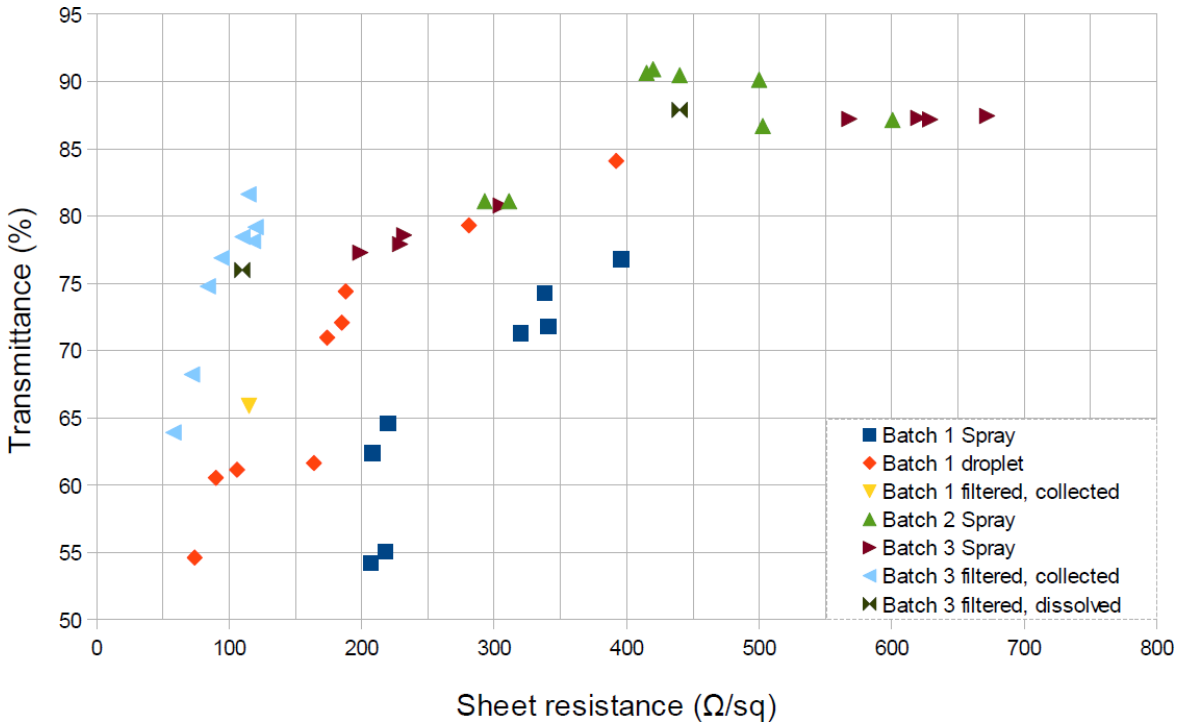

Figure 29: Initial resistance of the samples before any treatments as function of transmittance at 550 nm wavelength. Vacuum filtered samples prepared of batch 3 are clearly better than the rest.

over 100 Ω, but for droplet-dried samples the increase in resistance was very large and it was also significant for filtered samples. The chemical composition of the original dispersion of the samples was the same for the samples within the same batch. Annealing most likely reorganizes the microstructure of the films, either the way the DWCNTs and hemicellulose are connected to each other or by oxidizing some of the compounds and altering the microstructure that way. It is a possibility that the microstructure of spray-coated samples, the connections between the nanotubes for instance, is so non-optimal that annealing improves it while the microstructure of droplet-dried and filtered samples is already so good that annealing can only worsen it.

On the other hand it is also possible that the chemical composition of the samples was different: there could be some insulative impurity in the dispersion that was also soluble in water, which is entirely possible since even hemicellulose itself has both of those characteristics and the impurity could for example be hemicellulose molecules that are not connected to DWCNTs. In spray-coating everything that there is in the dispersion ends up as a part of the film whereas vacuum filtration can filter the nanotubes while letting some of the smaller molecules such as impurities go through. In droplet casting the slow drying process and large size of the droplet can either deposit most of the impurities to the edge of the film (which was removed in order to shape the film) as the depositions at the edge and in the middle of the droplet are always different, or the HC-DWCNT film could have aggregated first in which case the impurities would have landed on the film but not between the nanotubes.

The latter argument explains why annealing can improve spray-coated samples but not the other samples: annealing removes these impurities off spray-coated samples while the samples that do not have any impurities are only damaged instead. The reason why droplet cast samples are damaged more than filtered samples could be because of their uneven HC-DWCNT distribution: some parts of the film are thinner than others and even minor damage to the thinner parts can greatly reduce the viable pathways for charge transportation. The annealed filtered samples had uniform thickness and hence were relatively damaged less than the droplet cast samples. Thickness also affected spray-coated samples: sample 11 A was clearly thicker than B and it also benefited relatively more of annealing than B did as the sheet resistance of A decreased by 52 % while for B it decreased only 38 %.

Sample	Batch	Dep. Method	Initial $R_s(\Omega/sq)$	Anneal: $200°C$	Anneal: $230°C$	Anneal: $250°C$	Anneal: $270°C$	Anneal: $280°C$	Anneal: $300°C$
Annealing mode 0									
11 A	1	Spray	341			165	190		
11 B	1	Spray	396			244	277		
14 A	1	Droplet	105	148	192	255			
14 B	1	Droplet	175	247	325	451			
30	3	Filtered, peeled	85			114			
31	3	Filtered, peeled	70			94			
Annealing mode 2									
9 A	3	Spray	620	540	520	494		484	493
9 B	3	Spray	568	512	506	495		474	485
12 A	1	Spray	320			241	170		
12 B	1	Spray	338			265	210		
15 A	1	Droplet	194	256	279	323			
15 B	1	Droplet	92	117	132	147			
Annealing mode 3									
10 A	3	Spray	672	560	551	558		575	619
10 B	3	Spray	629	515	520	540		566	627

Table 1: Results of annealing: Annealing up to 250 $°C$ improved spray-coated samples while it damaged other samples. Mode 0 is a static oven without airflow, mode 2 is the heat blower with second fastest air flow setting and mode 3 with the fastest air flow setting. Annealing time was 20 min and all resistance values were measured with Finest 203 multimeter.

Sample	TiO_2 layer	Anneal	R_s before (Ω/sq)	R_s after (Ω/sq)	R_s after 11 d (Ω/sq)
36	40 μm	300 $°C$	115	434	142
37	40 μm	350 $°C$	119	348	251
38	40 μm	400 $°C$	94	286	321
39	60 μm	400 $°C$	110	375	349

Table 2: Results of annealing with TiO_2: None of the samples survived the process without increase in sheet resistance.

5.5.3 Annealing with TiO_2

Annealing with TiO_2 layer on the HC-DWCNT film did not protect it well enough to avoid the increase in resistance as shown in table 2. A well annealed TiO_2 layer should be transparent and colorless but samples annealed in 300 and 350 $°C$ were slightly yellow and only the sample annealed in 400 $°C$ was properly colorless. Only the sample annealed in the lowest temperature of 300 $°C$ had relatively small increase in sheet resistance of 23 %. Increasing the thickness of the TiO_2 layer up to 60 μm did not improve the protection, instead the thicker layer was not annealed well enough as it was colored yellow and would have required longer anneal time. The resistance measured right after the test was very high for all of the samples but the sample annealed in 300 $°C$ managed to recover most of its conductivity while the other samples sufered more permanent damage.

5.5.4 Immersing the samples in water

Immersing the HC-DWCNT films in acetone or isopropanol for 30 min had no effect on the performance of the samples while immersing in ethanol slightly increased the resistance. Interestingly immersing in water decreased the resistance of the spray-coated sample from 208 to 100 Ω/sq and from 220 to 120 Ω/sq. Hence immersing in water was also tested on other samples by immersing them for 10 min in water, which systematically improved the quality of spray-coated samples as shown in table 3 regardless of the HC-DWCNT batch used. Similar improvement was however not observed with droplet-dried samples.

This result indicates that there are clear differences in the microstructure or composition of spray-coated films compared to the other two methods. Dipping the samples in water could both remove the soluble impurities from blocking the tube connections and rearrange the microstructure. To test the effect of annealing on a sample that had already been improved by immersion sample 8 was annealed at 250 $°C$ with mode 3 which, judging by the earlier annealing tests, should have reduced the film resistance further. Yet the sheet resistance increased to 271 for film A and 308 Ω/sq for film B which are

Sample	Batch	Dep. Method	R_s (Ω/sq) before	R_s (Ω/sq) after
2 A	1	Spray	208	100
2 B	1	Spray	220	120
5 A	2	Spray	409	308
5 B	2	Spray	507	405
6 A	2	Spray	296	207
6 B	2	Spray	305	212
8 A	3	Spray	232	163
8 B	3	Spray	229	158
14 A	1	Droplet	107	105
14 B	1	Droplet	175	175
15 A	1	Droplet	187	194
15 B	1	Droplet	90	92
16 A	1	Droplet	166	142
16 B	1	Droplet	74	75

Table 3: Results of immersing samples in water: Immersing in water only improved spray-coated samples reliably. Sample 2 was kept underwater for 30 minutes while the others were kept for 10. All values were measured with the multimeter.

more than they were before the immersion. This means that impurities might not just be removed during annealing but they might also protect the rest of the film. Immersion was also tested on spray-coated samples that had already been annealed. Resistances were reduced also in these films, suggesting that the water immersion is more efficient means to improve conductivity of the films than annealing the HC-DWCNT films.

SEM images (figures 34 - 37) taken of spray-coated and other samples also show that there are both differences in the structure and chemical composition of the films depending on the deposition methods and whether the samples were immersed or not: Non-immersed spray-coated samples had more impurities and less uniform structure in microscopic scale than other samples. SEM imaging results are given in greater detail in chapter 6.

5.5.5 Summary of the post-treatment results

Ultimately dipping in water proved to be far better post-treatment than annealing: dipping in water cleaned the samples and could rearrange the poor microstructure of spray-coated samples, but annealing in addition to removing impurities also damaged the HC-DWCNT composite. Hence dipping in water improved conductivity of the spray-coated films more than annealing did. However, both of the methods could only improve spray-coated films as droplet-cast and vacuum filtered films had good microstructure and high purity in the first place.

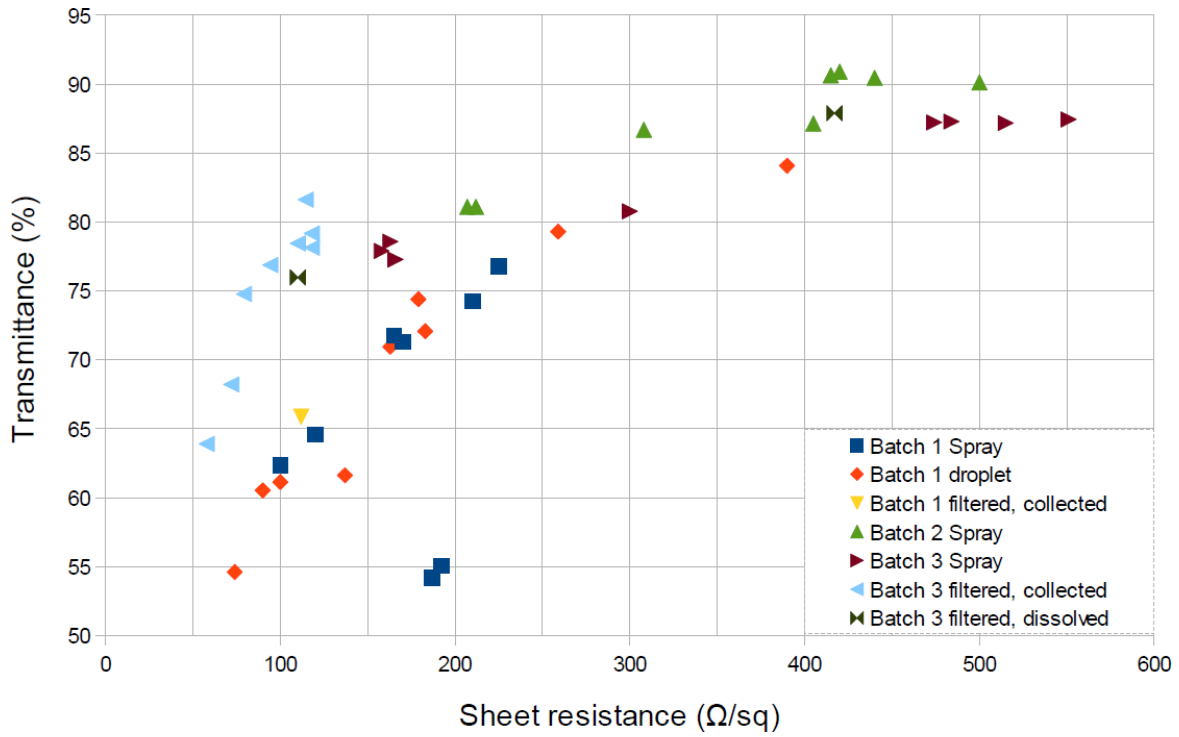

Figure 30: Lowest measured resistance of each sample after treatments as function of transmittance at 550 nm wavelength. Vacuum filtered samples without post-treatments are still better than other samples that were immersed in water or annealed.

Figure 30 shows the lowest measured resistance of the same samples as in figure 29 and it includes resistance measurements after post-treatments of the films. The spray-coated batch 1 samples could be improved to the point where they are about as good as the droplet-dried samples, the only exception in the figure being the two samples with about 55 % transmittance that were not immersed or annealed. Despite immersion in water the spray-coated batch 3 samples failed to catch up with the filtered batch 3 samples that had not been altered: for instance out of samples with 78 % transmittance the spray-coated one had sheet resistance of 158 Ω/sq while the filtered one had 118 Ω/sq, about one quarter less. Ultimately the most successful sample was prepared with filtration and peeling method of batch 3 and had sheet resistance of 114.6 Ω/sq and transmittance of 81.6 %. The error for this sample calculated with equation (4) is
$\delta R_s = \sqrt{2}(0.05R_s) = \sqrt{2} \cdot 0.05 \cdot 114.6\ \Omega/sq = 8.103\ \Omega/sq \approx 9\ \Omega/sq.$
With the errors taken into consideration the sheet resistance is $115 \pm 9\ \Omega/sq$.

5.5.6 Lifetime of the films

Lifetime of a prepared film could be defined as time it takes to lose 1/e fraction of the initial conductivity of the film. The results listed in table 4 are the comparison between the lowest measured sheet resistance and the latest measurement. The latest measurement was performed with 4-point method and it was performed on the same day for all the listed samples. The spray-coated and droplet-dried samples were at that point about five to seven months old while the filtered samples were newer but still at least one month old. This should not cause a large difference since most of the increase in resistance happened during the first week after the film deposition: for example sample 6 A had sheet resistance of 207 Ω/sq after immersion to water and it increased to 250 Ω/sq after seven days and after several months from that the resistance had further increased only by 6 Ω up to 256 Ω/sq. Only samples that had not been damaged by excessive annealing are shown in the table.

Batch 1 samples had very large increase in resistance, especially spray-coated samples which had an average increase of 65.3 %. Batch 2 and 3 spray-coated samples had much lower increase in average, 19.6 % and 12.9 %, however some of the difference may have been caused by immersion in water: the batch 1 samples in the table were not immersed while batch 2 and 3 samples were immersed in water. Batch 1 droplet-dried samples also had fairly large increase of 27.5 % so the difference between the methods was large. For filtered samples the increase was nonexistant for thicker samples and even the thin sample with high resistance showed only an increase of 6.8 %. In fact sample 28 had instead slightly improved during the time. Film thickness is again relevant as thicker films are showing better stability in case of droplet cast and filtered samples, but the development of spray-coated samples was much more inconsistent.

Sample	Batch	Dep. Method	Annealed	Dipped	Lowest $R_s(\Omega/sq)$	Latest $R_s(\Omega/sq)$	Increase %
12 A	1	Spray	yes	no	170	306.5	80.3
12 B	1	Spray	yes	no	210	333.1	58.6
18 A	1	Spray	no	no	187	307.6	64.5
18 B	1	Spray	no	no	192.1	303.1	57.8
16 A	1	Droplet	no	yes	137	179.1	30.8
16 B	1	Droplet	no	yes	74	92.0	24.2
5 A	2	Spray	yes	yes	308	357.3	16.0
5 B	2	Spray	yes	yes	405	485.4	19.8
6 A	2	Spray	yes	yes	207	256.0	23.7
6 B	2	Spray	yes	yes	212	252.3	19.0
7 A	3	Spray	yes	yes	166	170.9	2.9
7 B	3	Spray	yes	yes	300	368.4	22.8
28	3	Filtered, peeled	no	no	79.2	79.2	0.0
25	3	Filtered, dissolved	no	no	417	445.2	6.8
27	3	Filtered, dissolved	no	no	110	110.4	0.4

Table 4: Increase of resistance due time. Samples prepared with batch 3 and vacuum filtration showed very good stability. The R_s values with accuracy of one decimal were measured with 4-point method while the rest were measured with multimeter.

5.5.7 IR transmittance

The absorbance spectrum of the filtered samples is shown in figure 31 and the spectrum of the droplet-dried sample is in figure 32. The peeled sample had absorbance of 0.1216 at 550 nm and the dissolved sample had 0.1181 while their absorbances at 4000 nm were 0.0138 and 0.0154, so the dissolved sample had higher absorbance in infrared but lower in visible light. Because CaF_2 windows are soluble in water there is a possibility that the window substrate of the peeled sample was slightly thinner as it was immersed in water than the window used for the dissolved sample but since the absorption coefficient of CaF_2 is very small, about $5 \cdot 10^{-4}$ cm^{-1} [135], the difference of 0.005 is too large to be explained by the difference of window thickness. Hence the most likely cause for the difference in IR transmittance are the impurities caused by dissolution of the MCE filter. At least the impurities have clearly caused the two peaks at 6050 nm and 7820 nm, both the peeled sample and droplet-dried sample also have a small peak at 6050 nm but it is relatively much smaller than the peak of the dissolution sample. 6050 nm and 7820 nm could correspond to N-H and N-C bonds: MCE filters contain nitrogen which could have formed bonds with HC-DWCNT in acetone bath. Each sample also has small bands at 2900 nm and 3440 nm which correspond to stretching of O-H and C-H bonds in hemicellulose.

Apart from having higher absorbance in general due to having thicker layer of HC-DWCNT, the shape of absorbance spectrum of the droplet-dried sample is slightly different than the spectrum of the filtered samples: the bands at 2900 nm and 3440 nm are relatively smaller and absorbance at over 7000 nm is higher compared to the rest of the IR region. This hints towards the possibility that there would be a small difference in chemical composition of the samples: filtration probably removes some impurities that cause the change in absorbance spectrum.

The spectrum in figure 33 is combination of the measurements performed with Lambda 850 for transmittance in visible light and Magna-IR 750 for the transmittance in infrared. The spectrums do not meet because neither of the measurement devices could measure in near-infrared region from 900 nm to 1400 nm. The transmittance at 550 nm is 75.6 % and it is at its highest value of 97.0 % at 3600 nm. The sheet resistance of this sample was not measured but by comparing its transmittance at 550 nm to other samples prepared with filtration and peeling method its sheet resistance could be roughly estimated as 90 Ω/sq.

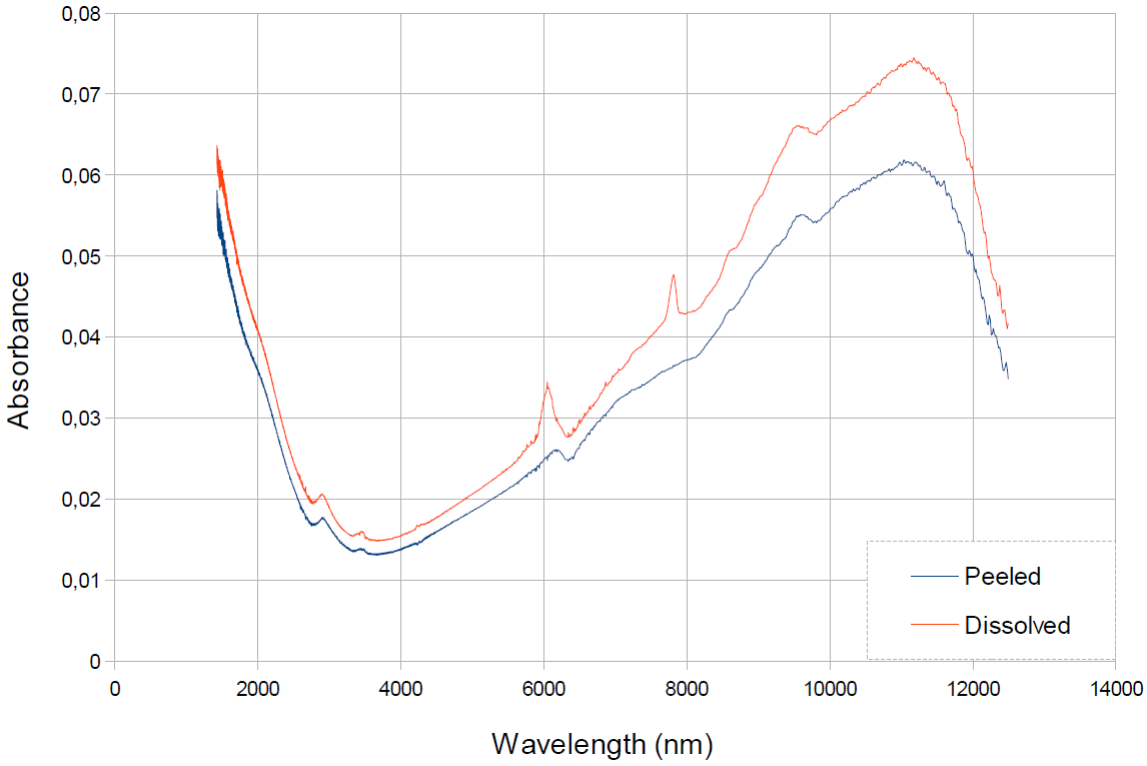

Figure 31: IR absorbance spectrum of filtered HC-DWCNT samples prepared with peeling or dissolution methods. Stronger peaks of the dissolved sample are caused by impurities.

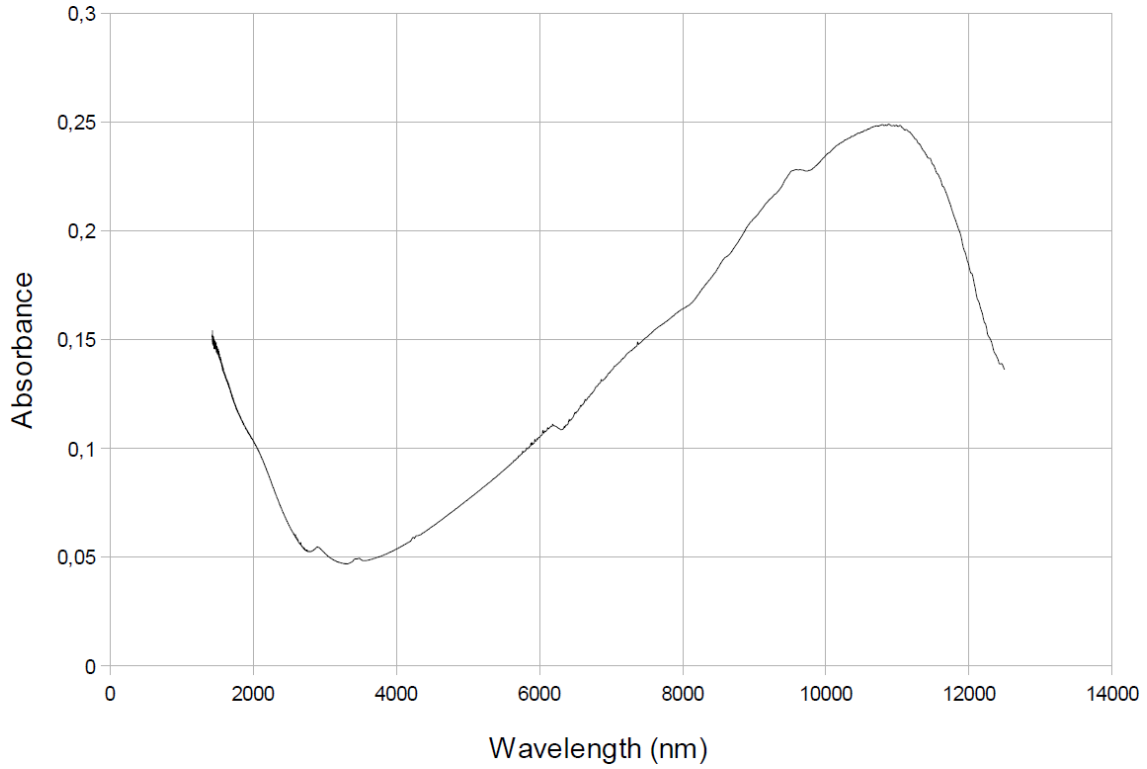

Figure 32: Absorbance spectrum of a droplet-dried HC-DWCNT sample in IR.

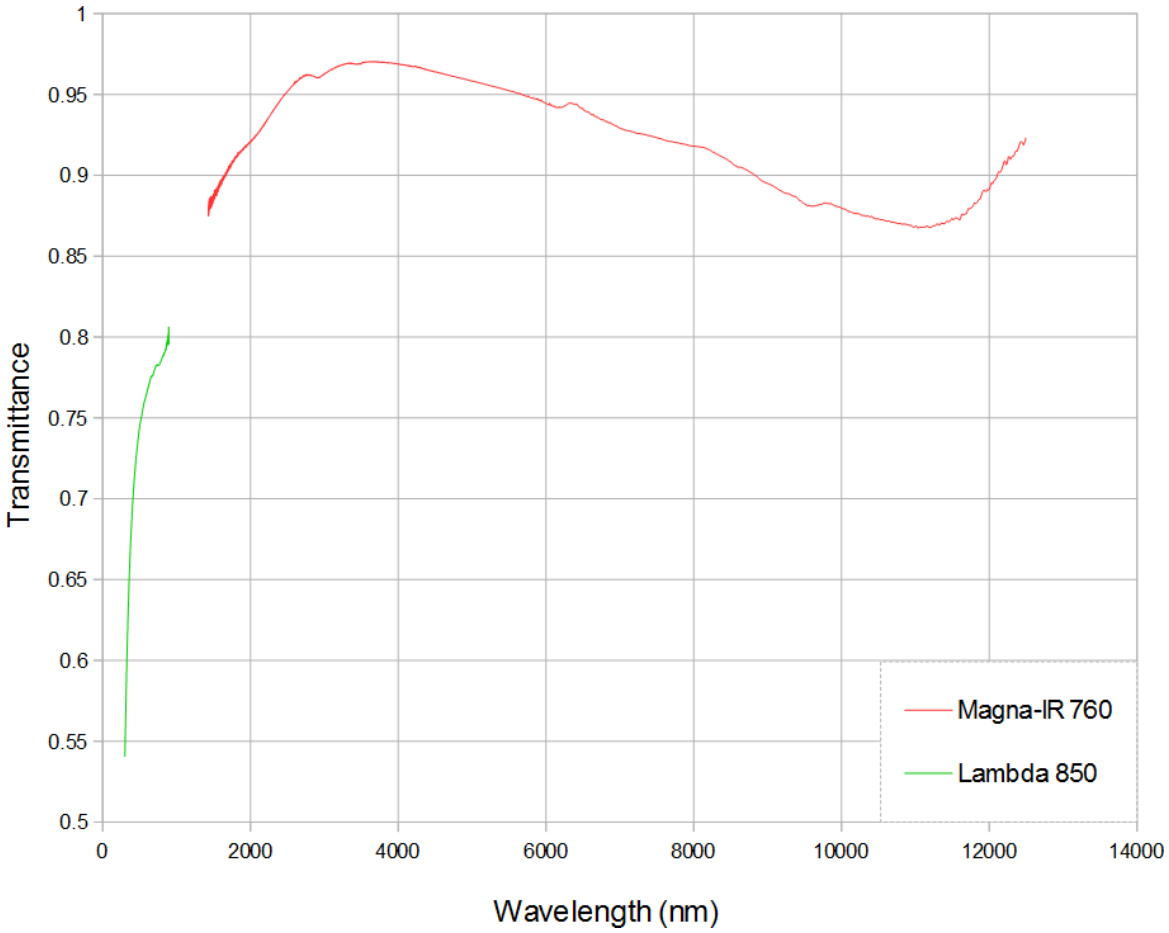

Figure 33: Transmittance spectrum of a sample prepared with filtering and peeling method. The spectrum is combined of spectrums given by two separate measurement devices.

6 SEM imaging

Raith eLINE scanning electron microscope (SEM) was used for imaging two spray-coated, two droplet-dried and one filtered sample in order to discover possible differences in the films produced with different deposition methods. SEM produces a beam of electrons that it focuses with electromagnetic lenses to a small spot on the sample surface. The beam interacts with the atoms on the surface of the sample, ionizing them and ejecting electrons off the atoms. These ejected electrons are called secondary electrons. As the beam scans the sample these secondary electrons are detected and by knowing the amount of secondary electrons from each spot an image can be formed. The amount of released secondary electrons depends on how many atoms are hit by the beam: if the beam hits for instance a tilted edge it releases more particles than when hitting a flat surface. This way it is possible to distinguish the edges and other non-uniformities of the surface.

If the sample surface is not conductive the electron beam can charge it, which redirects the beam as the negative charges repel each other. Since HC-DWCNT film is conductive it was enough that the film was connected via a metal clamp to the stage to ground the samples. The voltage used for accelerating the electrons was 15 kV and working distance was 9 mm.

6.1 Results and discussion

Images 34 and 35 are of a spray-coated sample with transmittance of 55 % that had not been annealed or immersed in water and they clearly show how the film is formed of miniature dried droplets: the gray areas in figure 34 are clean HC-DWCNT deposition and both the bright particles and dark spots and rings are different impurities that concentrate to the droplet edges. Figure 35 is an example of the intersections of these droplets and it shows that the micro scale deposition of HC-DWCNT can be very non-uniform. There is a possibility that there is only a small amount HC-DWCNT in the middle of the intersection that is filled with the dark substance made of impurities, but it is hard to say because the substance could hide HC-DWCNT particles underneath. These impurities were focused to the edges of the dried droplets and they could decrease the conductivity of the film if they act as an insulator between the droplet remains. The bright particles are some kind of crystals, and while they most likely do not affect the conductivity of the film much they can still increase scattering and absorbance of the film.

Another spray-coated sample that was imaged had transmittance of 81 % and it was both annealed and immersed in water. It did not have any clear droplet edges as the other sample and it had very low amount of crystallized impurities, hence immersion in

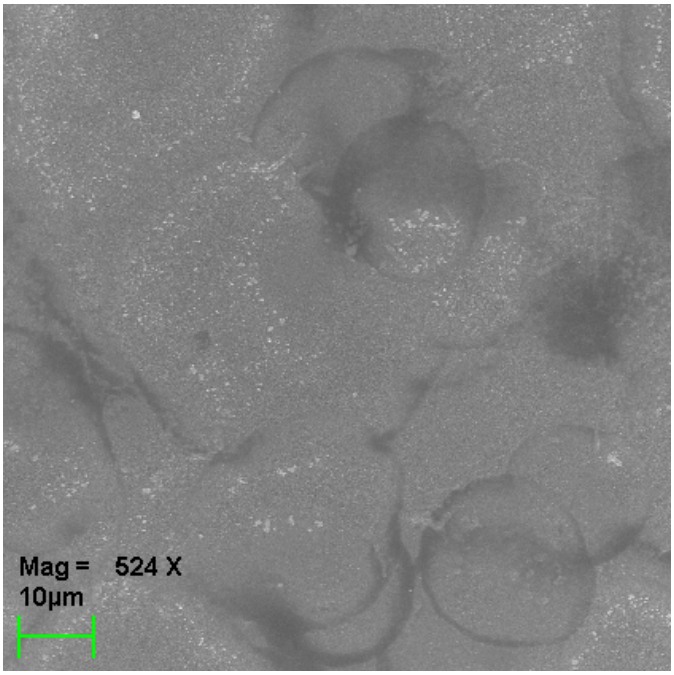

Figure 34: SEM image showing droplet edges on a spray-coated sample.

water can probably decrease the amount of haze slightly by removing crystals in addition to improving the microstructure and conductivity by re-depositing HC-DWCNT and removing impurities. While this sample is thinner than the other imaged spray-coated sample, these crystals were also much more common in droplet cast samples with similar transmittance that had not been immersed.

Figure 36 shows how droplet-dried films could at some points be very thick while at other points they almost had only one layer of HC-DWCNT particles. The bright spots in figure 36 A mark the glass substrate. The droplet-dry samples were not immersed in water but one of them had been annealed, however no significant differences were spotted between the samples. They both had similar crystal impurities like the spray-coated samples had but the dark substance could not be detected because it had either concentrated to the edge of the substrate from where it was removed along with the excess film or it had spread more uniformly. Ring like shapes in figures 36 B and 37 were very common across all the samples.

The sample that had been prepared with filtration and peeling method had transmittance of 91 %. The film in figure 37 is in many spots only one particle thick or the substrate is completely bare. This explains why samples with about 90 % transmittance had very high resistance: the DWCNTs on those samples had very few contacts to other tubes and with low amount of contacts and many dead ends the conductivity is also very low. If the transmittance was even higher the DWCNT density would be so low that individual nanotubes would be seen instead of an interconnected nanotubular film.

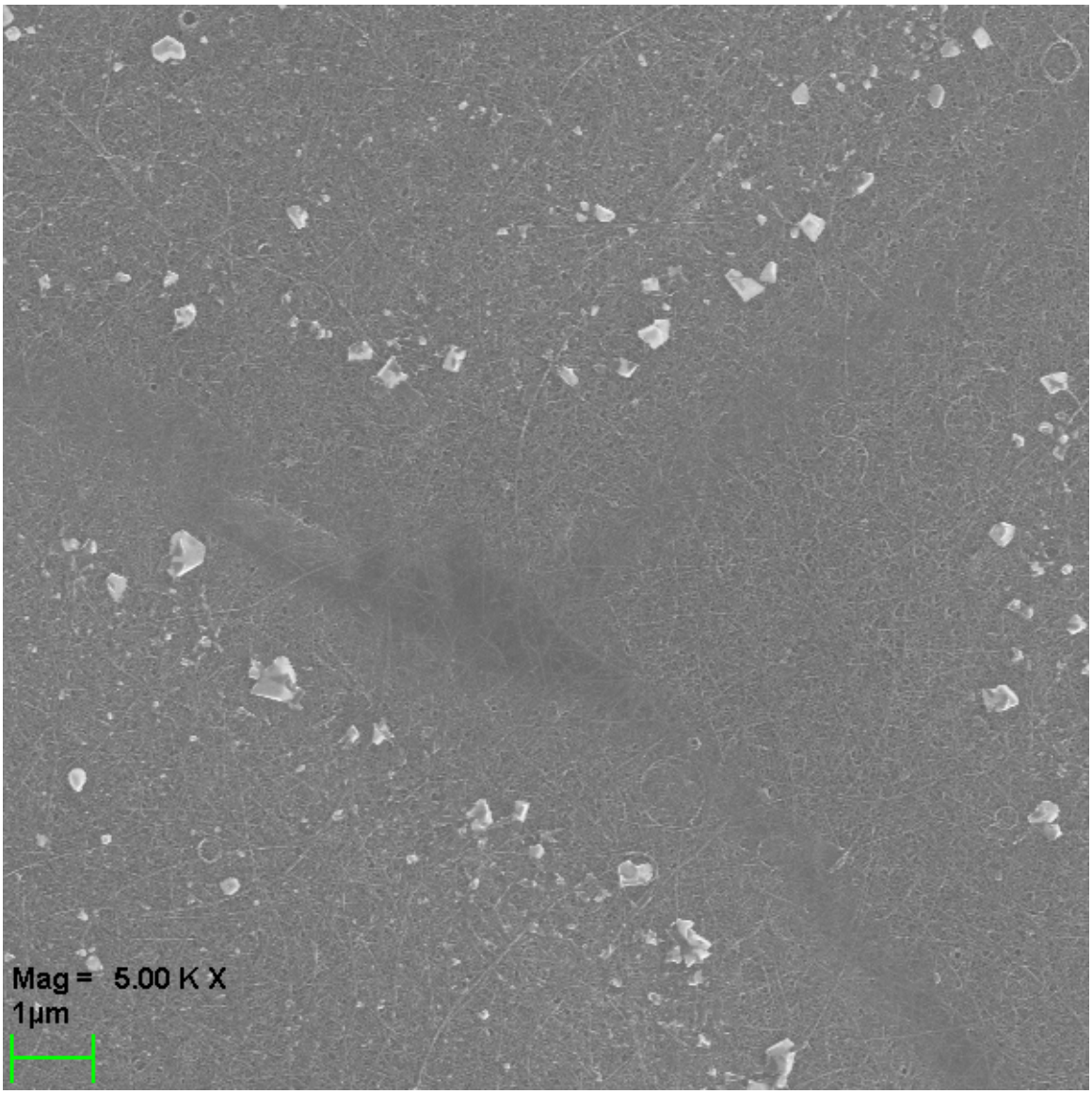

Figure 35: Intersection of three droplets on a spray-coated sample.

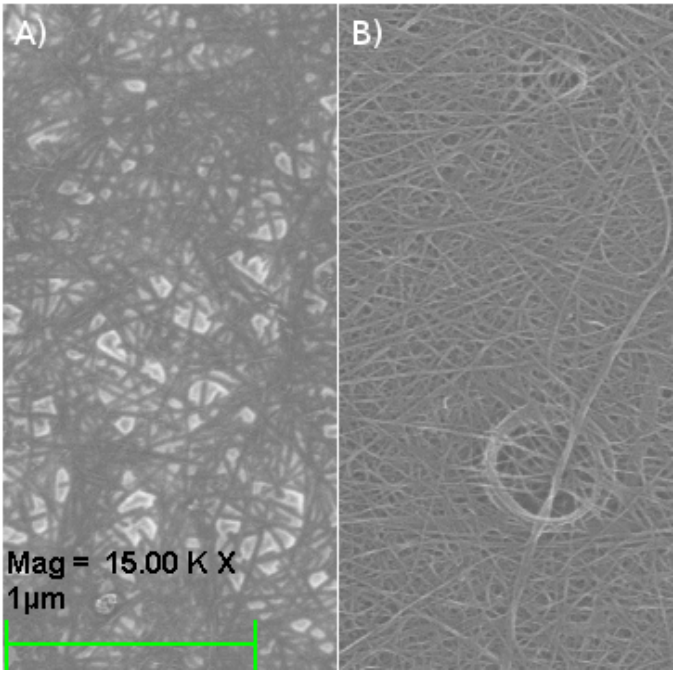

Figure 36: SEM image of a droplet-dried sample. A) and B) are both of the same sample, image A) has a very thin layer of HC-DWCNT on the substrate whereas B) has a very thick layer, showing how non-uniform droplet-dried films can be.

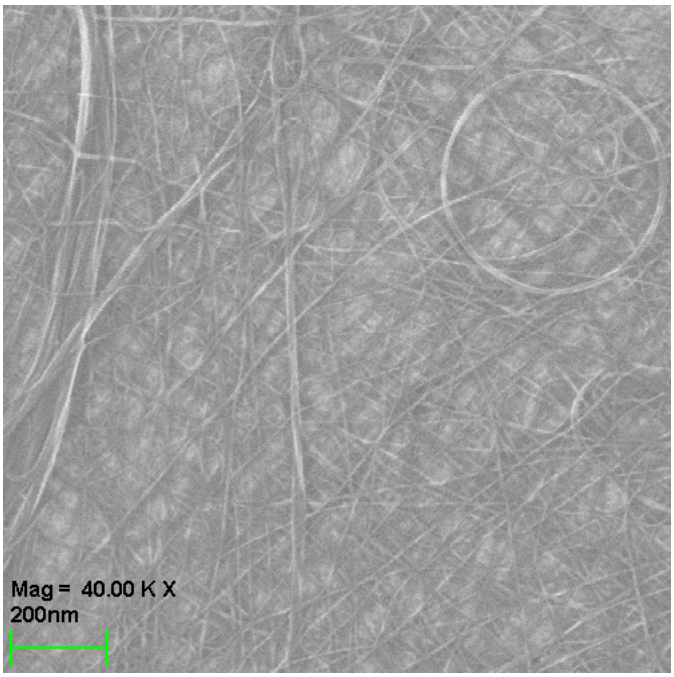

Figure 37: SEM image of a filtered sample that has transmittance of 91 %. The glass substrate is in many spots completely bare or only covered by a single HC-DWCNT particle.

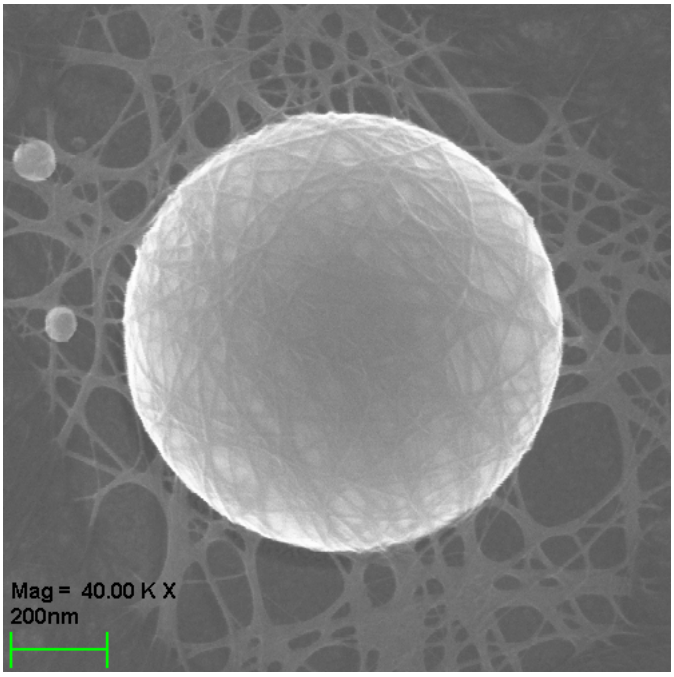

Figure 38: SEM image of a detached filter membrane particle underneath HC-DWCNT.

The filtered sample had occasional small spots covered by impurities but not similar crystallized impurities like the spray-coated and droplet-dried samples had. Instead it had numerous round particles shown in figure 38 covered by HC-DWCNT. Since the particles were covered by HC-DWCNT they had to have been on the filter before filtration because the peeling method does not flip the film over during transfer. Hence the particles are most likely loosely attached pieces of MCE filter membrane.

7 Thickness measurements and conductivity calculations

Tencor P-15 Stylus Profiler was used for measuring the thickness of the films. It is a contact profilometer that presses the surface of a sample with a stylus by using a specified contact force as the sample is moved beneath it. Changes in surface height alters the vertical position of the stylus which generates a signal. Four samples with different transmittance values ranging from 64% to 91% were measured with the profiler.

Conductivity of the samples was calculated by assuming that the samples were completely uniform and homogeneous. Conductivity σ_{DC} is given by

$$\sigma_{DC} = \frac{1}{R}\frac{l}{A} \tag{7}$$

in which l is the length of the sample and A is cross-sectional area, in other words height h of the sample multiplied by its width w. Since both length and width of the samples are 1 cm, (7) can be expressed as

$$\sigma_{DC} = \frac{1}{R_s h}. \tag{8}$$

The conductivity should increase as the thickness increases because as mentioned earlier in section 3 there should be less dead ends, DWCNTs that are not properly connected to other tubes. The relative amount of DWCNTs that actually conduct electricity should increase.

7.1 Results and discussion

The height profile of one of the samples is shown in figure 39. The film itself is quite thin, on average only 146.6 nm thick, but there are many spikes in the profile that are impurities. Because of the many impurities and curvature of the substrate this thickness value is only a rough estimate, which is also true for the other samples.

Values in table 5 were calculated with equation (8). For example sample 26 had height of 101.6 nm and sheet resistance of 118 so its conductivity was

$$\sigma_{DC26} = \frac{1}{118\ \Omega/sq\ \cdot\ 101.6\ nm}$$

$$\sigma_{DC26} = 83411\ S/m \approx 83\ kS/m$$

The height of the samples appears to be not directly proportional to the absorbance as it should be according to Beer-Lambert law (6). This means that the absorption coefficient of the samples has increased along with thickness, in other words the density

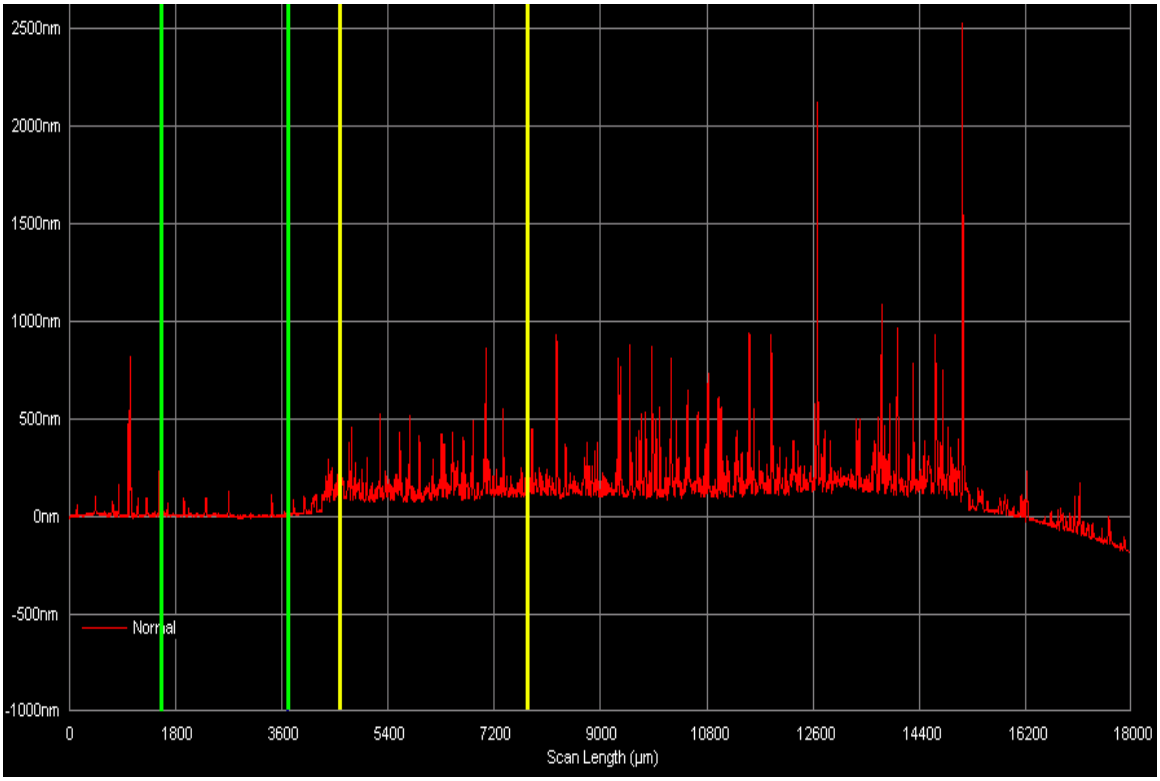

Figure 39: Height profile of sample 30 with transmittance of 68 %. The image is zoomed and does not show the entire sample. Green lines show from where the average height of the substrate was taken and yellow lines show the range from where the average height of the HC-DWCNT film was taken. The difference of the averaged heights is 146.6 *nm*. Because the glass itself was slightly curved the image had to be adjusted with the program for the sample to appear flat although effects of curvature can still be seen at the right edge of the image, which is why the only the left side was used for height measurements.

Sample	Absorbance	Transmittance (%)	Height (nm)	R_s (Ω/sq)	Conductivity (kS/m)
26	0.101	79	101.6	118	83
30	0.166	68	146.6	72	95
31	0.194	64	155.0	58	111

Table 5: Results of thickness measurements and calculated conductivity values. The R_s values were measured with the multimeter.

of the nanotubes in the films has increased. The conductivity of the samples also increases as the thickness and density increase, which is exactly as assumed.

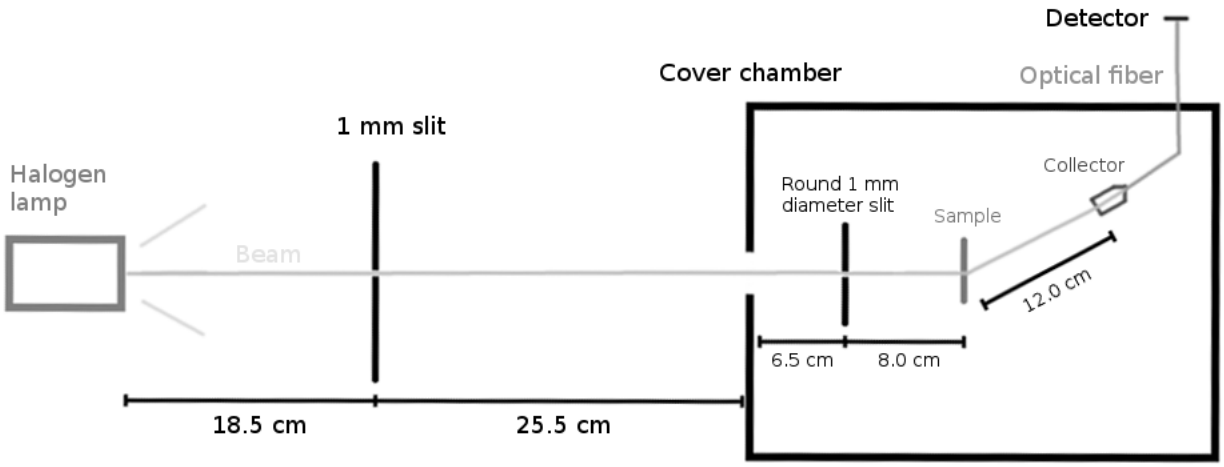

Figure 40: The setup used for scattering measurements. The collector had a diameter of 0.7 mm and it was connected to the detector via an optical fiber.

8 Scattering

Scattering means that light beams that pass through the sample change their path from the original direction. Scattering can be caused for example by collisions with the medium or by non-uniformities of the material such as density differences. Scattering in the prepared samples was strong enough to be clearly seen with naked eye so it was deemed necessary to measure it as well. The transmittance measurement device Lambda 850 could not be used for measuring scattered light as the detector and light source could not be moved with respect to each other so another setup was required.

8.1 Measurement setup

The scattering measurement setup is shown in figure 40 and the detector used was Horiba Jobin Yvon iHR320 0052-07-06. The detector detected the photons as counts per second, c/s, and for each measurement with different exposure time the exposure was reset and began from 0. The transmission of the samples was measured at angle 0 and scattered light intensity was measured at angles 5.5°, 10.5°, 15.5° and 20.5°. For each angle the measurement was repeated with different exposure times and the radiated power was determined by plotting counts per second as a function of time and fitting a line to the data. The scattering and transmittance was measured for three samples and a plain microscope slide was used for background measurement in order to eliminate the effect of the substrate.

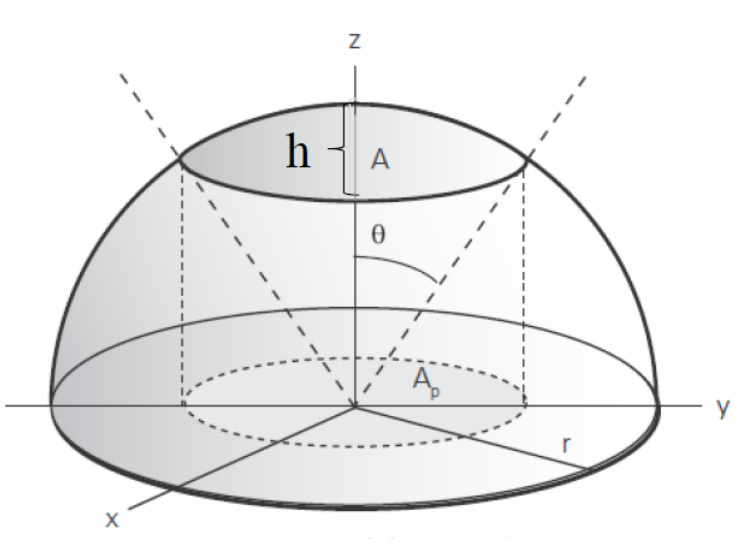

Figure 41: The surface area of a spherical cap.

Since the detector and the system were not originally designed for measuring transmittance or scattered light they possessed many faults for this kind of measurement. First of all the detector itself was not designed for measuring high intensities, it had a cap of how many counts it could measure, so the exposure times for measuring directly transmitted light were extremely small, and if the intensity of the lamp had been lowered then the intensity of the scattered light would have decreased as well and it would have taken a very long exposure time to measure the scattered portion. Secondly there was no proper sample mount available: the samples had to be held in place by pressing them against the sample table with a fastener. Hence every tilt and the position of the sample had to be tuned by hand. Thirdly the collector could only measure at an angle of bit over 20.5° and it also had to be moved manually for each measurement.

8.2 Calculating the portion of scattered light

The detected power P_d (measured in counts per second) was divided with the area of the spherical cap covered by the detector A_d to gain the detected intensity I_d as function of angle θ in radians:

$$I_d = \frac{P_d(\alpha)}{A_d}. \tag{9}$$

The surface area of a spherical cap A_{sc} illustrated in figure 41 is directly proportional to the radius of the sphere r and height of the cap h:

$$A_{sc} = 2\pi r h. \tag{10}$$

in which $h = r(1 - \cos\theta)$ and $\theta = \arcsin\frac{r_d}{r}$ where r_d is the radius of the detector. Since $\cos\left(\arcsin\frac{r_d}{r}\right) = \sqrt{1 - \left(\frac{r_d}{r}\right)^2}$ the equation (10) can be written as

$$A_d = 2\pi r^2\left(1 - \sqrt{1 - \left(\frac{r_d}{r}\right)^2}\right). \tag{11}$$

Since the radius of the half sphere $r = 0.12\ m$ and the radius of the detector is $r_d = 0.0035\ m$ the spherical area covered by the detector is

$$A_d = 2\pi \cdot (0.12m)^2 \cdot \left(1 - \sqrt{1 - \left(\frac{0.0035}{0.12m}\right)^2}\right) = 3.849 \cdot 10^{-5}\ m^2.$$

I_d was then plotted as a function of θ and an exponential decay function was fitted to the data to extrapolate the intensity $I(\theta)$ for the rest of the half sphere. Now the total power of the scattered light P_s can be gained by integrating the function $I(\theta)$ over the surface area of the half sphere:

$$P_s = \int_0^{2\pi r^2} I(\alpha)\,\mathrm{d}A. \tag{12}$$

As can be seen from equation (10), a small change in the surface area of the cap $\mathrm{d}A$ is directly proportional to a small change in its height $\mathrm{d}h$ which is equal to a small change of position in the z-axis $\mathrm{d}z$:

$$\mathrm{d}A = 2\pi r \mathrm{d}z. \tag{13}$$

By replacing $\mathrm{d}A$ in (12) with (13) we gain

$$P_s = \int_0^r I(\theta)\, 2\pi r \mathrm{d}z \tag{14}$$

$$P_s = 2\pi r \int_0^r I(\theta)\,\mathrm{d}z. \tag{15}$$

The relationship between the angle θ and the position in the z-axis can be derived with basic trigonometry:

$$\theta = \cos^{-1}\frac{z}{r}. \tag{16}$$

By replacing the variable θ in (15) with (16) we can now integrate the function

$$P_s = 2\pi r \int_0^r I(\cos^{-1}\frac{z}{r})\,\mathrm{d}z \tag{17}$$

and gain the total power of the scattered light P_s.

The portion of scattered light n_s is then given by

$$n_s = \frac{P_s}{P_{gdt} + P_{gs}} \tag{18}$$

in which P_{gdt} and P_{gs} are the powers of directly transmitted and scattered light in case of plain glass without HC-DWCNT film, in other words the total amount of light that passes through the substrate. The portion of directly transmitted light n_t is similarly given by

$$n_{dt} = \frac{P_{dt}}{P_{gdt} + P_{gs}}. \tag{19}$$

8.3 Results and discussion

Results of measuring the directly transmitted light are shown in figure 42. It was expected that the measurement system would not be optimal for measuring high intensities, and it proved to be true as the measurements with less than 0.01 s exposure time differed greatly from the measurements with higher exposure times which had coherent results. Especially the measurement done with 0.005 s showed that the real exposure time may be different than what the system was set to measure. The measurement points under 0.01 s were omitted from the fitting, as done in figure 43. The power of the directly transmitted light is given by the slope of the fitted line and it was determined similarly for the other samples.

The power of a scattered ray of light at each angle was also gained by plotting the counts as function of exposure time and then fitting a line to the measurement points. The power as a function of angle is given for each sample in figure 44 and the curve fit to those values of sample 40 after divining them with the area of the detector is shown in figure 45. The area of the detector was calculated earlier so the intensity for example at angle 5.5°, or 0.10 rad, is given by equation (9). The area of the detector is $3.849 \cdot 10^{-5}$ m^2 and the power at angle 5.5° is 280.4 c/s so the intensity is

$$I_d = \frac{280.4\ c/s}{3.849 \cdot 10^{-5}\ m^2},$$

$$I_d = 7284672\ c/(sm^2) \approx 7284\ kc/(sm^2).$$

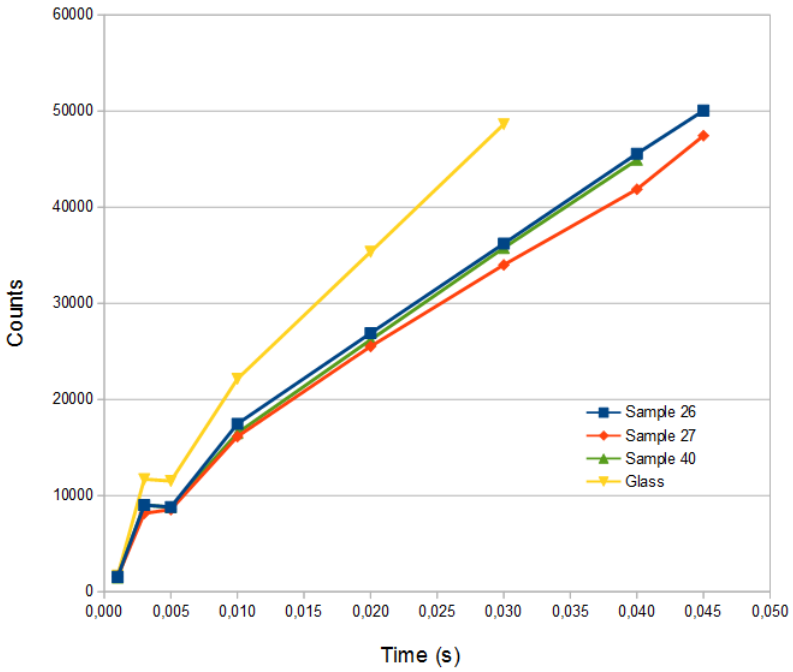

Figure 42: Directly transmitted light measured in counts as function of time for each sample.

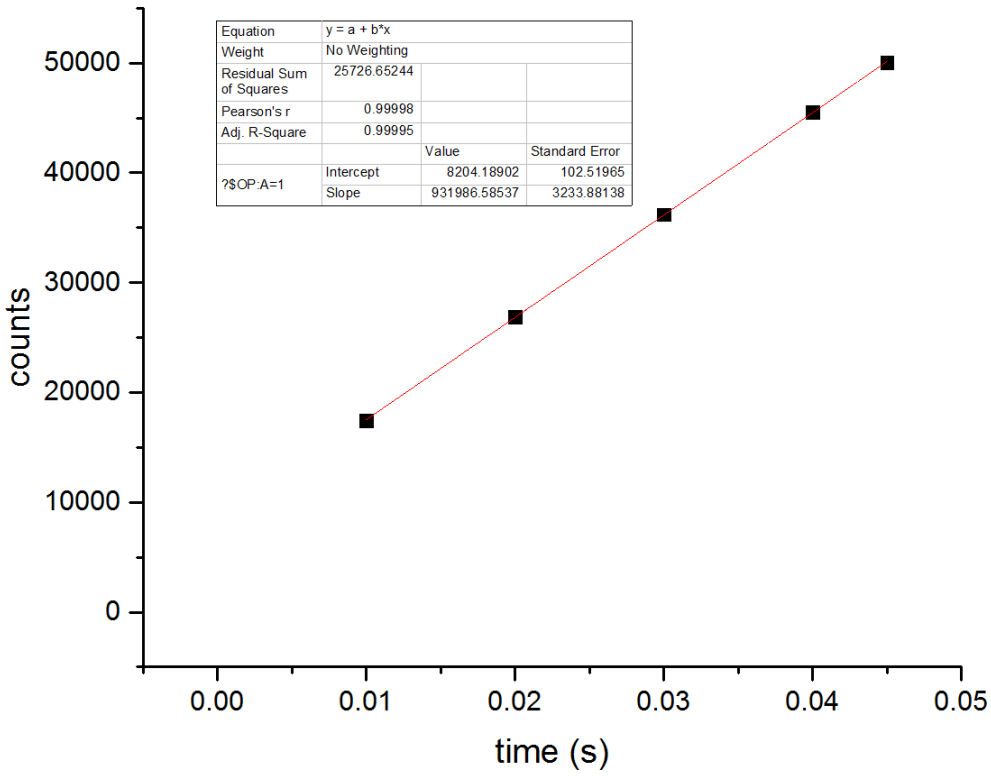

Figure 43: Directly transmitted light in counts for sample 26. The slope of the fitted line is the same as power of the directly transmitted light. Three measurement points which were measured in less than 0.01 seconds were omitted because of their unreliability.

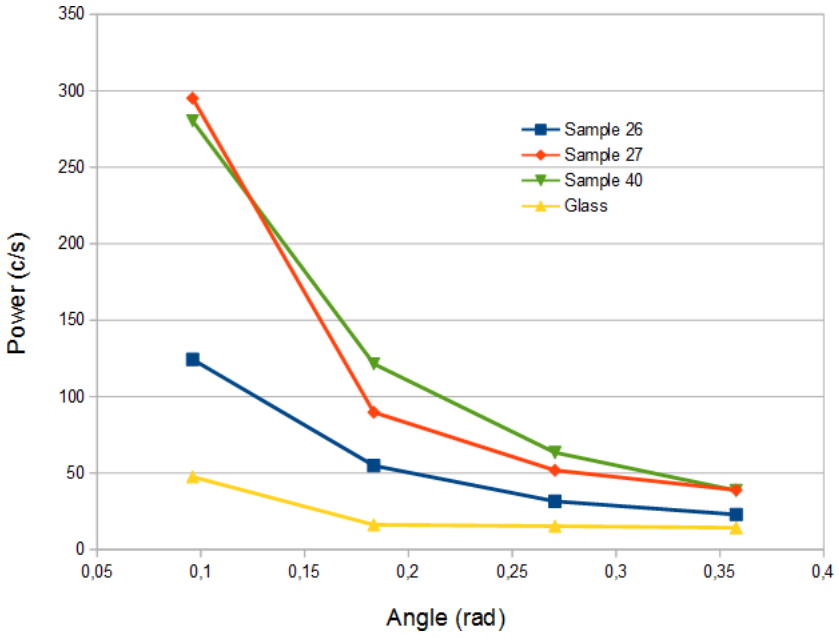

Figure 44: The measured power of scattered light as function of angle for each sample.

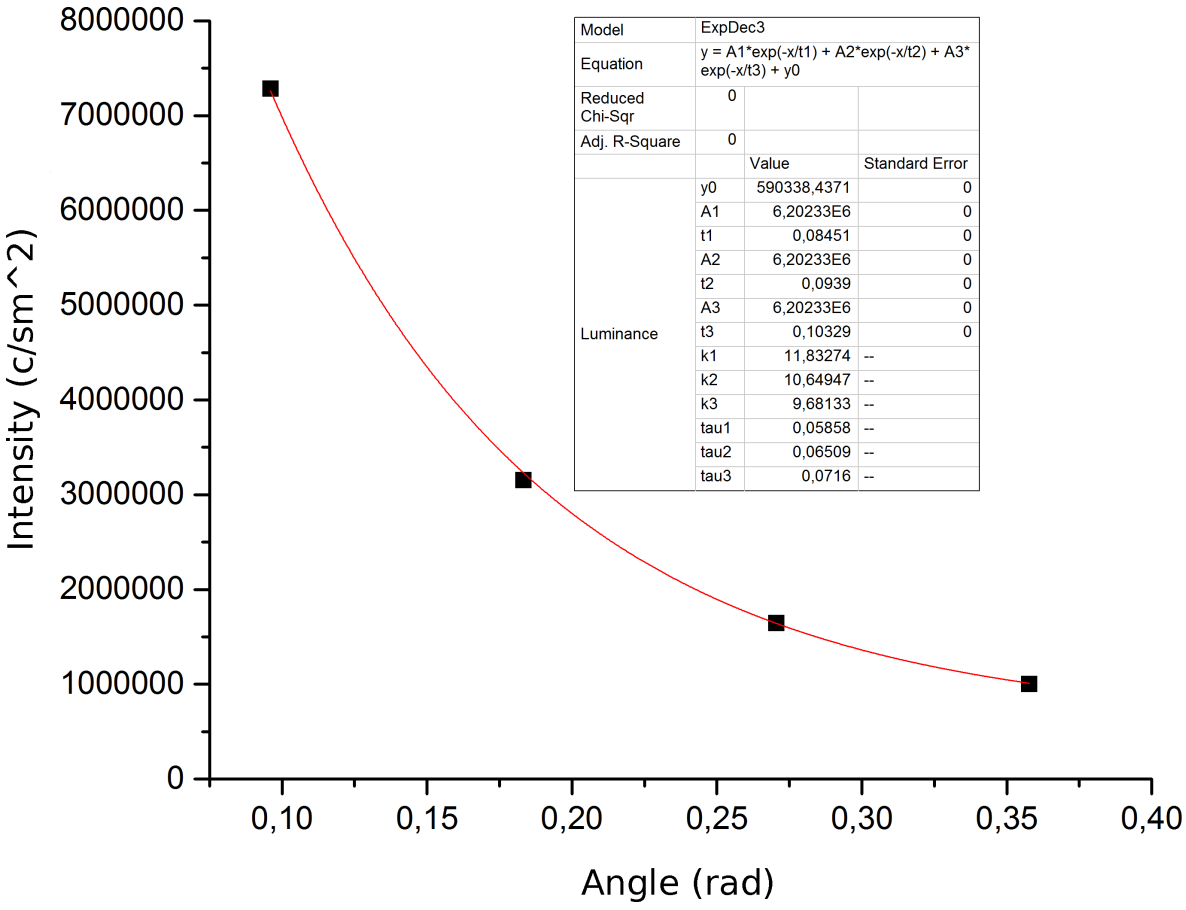

Model	ExpDec3		
Equation	y = A1*exp(-x/t1) + A2*exp(-x/t2) + A3*exp(-x/t3) + y0		
Reduced Chi-Sqr	0		
Adj. R-Square	0		
		Value	Standard Error
Luminance	y0	590338,4371	0
	A1	6,20233E6	0
	t1	0,08451	0
	A2	6,20233E6	0
	t2	0,0939	0
	A3	6,20233E6	0
	t3	0,10329	0
	k1	11,83274	--
	k2	10,64947	--
	k3	9,68133	--
	tau1	0,05858	--
	tau2	0,06509	--
	tau3	0,0716	--

Figure 45: Intensity of the scattered light as function of angle for sample 40 with an exponential decay fit. This curve was extrapolated up to $\pi/2$ *rad* and integrated in order to gain the total power of the scattered light.

Sample	Transmitted (kc)	Scattered (kc)	Transmitted portion (%)	Scattered portion (%)	Total	Lambda 850
26	932	48.3	68.5	3.6	72.1	79.2
27	874	93.0	64.3	6.8	71.1	76.0
40	948	68.2	69.7	5.0	74.7	76.8
glass	1324	35.9	97.4	2.6	100.0	100.0

Table 6: Results of transmittance and scattering measurements performed with iHR320. The table also includes transmittance values measured with Lambda 850.

After extrapolating the curve in figure 45 up to $\pi/2$ rad and integrating it from 0 rad to $\pi/2$ rad the gained total power of the scattered light is 68.2 kc/s while the power of the transmitted light is 947.7 kc/s. By comparing these values to the corresponding values for plain glass, 35.9 and 1324.0 kc/s, we gain the percentages of scattered and transmitted light with equations (18) and (19):

$$n_s = \frac{68.2\ kc/s}{1324.0\ kc/s + 35.9\ kc/s},$$

$$n_s = 0.0502 \approx 5.1\ \%,$$

$$n_{dt} = \frac{947.7\ kc/s}{1324.0\ kc/s + 35.9\ kc/s},$$

$$n_{dt} = 0.6969 \approx 69.7\ \%.$$

These results are gathered in table 6 and also shown graphically in figure 46. Since scattering portion of light was found to be several percents it is definitely a relevant factor for determining the quality of these films. The downside is that the results were not very coherent with the more accurate transmittance measurements performed with Lambda 850: only the combined percentage of transmittance and scattering of sample 40 came even close to the transmittance value given by Lambda 850 that does not even measure or add scattering to it. All values given by Lambda 850 were much higher than those given by iHR320. Hence the scattering percentages given here cannot be called absolute values but they do at least indicate a rough scale for the scattering percentage of HC-DWCNT films. All in all the amount of scattering in these films is not very high, in the scale of few percent, but still enough to be relevant.

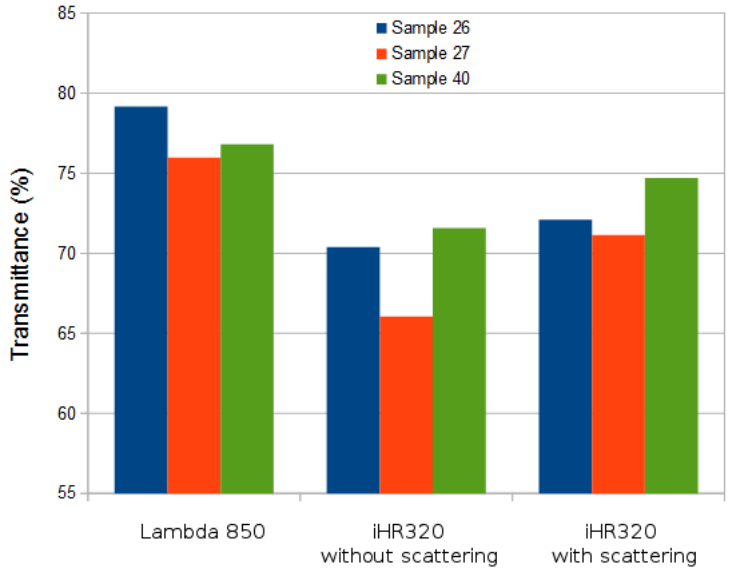

Figure 46: Comparison between the two transmittance measurement methods. Left columns represent direct transmittance measured with Lambda 850, middle columns are direct transmittance measured with iHR320 without taking scattering into account (direct transmittance of a sample divided by direct transmittance of glass) and columns on the right are the combined transmittance and scattering measured with iHR320. Transmittance measured with Lambda 850 was much higher than with iHR320 because iHR320 suffered from multiple error sources, but scattering in these samples is clearly significant enough that it should be taken into account when evaluating the quality of these films.

9 Conclusions

The best HC-DWCNT sample was prepared with vacuum filtration and had sheet resistance of $115 \pm 9\ \Omega/sq$ with 81.6 % transmittance at 550 nm and over 95 % in some of the IR region. Although HC-DWCNT cannot yet compete with other hybrid materials and doped CNT films in short-term quality, it does have potential as an alternative material, especially considering that the best HC-DWCNT films in this study were not doped or subjected to any kind of treatment that could improve the results further. Some of these other materials which were reviewed are presented in figure 47; AgNW hybrids and some other film types were omitted from the figure because of their infelixibility, high haze or too expensive vacuum preparation methods in order to better compare HC-DWCNT samples to other films with similar qualities. A very promising factor for future development of HC-DWCNT is that apart from nanobuds other pristine carbon films, SWCNT, DWCNT and most graphene films are clearly of lesser quality than HC-DWCNT films. If the few percent haze is also taken into account HC-DWCNT films are very close to HNO_3 doped DWCNTs and AuNP/SWCNT films, although the AgNP/DWCNT films by Lee et al. [112] still clearly hold the record of DWCNT hybrid films. Unfortunately the scattering measurement system was not accurate enough to produce exact values. HC-DWCNT films of the latest batch also showed very promising stability in room conditions, although the films were not very stable in high temperatures of over 200 $°C$.

The comparison of deposition methods revealed some important issues for future development. First of all the original dispersion contained insulating impurities which can be partly removed by simple immersion in water or filtration, which was found out by the different properties of spray-coated films and films produced with other methods. Because of this, along with the fact that the film structure shown in SEM images of spray-coated samples is far from optimal, regular spray-coating is not a good method from producing these films although immersion in water can improve them closer to the level of vacuum filtered films. Secondly the new deposition and transfer method, vacuum filtration combined with simple separation of the filter and film by lowering them to water, which leaves the HC-DWCNT film to float on the water surface, produced better samples than traditional dissolution of the filter membrane. This is the first time to our knowledge that this method is used for producing transparent conductive thin films with low sheet resistance: the only other vacuum filtered film peeled off in similar fashion had extremely large sheet resistance [134]. The only issue of the method was that some small particles of the filter membrane were attached to the film and transferred along with it, but this could of course be avoided with additional development.

All in all the use of hemicellulose for dispersing DWCNTs in water and connecting

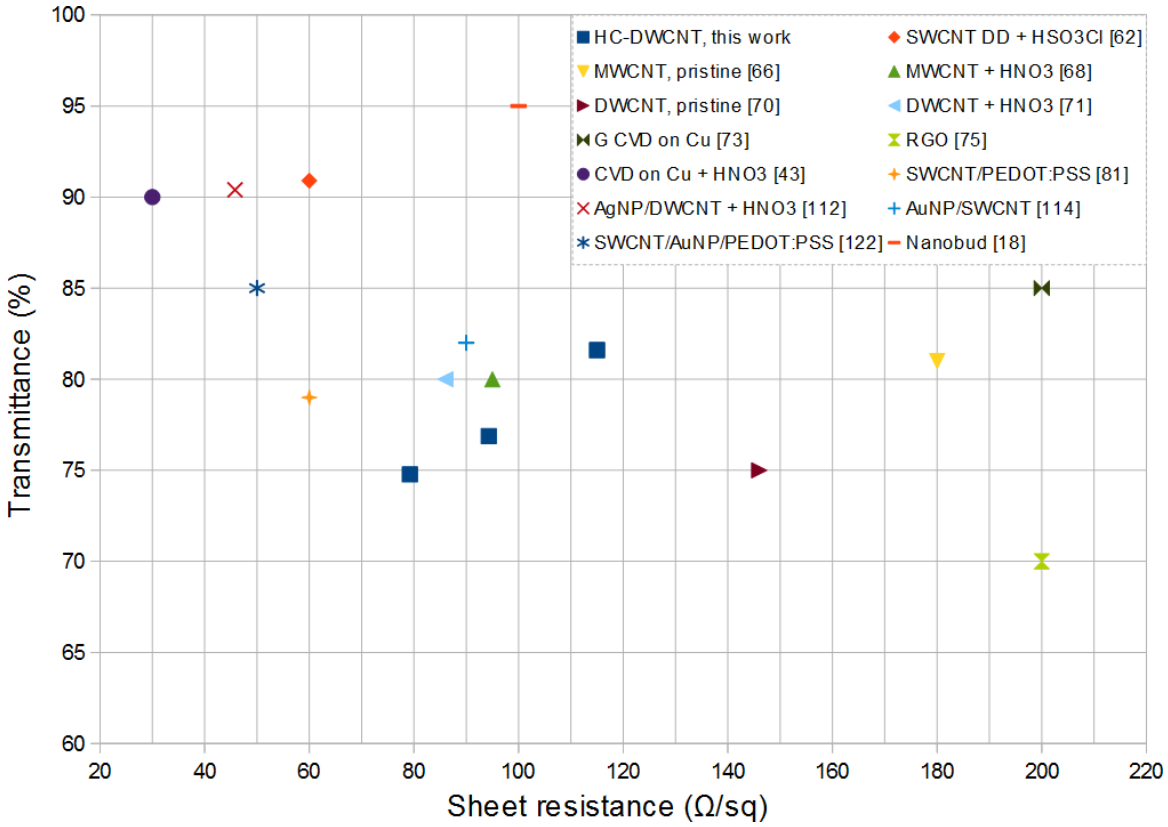

Figure 47: Comparison of HC-DWCNT films and some of the relevant carbon-based conductive films from literature with good flexibility, low haze and cost-efficient fabrication methods.

them to form transparent conductive films that are flexible, stable and also transparent in IR shows great potential for further research. Additionally the fairly new film deposition and transfer method is much cheaper and more scalable than traditional vacuum filtration in addition to its capability of producing higher-quality films.

References

[1] IHS Inc. Transparent electrode technology market report - 2013.

[2] Xinning Ho and Jun Wei. Films of carbon nanomaterials for transparent conductors. *Materials*, vol. 6(6):2155–2181, 2013.

[3] Liangbing Hu et al. Infrared transparent carbon nanotube thin films. *Applied Physics Letters*, 94:081103, 2009.

[4] Antonio Facchetti and Tobin Marks. *Transparent Electronics: From Synthesis to Applications*. John Wiley & Sons, 2010.

[5] M. Gulen et al. Role of annealing temperature on microstructural and electro-optical properties of ITO films produced by sputtering. *Journal of Materials Science: Materials in Electronics*, 24(2):467–474, 2013.

[6] Fumiaki N. Ishikawa et al. Transparent electronics based on transfer printed aligned carbon nanotubes on rigid and flexible substrates. *ACS Nano*, 3(1):73–79, 2009.

[7] Rufan Chang et al. Growth of half-meter long carbon nanotubes based on Schulz–Flory distribution. *ACS Nano*, 7(7):6156–6161, 2013.

[8] Changgu Lee et al. Measurement of the elastic properties and intrinsic strength of monolayer graphene. *Science*, 321(5887):385–388, 2008.

[9] Eric Pop et al. Thermal properties of graphene: Fundamentals and applications. *MRS Bulletin*, 37(12):1273–1281, 2012.

[10] Zhiyong Wang et al. Proximity-induced ferromagnetism in graphene revealed by the anomalous Hall effect. *Physical Review Letters*, 114(1):016603, 2015.

[11] R. R. Nair et al. Fine structure constant defines visual transparency of graphene. *Science*, 320(5881):1308, 2008.

[12] Qiaoliang Bao et al. Atomic-layer graphene as a saturable absorber for ultrafast pulsed lasers. *Adv. Funct. Mater*, 19(19):3077–3083, 2009.

[13] Mariana Pokrass et al. Saturable absorption of multi-walled carbon nanotubes/hybrid-glass composites. *Optical Materials Express*, 2(6):825–838, 2012.

[14] H. Kataura et al. Optical properties of single-wall carbon nanotubes. *Synthetic Metals*, 103(1-3):2555–2558, 1999.

[15] Brian W. Smith et al. Encapsulated C_{60} in carbon nanotubes. *Nature*, 396(6709):323–324, 1998.

[16] Albert G. Nasibulin et al. A novel hybrid carbon material. *Nature Nanotechnology*, 2(3):156–161, 2007.

[17] Kehan Yu et al. Carbon nanotube with chemically bonded graphene leaves for electronic and optoelectronic applications. *Journal of Physical Chemistry Letters*, 2(13):1556–1562, 2011.

[18] Canatu. CNB^{TM} hi-contrast film datasheet 2015 05 18. `http://www.canatu.com/downloads/brochure/Canatu-Hi-Contrast_brochure.pdf`. [Viewed 27-9-2015].

[19] Max M. Shulaker et al. Carbon nanotube computer. *Nature*, 501(7468):526–530, 2013.

[20] Dingshan Yu and Liming Dai. Self-assembled graphene/carbon nanotube hybrid films for supercapacitors. *Journal of Physical Chemistry Letters*, 1(2):467–470, 2010.

[21] Dirk M. Guldi et al. Single-wall carbon nanotubes as integrative building blocks for solar-energy conversion. *Angewandte Chemie*, 117(13):2051–2054, 2005.

[22] Kalpna Varshney. Carbon nanotubes: A review on synthesis, properties and applications. *International Journal of Engineering Research and General Science*, 2(4):660–677, 2014.

[23] Hong Wang et al. Catalysts for chirality selective synthesis of single-walled carbon nanotubes. *Carbon*, 81:1–19, 2015.

[24] Stephan P. Turano and Jud Ready. Chemical vapor deposition synthesis of self-aligned carbon nanotube arrays. *Journal of Electronic Materials*, 35(2):192–194, 2006.

[25] Pavel Nikolaev et al. Gas-phase catalytic growth of single-walled carbon nanotubes from carbon monoxide. *Chemical Physics Letters*, 313(1-2):91–97, 1999.

[26] Antti Kaskela et al. Aerosol-synthesized swcnt networks with tunable conductivity and transparency by a dry transfer technique. *Nano Letters*, 10(11):4349–4355, 2010.

[27] A. F. Ismail et al. A review of purification techniques for carbon nanotubes. *NANO: Brief Reports and Reviews*, 3(3):127–143, 2008.

[28] Aiping Yu et al. Application of centrifugation to the large-scale purification of electric arc-produced single-walled carbon nanotubes. *Journal of the American Chemical Society*, 128(30):9902–9908, 2006.

[29] Yoko Matsuzawa et al. Effective nondestructive purification of single-walled carbon nanotubes based on high-speed centrifugation with a photochemically removable dispersant. *Journal of Physical Chemistry C*, 118(9):5013–5019, 2014.

[30] K. S. Novoselof et al. Electric field effect in atomically thin carbon films. *Science*, 306(5696):666–669, 2004.

[31] Qingbin Zheng et al. Graphene oxide-based transparent conductive films. *Progress in Material Science*, 64:200–247, 2014.

[32] Phaedon Avouris and Christos Dimitrakopoulos. Graphene: synthesis and applications. *Materials Today*, 15(3):86–97, 2012.

[33] Khaled Parvez et al. Exfoliation of graphite into graphene in aqueous solutions of inorganic salts. *Journal of the American Chemical Society*, 136(16):6083–6091, 2014.

[34] Daniel R. Dreyer et al. The chemistry of graphene oxide. *Chemical Society Reviews*, 39(1):228–240, 2010.

[35] Xiluan Wang et al. Size fractionation of graphene oxide sheets by pH-assisted selective sedimentation. *Journal of the American Chemical Society*, 133(16):6338–6342, 2011.

[36] Zhuangchun Wu et al. Transparent, conductive carbon nanotube films. *Science*, 305(5688):1273–1276, 2004.

[37] James E. Morris and Krzysztof Iniewski. *Graphene, Carbon Nanotubes, and Nanostructures: Techniques and Applications*. CRC Press, 2013.

[38] E. S. W. Kong. *Nanomaterials, Polymers and Devices: Materials Functionalization and Device Fabrication*. John Wiley & Sons, 2015.

[39] Sung-Wook Choi et al. Patterning of hierarchically aligned single-walled carbon nanotube langmuir-blodgett films by microcontact printing. *Langmuir*, 26(19):15680–15685, 2010.

[40] L. Fu and A. M. Yu. Carbon nanotubes based thin films: Fabrication, characterization and applications. *Reviews on Advanced Materials Science*, 36:40–61, 2014.

[41] Mohammad Reza Golobostanfard et al. Incorporating carbon nanotubes in sol-gel synthesized indium tin oxide transparent conductive films. *Langmuir*, 30(39):11785–11791, 2014.

[42] Albert G. Nasibulin et al. Multifunctional free-standing single-walled carbon nanotube films. *ACS Nano*, 5(4):3214–3221, 2011.

[43] Sukang Bae et al. Roll-to-roll production of 30-inch graphene films for transparent electrodes. *Nature Nanotechnology*, 5(8):574–578, 2010.

[44] Libo Gao et al. Face-to-face transfer of wafer-scale graphene films. *Nature*, 505(7482):190–194, 2014.

[45] Evgeniya H. Lock et al. High-quality uniform dry transfer of graphene to polymers. *Nano Letters*, 12(1):102–107, 2012.

[46] Nicholas Petrone et al. Chemical vapor deposition-derived graphene with electrical performance of exfoliated graphene. *Nano Letters*, 12(6):2751–2756, 2012.

[47] Ji Won Suk et al. Transfer of cvd-grown monolayer graphene onto arbitrary substrates. *ACS Nano*, 5(9):6916–6924, 2011.

[48] Bing Deng et al. Roll-to-roll encapsulation of metal nanowires between graphene and plastic substrate for high-performance flexible transparent electrodes. *Nano Letters*, 15(6):4206–4213, 2015.

[49] Yu Wang et al. Electrochemical delamination of CVD grown graphene film: Toward the recyclable use of copper catalyst. *ACS Nano*, 5(12):9927–9933, 2011.

[50] Christie Thomas Cherian et al. 'Bubble-free' electrochemical delamination of CVD graphene films. *Small*, 11(2):189–194, 2015.

[51] Libo Gao et al. Repeated growth and bubbling transfer of graphene with millimetre-size single-crystal grains using platinum. *Nature Communications*, 3:699, 2011.

[52] Wei Chen. *Doped Nanomaterials and Nanodevices, Chapter: Doping of Carbon Nanotubes*. American Scientific Publishers, 2010.

[53] Bhupesh Chandra et al. Stable charge-transfer doping of transparent single-walled carbon nanotube films. *Chemistry of Materials*, 22(18):5179–5183, 2010.

[54] Seung Bo Yang et al. Recent advances in hybrids of carbon nanotube network films and nanomaterials for their potential applications as transparent conducting films. *Nanoscale*, 3:1361–1373, 2011.

[55] Amal Kasry et al. Chemical doping of large-area stacked graphene films for use as transparent, conducting electrodes. *ACS Nano*, 4(7):3839–3844, 2010.

[56] Hadi Hosseinzadeh Khaligh and Irene A. Goldthorpe. Failure of silver nanowire transparent electrodes under current flow. *Nanoscale Research Letters*, 8(1):235, 2013.

[57] Hongjun Gao et al. Chemical vapor doping of transparent and conductive films of carbon nanotubes. *Chemical Physics Letters*, 546:109–114, 2012.

[58] K. Mustonen et al. Gas phase synthesis of non-bundled, small diameter single-walled carbon nanotubes with near-armchair chiralities. *Applied Physics Letters*, 107(1):013106, 2015.

[59] Ilya V. Anoshkin et al. Hybrid carbon source for single-walled carbon nanotube synthesis by aerosol cvd method. *Carbon*, 78:130–136, 2014.

[60] Olivier Reynaud et al. Aerosol feeding of catalyst precursor for cnt synthesis and highly conductive and transparent film fabrication. *Chemical Engineering Journal*, 255:134–140, 2014.

[61] Jing Gao et al. Optimizing processes of dispersant concentration and post-treatments for fabricating single-walled carbon nanotube transparent conducting films. *Applied Surface Science*, 277:128–133, 2013.

[62] David S. Hecht et al. High conductivity transparent carbon nanotube films deposited from superacid. *Nanotechnology*, 22(7):075201, 2011.

[63] Sae Jin Sung et al. New insights into the oxidation of single-walled carbon nanotubes for the fabrication of transparent conductive films. *Carbon*, 81:525–534, 2015.

[64] Yeji Kim et al. Industrially feasible approach to transparent, flexible, and conductive carbon nanotube films: Cellulose-assisted film deposition followed by solution and photonic processing. *Applied Physics Express*, 6(2):025101, 2013.

[65] Yanqing Wang and Bunshi Fugetsu. Mono-dispersed ultra-long single-walled carbon nanotubes as enabling components in transparent and electrically conductive thin films. *Carbon*, 82:152–160, 2015.

[66] Walid Aloui et al. Transparent and conductive multi walled carbon nanotubes flexible electrodes for optoelectronic applications. *Superlattices and Microstructures*, 64:581–589, 2013.

[67] Daewoong Jung et al. Highly conductive flexible multi-walled carbon nanotube sheet films for transparent touch screen. *Japanese Journal of Applied Physics*, 52(3), 2013.

[68] Luowen Peng et al. Transparent, conductive, and flexible multiwalled carbon nanotube/graphene hybrid electrodes with two three-dimensional microstructures. *Journal of Physical Chemistry C*, 116(8):4970–4978, 2012.

[69] Naoki Imazu et al. Fabrication of flexible transparent conductive films from long double-walled carbon nanotubes. *Science and Technology of Advanced Materials*, 15(2):025005, 2014.

[70] Alexander A. Green and Mark C. Hersam. Processing and properties of highly enriched double-wall carbon nanotubes. *Nature Nanotechnology*, 4(1):64–70, 2009.

[71] Peng-Xiang Hou et al. Double-wall carbon nanotube transparent conductive films with excellent performance. *Journal of Materials Chemistry A*, 2:1159–1164, 2014.

[72] Keun Soo Kim et al. Large-scale pattern growth of graphene films for stretchable transparent electrodes. *Nature*, 457(7230):706–710, 2009.

[73] Weiwei Cai et al. Large area few-layer graphene/graphite films as transparent thin conducting electrodes. *Applied Physics Letters*, 95:123115, 2009.

[74] Xuesong Li et al. Transfer of large-area graphene films for high-performance transparent conductive electrodes. *Nano Letters*, 9(12):4359–4363, 2009.

[75] Atiye Nekahi et al. Transparent conductive thin film of ultra large reduced graphene oxide monolayers. *Applied Surface Science*, 295:59–65, 2014.

[76] Jing Ning et al. Electrical and optical properties of layer-stacked graphene transparent electrodes using self-supporting transfer method. *Synthetic Metals*, 203:215–220, 2015.

[77] Fethullah Güneş et al. Layer-by-layer doping of few-layer graphene film. *ACS Nano*, 4(8):4595–4600, 2010.

[78] Ivan Khrapach et al. Novel highly conductive and transparent graphene-based conductors. *Adv. Mater.*, 24(21):2844–2849, 2012.

[79] Bu-Jong Kim et al. Sheet resistance, transmittance, and chromatic property of CNTs coated with PEDOT:PSS films for transparent electrodes of touch screen panels. *Thin Solid Films*, 572:68–72, 2014.

[80] Bu-Jong Kim et al. Properties of cnts coated by PEDOT:PSS films via spin-coating and electrophoretic deposition methods for flexible transparent electrodes. *Surface and Coatings Technology*, 271:22–26, 2015.

[81] Jing Zhang et al. Incorporation of single-walled carbon nanotubes with PEDOT/PSS in DMSO for the production of transparent conducting films. *Diamond and Related Materials*, 22:82–87, 2012.

[82] Sukanta De et al. Transparent, flexible, and highly conductive thin films based on polymer-nanotube composites. *ACS Nano*, 3(3):714–720, 2009.

[83] Mansu Kim and Young Chul Kim. Single wall carbon nanotube/poly(3,4-ethylenedioxythiophene) nanocomposite film as a transparent electrode for flexible organic light-emitting diodes. *Synthetic Metals*, 198:31–35, 2014.

[84] Gaozhi Xiao et al. Highly conductive and transparent carbon nanotube composite thin films deposited on polyethylene terephthalate solution dipping. *Thin Solid Films*, 518(10):2822–2824, 2010.

[85] L.N. Saw et al. Transparent, electrically conductive, and flexible films made from multiwalled carbon nanotube/epoxy composites. *Composites Part B: Engineering*, 43(8):2973–2979, 2012.

[86] Sasmita Nayak et al. Preparation of transparent and conducting carbon nanotube/n-hydroxymethyl acrylamide composite thin films by in situ polymerization. *Carbon*, 50(11):4269–4276, 2012.

[87] Sergio H. Domingues et al. Transparent and conductive thin films of graphene/polyaniline nanocomposites prepared through interfacial polymerization. *Chemical Communications*, 47:2592–2594, 2011.

[88] Desalegn Alemu et al. Highly conductive PEDOT:PSS electrode by simple film treatment with methanol for ITO-free polymer solar cells. *Energy & Environmental Science*, 5(11):9662–9671, 2012.

[89] Masahiro Hokazono et al. Thermoelectric properties and thermal stability of PEDOT:PSS films on a polyimide substrate and application in flexible energy conversion devices. *Journal of Electronic Materials*, 43(6):2196–2201, 2014.

[90] Yue-Feng Liu et al. Improved efficiency of indium-tin-oxide-free organic light-emitting devices using PEDOT:PSS/graphene oxide composite anode. *Organic Electronics*, 26:81–85, 2015.

[91] Shicai Xu et al. Graphene–silver nanowire hybrid films as electrodes for transparent and flexible loudspeakers. *CrystEngComm*, 16(17):3532–3539, 2014.

[92] Donghwa Lee et al. Highly stable and flexible silver nanowire–graphene hybrid transparent conducting electrodes for emerging optoelectronic devices. *Nanoscale*, 5(17):7750–7755, 2013.

[93] Iskandar N. Kholmanov et al. Improved electrical conductivity of graphene films integrated with metal nanowires. *Nano Letters*, 12(11):5679–5683, 2012.

[94] Mi-Sun Lee et al. High-performance, transparent, and stretchable electrodes using graphene−metal nanowire hybrid structures. *Nano Letters*, 13(6):2814–2821, 2013.

[95] Donghwa Lee et al. High-performance flexible transparent conductive film based on graphene/agnw/graphene sandwich structure. *Carbon*, 81(1):439–446, 2015.

[96] P. Meenakshi et al. Investigations on reduced graphene oxide film embedded with silver nanowire as a transparent conducting electrode. *Solar Energy Materials and Solar Cells*, 128:264–269, 2014.

[97] Hsi-Wen Tien et al. Using self-assembly to prepare a graphene-silver nanowire hybrid film that is transparent and electrically conductive. *Carbon*, 58:198–207, 2013.

[98] Dong Chul Choo and Tae Whan Kimz. Conducting transparent thin films based on silver nanowires and graphene-oxide flakes. *Journal of The Electrochemical Society*, 162(6):H419–H421, 2015.

[99] Young Soo Yun et al. Transparent conducting films based on graphene oxide/silver nanowire hybrids with high flexibility. *Synthetic Metals*, 162(15–16):1364–1368, 2012.

[100] Hye Jin Han et al. Preparation of transparent conducting films with improved haze characteristics using single-wall carbon nanotube-silver nanowire hybrid material. *Synthetic Metals*, 199:219–222, 2015.

[101] Andrew J Stapleton et al. Highly conductive interwoven carbon nanotube and silver nanowire transparent electrodes. *Science and Technology of Advanced Materials*, 14(3):035004, 2013.

[102] Takehiro Tokuno et al. Hybrid transparent electrodes of silver nanowires and carbon nanotubes: a low-temperature solution process. *Nanoscale Research Letters*, 7(1):281, 2012.

[103] Mao xiang Jing et al. High performance of carbon nanotubes/silver nanowires-PET hybrid flexible transparent conductive films via facile pressing-transfer technique. *Nanoscale Research Letters*, 9(1):588, 2014.

[104] Liangjing Shi et al. A long-term oxidation barrier for copper nanowires: graphene says yes. *Physical Chemistry Chemical Physics*, 17:4231–4236, 2015.

[105] Iskandar N. Kholmanov et al. Reduced graphene oxide/copper nanowire hybrid films as high-performance transparent electrodes. *ACS Nano*, 7(2):1811–1816, 2013.

[106] Zhaozhao Zhu et al. Transparent conducting electrodes based on thin, ultra-long copper nanowires and graphene nano-composites. *Proceedings of the SPIE*, 9177:91770J, 2014.

[107] Jung-Yong Lee et al. Solution-processed metal nanowire mesh transparent electrodes. *Nano Letters*, 8(2):689–692, 2008.

[108] Liangbing Hu et al. Scalable coating and properties of transparent, flexible, silver nanowire electrodes. *ACS Nano*, 4(5):2955–2963, 2010.

[109] Colin Preston et al. Optical haze of transparent and conductive silver nanowire films. *Nano Research*, 6(7):461–468, 2013.

[110] Katsuyuki Naito et al. Transparent conducting film composed of graphene and silver nanowire stacked layers. *Synthetic Metals*, 175:42–46, 2013.

[111] Hsi-Wen Tien et al. The production of graphene nanosheets decorated with silver nanoparticles for use in transparent, conductive films. *Carbon*, 49(5):1550–1560, 2011.

[112] Shie-Heng Lee et al. Highly transparent and conductive thin films fabricated with nano-silver/double-walled carbon nanotube composites. *Journal of Colloid and Interface Science*, 364(1):1–9, 2011.

[113] Wen-Yin Ko and Kuan-Jiuh Lin. Highly conductive, transparent flexible films based on metal nanoparticle-carbon nanotube composites. *Journal of Nanomaterials*, 2013:Article ID 505292, 2013.

[114] Seung Bo Yang et al. Multistep deposition of gold nanoparticles on single-walled carbon nanotubes for high-performance transparent conducting films. *Journal of Physical Chemistry C*, 116(48):25581–25587, 2012.

[115] Chen Feng et al. Flexible, stretchable, transparent conducting films made from superaligned carbon nanotubes. *Advanced Functional Materials*, 12(6):885–891, 2010.

[116] Ying Zhou et al. Building interconnects in carbon nanotube networks with metal halides for transparent electrodes. *Carbon*, 87:61–69, 2015.

[117] Tengfei Qiu et al. Hydrogen reduced graphene oxide/metal grid hybrid film: towards high performance transparent conductive electrode for flexible electrochromic devices. *Carbon*, 81:232–238, 2015.

[118] Sung Man Kim et al. Hybrid transparent conductive films of multilayer graphene and metal grid for organic photovoltaics. *Japanese Journal of Applied Physics*, 52(12R):125103, 2013.

[119] Yu Zhu et al. Rational design of hybrid graphene films for high-performance transparent electrodes. *ACS Nano*, 5(8):6472–6479, 2011.

[120] Tongchuan Gao et al. Hierarchical graphene/metal grid structures for stable, flexible transparent conductors. *ACS Nano*, 9(5):5440–5446, 2015.

[121] Sunna Hwang et al. Formation of electrically conducting, transparent films using silver nanoparticles connected by carbon nanotubes. *Thin Solid Films*, 562:445–450, 2014.

[122] Na-Ri Shin et al. Highly conductive PEDOT:PSS electrode films hybridized with gold-nanoparticle-doped-carbon nanotubes. *Synthetic Metals*, 192:23–28, 2014.

[123] Iskandar N. Kholmanov et al. Nanostructured hybrid transparent conductive films with antibacterial properties. *ACS Nano*, 6(6):5157–5163, 2012.

[124] Xiao-Zhao Zhu et al. The application of single-layer graphene modified with solution-processed TiO_x and PEDOT:PSS as a transparent conductive anode in organic light-emitting diodes. *Organic Electronics*, 14(12):3348–3354, 2013.

[125] Yuan-Li Huang et al. Self-assembly of silver–graphene hybrid on electrospun polyurethane nanofibers as flexible transparent conductive thin films. *Carbon*, 50(10):3473–3481, 2012.

[126] Sondra L. Hellstrom et al. Strong and stable doping of carbon nanotubes and graphene by MoO_x for transparent electrodes. *Nano Letters*, 12(7):3574–3580, 2012.

[127] Sung Ho Kim et al. Carbon nanotube and graphene hybrid thin film for transparent electrodes and field effect transistors. *Advanced Materials*, 26(25):4247–4252, 2014.

[128] Qingbin Zheng et al. Highly transparent and conducting ultralarge graphene oxide/single-walled carbon nanotube hybrid films produced by langmuir–blodgett assembly. *Journal of Materials Chemistry*, 22:25072–25082, 2012.

[129] Mohammad Reza Golobostanfard et al. Carbon nanotube/indium tin oxide hybrid transparent conductive film: Effect of nanotube diameter. *Solar Energy Materials and Solar Cells*, 132:418–424, 2014.

[130] Ian Y.Y. Bu and Matthew T. Cole. A highly conductive and transparent solution processed azo/mwcnt nanocomposite. *Ceramics International*, 40(1A):1099–1104, 2014.

[131] Hao Sun et al. Novel graphene/carbon nanotube composite fibers for efficient wire-shaped miniature energy devices. *Advanced Materials*, 26(18):2868–2873, 2014.

[132] Jae Young Kim et al. Graphene–carbon nanotube composite as an effective conducting scaffold to enhance the photoelectrochemical water oxidation activity of a hematite film. *RSC Advances*, 2:9415–9422, 2012.

[133] Yasodinee Wimalasiri and Linda Zou. Carbon nanotube/graphene composite for enhanced capacitive deionization performance. *Carbon*, 59:464–471, 2013.

[134] Ashok K. Sundramoorthy et al. Lateral assembly of oxidized graphene flakes into large-scale transparent conductive thin films with a three-dimensional surfactant 4-sulfocalix[4]arene. *Scientific Reports*, 5(Article number: 10716), 2015.

[135] Corning Incorporated. Calcium fluoride product sheet. `https://lightmachinery.com/media/1542/h0607_caf2_product_sheet.pdf`. [Viewed 26-9-2015].